DEUTERIUM NUCLEAR MAGNETIC RESONANCE OF PHOSPHOLIPIDS AT HIGH PRESSURE

BOYAN BONEV

DEUTERIUM NUCLEAR MAGNETIC RESONANCE OF PHOSPHOLIPIDS AT HIGH PRESSURE

By

Boyan Bonev

Eng.-phys., M. Sc. Physics, "St. Kliment Ochridski" University of Sofia

A THESIS SUBMITTED TO THE SCHOOL OF GRADUATE STUDIES IN PARTIAL FULFILLMENT OF THE REQUIREMENTS FOR THE DEGREE OF DOCTOR OF PHILOSOPHY

DEPARTMENT OF PHYSICS AND PHYSICAL OCEANOGRAPHY

MEMORIAL UNIVERSITY OF NEWFOUNDLAND

AUGUST 2, 1996

Abstract

The effect of hydrostatic pressure on saturated diacyl phospholipids was studied using deuterium NMR. A probe for deuterium NMR studies of soft materials was constructed to operate at pressures up to 2.7 kbar. The response of the bilayer to hydrostatic pressure was found to be highly anisotropic in that the bilayer thickness was observed to increase as the pressure was raised. From the temperature and pressure dependence of the first spectral moments in perdeuterated DMPC, it was concluded that the effect of temperature on area per lipid decreased with pressure. The main transition in DMPC-d_{54} was analyzed in terms of a Landau-type free energy model. In another series of experiments lipid headgroups were found to tilt toward the bilayer normal, in response to a pressure-induced reduction in the area per lipid molecule in the bilayer. Experiments where temperature was varied at high and low pressure led to the conclusion that the headgroup response to temperature consists of two effects - a headgroup tilt and a temperature-induced methylene disorder. In a study of perdeuterated DLPC high pressure was found to remove the overlap between the main and the subtransition and to result in the appearance of a true gel phase below the liquid crystalline phase. The low temperature end of the liquid crystalline phase was found to be dominated by an intermolecular ordering process which substantially slowed the motions. In perdeuterated DPPC, high pressure was seen to promote the formation of a number of low temperature phases. When temperature was lowered, the system was observed to pass through the liquid

crystalline phase, a possibly interdigitated phase, a phase that might reflect domination by intermolecular correlations, rather than chain order, and a highly ordered crystalline phase. Cholesterol in a DPPC membrane was found to reduce the effects of hydrostatic pressure on the membrane in the sense that aside from the pressure-induced temperature shift the ambient pressure phase behaviour was retained even at 2.2 kbar. No evidence was found to suggest that the positioning of the cholesterol molecule in the bilayer might be affected by pressure.

Table of Contents

List of Tables

List of Figures

Acknowledgements

It is a special pleasure to thank everyone who helped in preparation of this thesis. In the first place I am deeply indebted to my supervisor Professor Michael Morrow, who made this work possible, for his talented guidance, tremendous help throughout all stages of this project and financial support. I want to thank, as well, Professors Michel Lafleur and Mark Whitmore for sharing their results and for the insightful discussions. I am also very grateful to Dr. John Katsaras for his fruitful suggestions and to Professors Nathan Rich and Mark Whitmore for their help and advice as members of my supervisory committee.

It is a pleasure to acknowledge William Kieley for his expert assistance and advice during the construction of the high pressure probe, Juli Atherton for her help in data acquisition and analysis, Wen Li for the discussion and for her help with Figure 1.2 and Dr. Rod Byrne for his invaluable consultations on LaTeX.

I have benefited greatly from my interaction with my fellow graduate students and friends at the Physics Department, present and past.

My computer skills have greatly improved, which became possible with the help of Rod Campbell, Allan Goulding, David Press, Chris Stevenson and Fred Perry.

My years at Memorial would not have been the same without the friendly staff of the Physics Department; special thanks to Daphne Corbett and Mrs. J. Barron.

Finally, I wish to thank my parents, Boyan Bonev and Nadejda Hadjiivanova, for their understanding, encouragement and support.

I also wish to acknowledge the donation of Celazole by the Hoechst Celanese Corporation.

This thesis is written without any caffeine consumption.

Chapter 1

Phospholipids

Lipids constitute one of the major classes of biologically important organic molecules. They form the central architectural feature of biological membranes, the lipid bilayer [1-4]. The membrane lipids in general have an amphiphilic structure. The hydrophilic part is normally a polar group (charged or zwitterionic) and the hydrophobic part is aliphatic.

Among all lipid families, phospholipids have been subject to the most intense scrutiny and are presently best understood. The role of the phospholipids as essential membrane components is attributed to their lyotropic behavior, i.e., to their ability to spontaneously form bilayer mesophases when dispersed in water [1, 3-7]. This behaviour is driven by the so called *hydrophobic interactions*. Geometric factors, reflecting the relative size of the polar region (headgroup) and the hydrophobic region (tails), as well as the degree of hydration, determine the type of liquid crystal aggregates formed [1].

1.1 Description and classification

Phospholipids display a rich diversity of phases as temperature (thermotropic mesomorphism) or hydration (lyotropic mesomorphism) is varied. A number of lamellar (L, P), hexagonal (H), cubic(Q) and crystalline (C) phases have been identified. A popular and comprehensive description of these phases has been proposed by Luzzati [8], although a complete and unified nomenclature is currently not available.

The various lipid mesophases in Luzzati's notation are described by a Latin letter on the basis of their general topology and geometry, with a subscript, specifying the state of the hydrocarbon chains. The meaning of the various symbols is summarized in table 1.1 (from [5]).

Phase structure		*Hydrocarbon chain state*	
L	-lamellar	α	-fluid (disordered)
P	-rippled	β	-normal (partially ordered gel)
H	-two-dimensional hexagonal	β'	-tilted (partially ordered gel)
H_I	-hexagonal	δ	-helical
H_{II}	-inverted hexagonal	c	-crystalline
R	-rhombohedral		
Q	-cubic		
C	-crystalline		

Table 1.1: Luzzati's nomenclature.

Stable phases for phospholipids with two hydrocarbon chains are usually lamellar [8-11] or, for lipids with a smaller headgroup [12], hexagonal.

Phospholipids have a phosphate group as part of their polar headgroup. A major family of membrane lipids is the glycerophospholipids. The focus of the present work is largely on glycerophospholipids. Their general structure includes two nonpolar hydrocarbon chains, esterified (or etherified) to a glycerol (often called the backbone), to which a phosphate group is also esterified, usually at position 3'. The phosphate, in turn, is esterified to an alcohol. A very common membrane lipid class, the phosphatidylcholines, has a choline group attached to the phosphate.

The phospholipid hydrocarbon chains are residues of esterified fatty acids. These fatty acid residues may be saturated or unsaturated. Saturated (alkyl) chains contain no double bonds.

Phospholipids with one or two saturated chains are ubiquitous in lung surfactants and in cell membranes. Table 1.2 lists saturated fatty acids associated with the

diacylphospholipids discussed in this work together with an example of a monounsaturated acid.

Structure	*Systematic name*	*Common name*	*Δ-system*
$CH_3(CH_2)_{10}COOH$	*n*-Dodecanoic	Lauric	12:0
$CH_3(CH_2)_{12}COOH$	*n*-Tetradecanoic	Myristic	14:0
$CH_3(CH_2)_{14}COOH$	*n*-Hexadecanoic	Palmitic	16:0
$CH_3(CH_2)_{16}COOH$	*n*-Octadecanoic	Stearic	18:0
$CH_3(CH_2)_7CH{=}CH(CH_2)_7COOH$		Oleic	18:1cΔ^9

Table 1.2: Fatty acids nomenclature.

The complete names of the phospholipids are formed by preceding the backbone name with the names of the chains and appending the headgroup name at the end. One example of a diacylphospholipid is 1,2-dipalmitoyl-*sn*-glycero-3-phosphatidylcholine (DPPC). This lipid, abundant in membranes and surfactants, has a glycerol backbone, two palmitic chains and a phosphorylcholine headgroup. The structure of the 12 carbon homolog, 1,2-dilauroyl-*sn*-glycero-3-phosphatidylcholine (DLPC), is shown in Figure 1.1. Figure 1.2 illustrates the approximate orientation of the various parts of an isolated DLPC molecule (produced by Cerius-2).

Phospholipids are the major components of cell membranes. They play an active role in cell division and fusion, endo- and exocytosis, transport, etc. Phospholipids determine the passive behaviour of the membrane and serve as a structured solvent for enzymes, channels and other functional membrane components.

Another lipid discussed in this work, is cholesterol. The cholesterol molecule consists of a rigid sterol core, composed of four fused hydrocarbon rings, with a hydrocarbon chain at position 17 and a polar (hydroxyl) headgroup at position

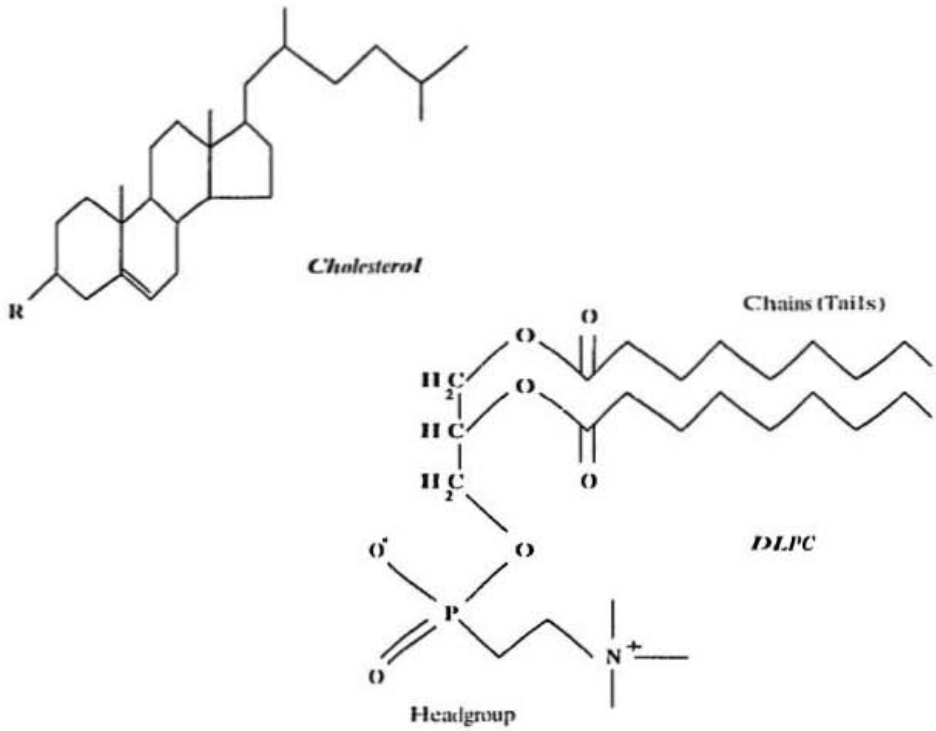

Figure 1.1: Structure of DLPC and cholesterol.

3 (figure 1.1). The molecule is amphiphilic, but cholesterol forms liquid crystal mesophases more readily in combination with phospholipids than on its own. Cholesterol plays a very important role in eukaryotic cell growth and is also a precursor to a number of hormones and bile salts. It is found in the phospholipid array of plasma membranes of most mammalian cells, where it participates in regulating bilayer fluidity, permeability and other properties.

1.2 Lipid bilayers

The diacylphosphatidylcholines (diacyl PCs) in water form a number of mesophases. A common feature of these is the phospholipid bilayer, formed spontaneously by the dispersion in water of diacyl PCs with more than 10 carbons in their hydrocarbon

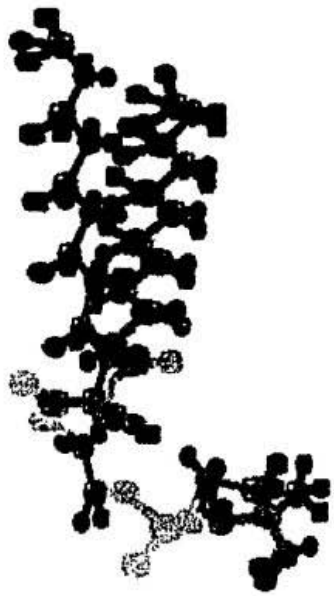

Figure 1.2: Model of an isolated molecule of DLPC. (Produced by Cerius 2.)

chains. Dry phospholipids are crystalline [13], but multibilayers form even at very low levels of hydration. The molecules in a bilayer are organized such that the hydrocarbon chains of each monolayer are parallel and form the hydrophobic region of the monolayer, while the polar headgroups lie in a different plane, forming the hydrophilic surface of the monolayer. Two monolayers orient with their hydrophobic faces towards each other to form the phospholipid bilayer. Bilayers are separated by the water subphase. At higher levels of hydration the multibilayers organize in larger closed structures called liposomes. The latter are vesicular aggregates which may contain one or many bilayers and have a water subphase enclosed in the vesicle. The single bilayer liposomes are called unilamellar vesicles (ULV) and are usually produced by sonication of the lipid/water suspension, while the multibilayer

ones are called multilamellar vesicles (MLV) and are obtained by gentle stirring or vortexing. The sizes of MLV are generally larger than those of ULV. The thickness of the bilayer, though, is small compared to the size of either.

The thermotropic behaviour of diacyl PC's is dominated by the state of their phospholipid chains. At low temperatures, the hydrocarbon chains are in the *all-trans* (t) conformation, that is, all carbon atoms on one chain lie in one plane. This is the ground state of the chain [14, 15]. It corresponds to a C-C-C-C dihedral angle of 0°. Another stable conformation of the acyl chains is the *gauche* (g) conformation, where the dihedral angle is ±120°. A gauche conformation changes the direction of the chain. This disrupts the order in the bilayer and is sterically unfavourable. Combinations of two gauche and one or more trans bonds (kinks and jogs) on the other hand, although less energetically favourable, disrupt the bilayer much less and are common in the excited state of the chains [14, 15]. At high temperature the phospholipid chains are in a disordered state, dominated by gauche conformations. They behave in that state much like melted paraffins. This is the *liquid crystalline*, or L_α phase. Caution must be exercised in using the expression *liquid crystal* - here it is used in a more restricted sense to describes the fluid state of the chains, rather than in its more common meaning referring largely to the mesomorphic states of matter (cf. [16]). At lower temperatures the lipid chains are predominantly straight (fewer gauche conformations) and tilted ($L_{\beta'}$) or not tilted (L_β) with respect to the bilayer normal. In addition, a bilayer modulation may occur in some cases to accommodate some of the mismatch between the headgroup and the chain volume, resulting in so called rippled (P) phases. In the ordered phase there is also evidence of molecular ordering within the plane of the bilayer.

Phase transitions and headgroups.

The phase conversion between the disordered (liquid crystalline phase) and the

more ordered phases in pure phospholipids is observed as a discontinuity in a number of experimental parameters. From the differential scanning calorimetry perspective, a sharp discontinuity in the enthalpy marks the transition. This is seen as a peak in the heat capacity of the system [17, 18]. X-ray crystallography [5, 6, 11, 13] and small angle neutron scattering (SANS) measurements [6, 19] report a discontinuity in the bilayer thickness. The onset of lateral molecular order below the phase transition can be observed by wide angle X-ray diffraction [5]. NMR moments and lineshape analysis indicate a discontinuous change in the orientational order of the acyl chains and the area per lipid molecule across the transition [20-22]. These and other experiments provide abundant evidence that the *main* bilayer transition, observed between the L_α and the $P_{\beta'}$ phases [11, 23], is of first order. It has been suggested, though, that the main transition in diacyl PC's occurs close to a critical point [22, 24-30]. On the basis of a systematic study of the discontinuity in the area per lipid molecule across the main transition, Morrow and coworkers [22] conclude that the main transition in shorter chain diacyl PCs occurs closer to a critical point than in longer chain homologs. The results of that study also imply that this discontinuity may disappear in lipids with less than 14 carbons in the acyl chains. The shortest chain diacyl PC, which forms stable bilayer aggregates, is DLPC which has 12 carbons on its chains. The observation of the $L_\alpha \rightarrow P_{\beta'}$ transition in this lipid is obstructed by the intervention of a transition into the L_c phase [22, 31-36].

At lower temperature the diacyl PCs undergo a phase conversion between the $P_{\beta'}$ and the $L_{\beta'}$ phases. This is the *pretransition*. The shorter chain diacyl PC homologs (12 and 14 carbons) enter a crystalline (L_c) phase across the *subtransition*. This phase is also observable in longer chain diacyl PCs after incubation at subzero temperatures over a long period of time [31, 37]. It is important to remember that these transitions occur between phases which are characterized by different order

and motional properties in the chain region. The topology of the sample (MLV in this case) does not change.

In membranes, the phosphatidylcholine headgroup is oriented almost parallel to the bilayer surface [38, 39]. This orientation can be affected by various perturbing agents. In the presence of membrane surface charge, for example, the headgroup undergoes a tilt towards, or away from the membrane surface [39-49]. Headgroup orientation is also affected by changes in hydration [50, 51].

1.3 Membranes at high pressure

The effects of hydrostatic pressure on phospholipid membranes have become the focus of substantial scientific interest in relation to issues like deep sea diving, physiology of ocean floor life forms and lipid systems in oil wells. Of particular interest are conditions like the high pressure nervous syndrome and pressure excitability in peripheral nerves. The experimental approaches used include electron spin resonance (ESR) [52, 53], dilatometry [54-58], differential scanning calorimetry [56, 59, 60], Raman, UV and IR spectroscopy [61-79], magnetic resonance [80-88], neutron scattering [19, 89-91], X-ray diffraction [92-95], light transmission [96, 97] and fluorescence [98, 99]. Theoretical models have been developed to discuss the effects of pressure on the main transition in phospholipids (Whitmore, unpublished results) and the mechanisms of incorporation of a local anaesthetic into the membrane [100, 101].

Research on membranes at high pressures has developed in a number of directions, among which are the study of the properties and phase behaviour of pure lipids at elevated pressure [19, 54, 56, 80, 81, 83, 85-88, 90, 91, 97, 102, 103], lipid-cholesterol interactions [72, 89] lipid-protein interactions [77, 78] and the effects of local anesthetics on lipid bilayers [52, 53, 55, 59, 72, 74, 84, 96, 104]. Live and intact

cells, as well as native cellular and organelle membranes, have also been investigated at elevated pressure [75, 105-111].

The main transition temperature in phospholipids has been observed to increase at elevated pressure by about 22°C per kbar [19, 51, 55, 83, 90, 112]. A number of high pressure phases have been reported, including an interdigitated phase [19, 56, 60, 61, 62, 65, 70, 82, 83, 85, 87, 88, 90, 97, 102, 103]. NMR spectra, presumably corresponding to six of these phases, have been identified [83]. These phases are identified as the liquid crystalline and five gel phases, described by Wong [102]. ^{2}H NMR experiments on lipids deuterated at specific places along the chains, show the distribution of methylene order along the chains. In particular, a substantial increase in the order is observed towards the ends of the chains in the interdigitated phase [86]. All phases can be observed in DPPC at pressures below 2 kbar.

Hydrostatic pressure produces lateral compression of the bilayer, the degree of which can be estimated from changes in the bilayer thickness. Pressure has been found to increase the thickness of the bilayer [90] and at the same time to decrease the bilayer volume [56, 57]. The volume compressibility of the bilayer, though, is one or two orders of magnitude smaller than the compressibility in the lateral and axial directions [113] and can often be neglected. Therefore, it is reasonable to assume that a lateral bilayer compression occurs at a rate proportional to the inverse of the change in bilayer thickness (see chapter 4). Deuterium NMR provides a way of estimating the change in membrane thickness.

Pressure is found to have an ordering effect on the acyl chains [83, 84]. Addition of a membrane-soluble local anesthetic is shown to disorder the bilayer. Subsequent application of high pressure has been observed to re-establish molecular order and, therefore, to act in its capacity of an anesthetic antagonist [84].

Experiments at elevated pressure provide information on the properties of phospholipids from the perspective of another thermodynamic dimension. The response of the bilayer to volume compression is very anisotropic and can be useful in gaining new insights into the mechanical and structural properties of the bilayer. The effects of volume compression on the phase behaviour of the phospholipids can lead to a better understanding of their ambient pressure phases.

1.4 This work

This is a study of the effects of hydrostatic compression on the molecular and phase properties of diacyl phospholipids. The design features of a new deuterium NMR probe for high pressure experimentation with soft materials are presented. The effects of pressure on the first order character of the phospholipid main transition are studied in terms of the discontinuity at the transition in the mean orientational order in DMPC. The proximity of the transition to a critical point is discussed. A phenomenological model is used to analyse the ambient and the high pressure behaviour of the system. A systematic study of the phase behaviour of DLPC at different pressures is presented. It is shown that pressure can be used to decouple the main transition and subtransition, which overlap at ambient pressure. The effect of pressure on the recently reported L_x phase is investigated, as well as the relative stability of the L_x and the gel phases with respect to the crystalline phase. It is suggested that DLPC undergoes a transition into the gel phase beyond a critical point. The response of the phosphocholine headgroup to a change in the area per lipid molecule is investigated in both DMPC and DPPC. High pressure is used as a tool for changing the orientation of the polar headgroup in a continuous way. A new mechanism governing the ambient pressure response of the headgroup to temperature is proposed. The phase behaviour of DPPC is studied at constant

pressure and at constant temperature. The boundaries of some high pressure phases are determined more accurately. The stability of the ordered crystalline and X phases is discussed. The effects of pressure on the phase behaviour and dynamical properties of a cholesterol-containing bilayer are studied.

Chapter 2

NMR Background

Nuclear magnetic resonance (NMR) is based on the principle of resonant energy transfer in a nuclear system in a magnetic field. This effect can only be observed in systems with nuclear spin $I \neq 0$.

The experiment includes a source of a constant external magnetic field $\mathbf{H}_0$, a spin system and a coil, with axis transverse to the external magnetic field. The coil plays the role of a coupling element between an excitation source of transverse time-dependent magnetic field and at the same time it provides the front end interface of the detector.

The interaction between an isolated spin and the magnetic field can be described by the Zeeman Hamiltonian

$$H_z = -\gamma \mathbf{H}_0 . \mathbf{I} \tag{2.1}$$

Here γ is the gyromagnetic ratio of the nuclear spin **I**. The preferred orientation in the spin system is along the external magnetic field. This results in a nonzero net macroscopic polarization. Let M_0 be the magnetization of the spin system at equilibrium. A semi-classical picture can be used to describe the dynamics of the spin system following a perturbation from equilibrium. The z-component of the magnetization, M_z, along $\mathbf{H}_0$, relaxes towards M_0, while the transverse components, M_x and M_y, relax to zero. The interaction can be described by the Bloch equations [114-116]

$$\frac{dM_z}{dt} = \frac{M_0 - M_z}{T_1} + \gamma(\mathbf{M} \times \mathbf{H})_z$$

$$\begin{aligned} \frac{dM_x}{dt} &= \gamma(\mathbf{M} \times \mathbf{H})_x - \frac{M_x}{T_2} \\ \frac{dM_y}{dt} &= \gamma(\mathbf{M} \times \mathbf{H})_y - \frac{M_y}{T_2}. \end{aligned} \tag{2.2}$$

The time constants for the relaxation are T_1 for the longitudinal component and T_2 for both transverse components of the magnetization.

This chapter presents a brief description of deuterium NMR theory and its relevance to membrane biophysics.

2.1 Deuterium NMR - theoretical remarks

Membranes fall in the category of partially ordered systems. More specifically, they are liquid crystals. The molecules in the lipid bilayer display some degree of orientational and positional order while complete crystal-like order is absent. Model membranes, discussed in this text, are generally in the form of MLV. The molecular motions in these systems are more restricted than in isotropic solutions, yet they have much more freedom than in the ordered systems. Deuterium NMR is a method for studying these motions which provide information on their magnitude, time scale and symmetry. The lipid motions in the membrane are anisotropic. As a result, the orientation dependent second order (tensor) spin interactions are not completely averaged out. These include the quadrupole and dipolar interactions and the chemical shifts.

Deuterium NMR (^{2}H NMR) utilizes some of the unique properties of this isotope. Hydrogen can be relatively easily substituted by deuterium in a number of organic molecules without altering the chemical and biochemical properties of the compounds. In addition, a site-specific substitution is possible, allowing information about a given part of the molecule to be obtained without interference from the rest of the system. Deuterium, a spin one nucleus, has a quadrupole moment small

enough that pulse techniques can be applied (typical line width is less than 250 kHz) and that the quadrupole interaction can be regarded as a first order perturbation to the Zeeman Hamiltonian (about 23 MHz in a 3.7 T magnetic field).

The complete Hamiltonian of the system consists of Zeeman, quadrupole, dipolar and chemical shift parts:

$$H = H_Z + H_Q + H_D + H_C. \tag{2.3}$$

For a carbon-deuterium bond in a methylene group the last two make contributions of the order of 10 kHz and 1 kHz, respectively, and can be neglected [117]. In this case the system can be treated as an isolated spin problem with the quadrupole interaction as a first order perturbation.

Figure 2.1 shows the splitting of the ground state of a system of spin $I = 1$ in external magnetic field $\mathbf{H_0}$. The ground level is split into three levels (left) with energies $E_m = -m\hbar\omega_0$. Here $m = 0, \pm 1$ and ω_0 is the Larmor frequency.

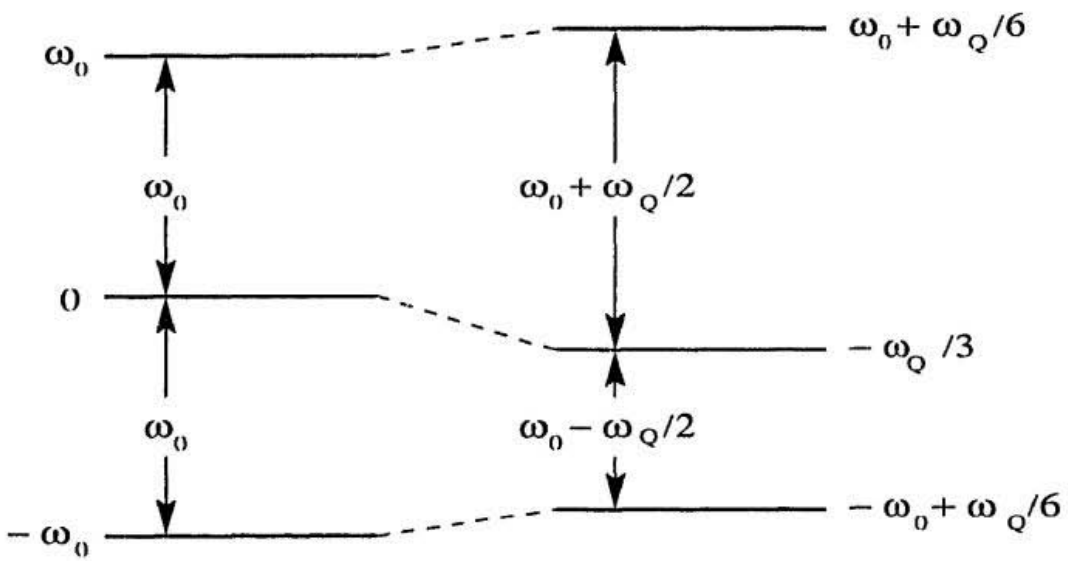

Figure 2.1: Zeeman and quadrupole splitting of the ground level in a spin one nucleus.

In a carbon deuterium chemical bond, the electron density has a highly

anisotropic distribution which creates an electric field gradient at the site of the nucleus. The quadrupole moment of the deuteron interacts with this gradient, producing a shift in the Zeeman levels. This shift can be evaluated by expanding the electric potential $V(\mathbf{r})$ in a Taylor's series. It can be shown, then, that the first non vanishing term in the resulting series for the quadrupole energy contains the second spatial derivatives of $V(\mathbf{r})$. These derivatives form a symmetric traceless second order tensor, called the electric field gradient (EFG) tensor. The quadrupole Hamiltonian can be expressed, by means of the Wigner-Eckart theorem, in the principal axes system of this tensor. Since the electric field gradient has a preferred direction, it is appropriate to introduce an asymmetry parameter

$$\eta = \left| \frac{V_{x'x'} - V_{y'y'}}{V_{z'z'}} \right| \tag{2.4}$$

reflecting the relative contribution of the diagonal elements $V_{x'x'}$, $V_{y'y'}$, $V_{z'z'}$ of the EFG tensor. Then the quadrupole Hamiltonian is [114, 116, 118-120]

$$H_Q = \frac{e^2qQ}{4I(2I-1)}[(3I_{z'}^2 - I^2) + \eta(I_{x'}^2 - I_{y'}^2)]. \tag{2.5}$$

Here $e^2qQ/h \approx 167$ kHz is the quadrupole coupling constant for deuterium in a carbon deuterium bond.

The quadrupole shift of the Zeeman lines can be determined by expressing the quadrupole Hamiltonian in spherical coordinates in the laboratory frame and then taking H_Q as a first order perturbation to the Zeeman Hamiltonian. The resulting Hamiltonian depends on I_z alone. Then the $m = \pm 1$ Zeeman levels are shifted upwards by an amount

$$\Delta = \frac{e^2qQ}{8}[(3\cos^2\beta - 1) + \eta \sin^2\beta \cos 2\alpha] \tag{2.6}$$

while the $m = 0$ level is lowered by 2Δ. The two Euler angles α and β describe the orientation of the EFG principal axes in the laboratory frame. The resulting

quadrupole splitting for a localized deuteron is

$$\omega_Q = \frac{3e^2qQ}{4h}[(3\cos^2\beta - 1) + \eta\sin^2\beta\cos 2\alpha]. \tag{2.7}$$

In this way the quadrupole interaction removes the degeneracy and the single Zeeman line of frequency ω_0 splits into two lines at $\omega_0 + 3\Delta/h$ and $\omega_0 - 3\Delta/h$. the shifted levels are shown in Figure 2.1 (right). The above expression also shows that the quadrupole splitting depends on the spatial orientation of the EFG with respect to the external magnetic field.

Almost all situations of practical interest involve deuterons which are not stationary but are, rather, part of molecules undergoing various motions. In the presence of molecular motions, it is more appropriate to discuss the average orientation of the EFG principal axes system, rather than its instantaneous one. This is usually done in terms of an *order parameter*, S_{ij} [119].

Instead of expressing the orientation of the EFG principal axes with respect to the laboratory frame of reference, it is suitable to introduce a molecular coordinate system and to describe the EFG orientation with respect to this system. This is appropriate in the case of carbon-deuterium bonds, since the essential part of the EFG is produced by the molecular electron distribution and the gradient appears stationary in such a molecular frame of reference. In this case, α, β and γ can be chosen to specify the Euler angles of the EFG system with respect to the molecular frame of reference and α', β' and γ' can be used to describe the orientation of the molecular axes of motion with respect to the laboratory coordinate system. The symmetry of the molecular motion and that of the laboratory frame leave γ, α' and γ' arbitrary and they can be set to zero. Then the average quadrupole splitting in the presence of molecular motion can be expressed in terms of the diagonal elements

of the order parameter tensor [117, 118, 119] as

$$\begin{aligned}\langle\omega_Q\rangle &= \frac{3c^2qQ}{4h}\frac{1}{2}(3\cos^2\beta' - 1)\langle[(3\cos^2\beta - 1) + \eta\sin^2\beta\cos 2\alpha]\rangle \\ &= \frac{3c^2qQ}{4h}[S_{zz} + \frac{1}{3}\eta(S_{xx} - S_{yy})].\end{aligned} \tag{2.8}$$

The order parameter elements are obtained by taking the average over the molecular motions. If the molecular reorientations are such that $S_{xx} = S_{yy}$, the quadrupole splitting,

$$\langle\omega_Q\rangle = \frac{3c^2qQ}{4h}(3\cos^2\beta' - 1)S_{zz}, \tag{2.9}$$

no longer depends on η. In a different situation, an axially symmetric EFG can result in an asymmetric deuterium line if the motions of the molecule are of lower symmetry.

A phospholipid dispersion in water is usually in the form of MLV. The molecular axes in such vesicles are approximately normal to, or slightly tilted with respect to the surface of the vesicle, thus assuming all possible orientations with respect to the external magnetic field. The different quadrupole splittings from molecules of different orientation with respect to the magnetic field result in a powder (or Pake) spectral line shape [117, 119] given by

$$\begin{aligned}f(x) &= \frac{1}{\sqrt{6}}\left[\frac{1}{(\frac{1}{2}+x)^{\frac{1}{2}}} + \frac{1}{(\frac{1}{2}-x)^{\frac{1}{2}}}\right] \quad , \quad 0 \le x \le \frac{1}{2} \\ f(x) &= \frac{1}{\sqrt{6}}\frac{1}{(\frac{1}{2}+x)^{\frac{1}{2}}} \quad , \quad \frac{1}{2} < x \le 1.\end{aligned} \tag{2.10}$$

where x is the scaled frequency. This is an expression for the deuterium lineshape for $\eta = 0$ and in the absence of relaxation, which would broaden the lines. A plot of the above equation is shown in Figure 2.2. When $\eta \neq 0$ the spectra are much more complex and analysis may require numerical calculations.

For symmetric lineshapes, like the one shown in Figure 2.2, the spectral moments

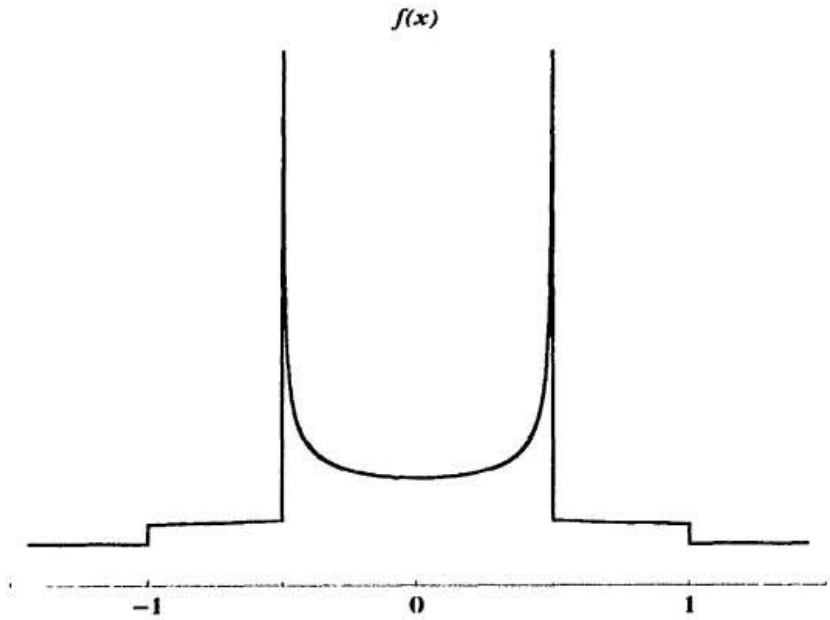

Figure 2.2: Spectral function f(x) for an axially symmetric motion.

can be defined as [117-119, 121]

$$M_n = \frac{\int_0^\infty f(\omega)\omega^n d\omega}{\int_0^\infty f(\omega)d\omega}. \tag{2.11}$$

The integral in the denominator is half the area under the spectrum and $f(\omega)$ is the spectral lineshape function. It can be shown that for an axially symmetric lineshape [119]

$$\begin{aligned} M_1 &= \frac{2}{3\sqrt{3}}\langle\omega_Q\rangle \\ &= \frac{e^2qQ}{h\sqrt{3}}S_{CD}. \end{aligned} \tag{2.12}$$

Here the second equality was obtained by expressing $\langle\omega_Q\rangle$ in terms of S_{CD} for a molecular axis, oriented along the magnetic field, using Equation 2.9. When perdeuterated hydrocarbon chains are studied the order parameter averaged over

all segments in the chain and $\overline{S_{CD}}$ must be used in Equation 2.12.

Equation 2.12 illustrates the importance of the first spectral moments to membrane studies. It shows M_1 as a useful indicator of mean orientational order in the hydrocarbon region. M_1 is thus extremely sensitive to phase transitions which affect this order [22, 119]. First spectral moments in the liquid crystalline phase are also used to estimate the acyl chain axial extension per methylene group in the hydrocarbon region of the membrane (cf. Equation 4.1 [22]).

2.2 NMR techniques

The NMR pulse sequence used in all experiments described hereafter is the *quadrupole echo* sequence [122]. It consists of two radio frequency (r.f.) pulses, separated by a time τ and shifted in phase by $\pi/2$. Each pulse tips the magnetization 90° away from equilibrium ($\pi/2$ pulse). A precession of the magnetization, called the free induction decay (FID), is initiated by the first pulse. Following the second pulse, a refocusing of the nuclear magnetization occurs at a time 2τ after the first pulse. The time 2τ can be chosen long enough that the echo will occur after the probe ringdown and beyond the dead time of the receiver. A necessary condition for implementation of the quadrupole echo sequence is that the longitudinal relaxation has to be slow $T_1 \gg \tau$. Here T_1 is the longitudinal relaxation time. The evolution of an isolated spin system following the two pulses can be described rigorously in terms of the density matrix formalism [117].

When the pulse separation is increased, the echo occurs at a later time with a concomitant decrease in amplitude. This loss of magnetization is a result of slow reorientation and is characterized by the transverse relaxation time T_{2e}. A series of increasing τ's with the corresponding decreasing echo amplitudes provides a means of measuring this parameter. If a single exponential decay mechanism is assumed,

the transverse relaxation rate can be calculated from

$$A(2\tau) = A(0)e^{-2\tau/T_{2e}}. \tag{2.13}$$

The subscript e here stands for 'echo', describing the method used for measuring the transverse relaxation.

A connection can be established between the transverse relaxation rate and the correlation times of the system by means of the density matrix formalism. The correlation function characteristic time (the correlation time) provides information on the timescale of the molecular motions. By means of an expansion of the density operator in terms of a complete set of orthonormal operators [119-121, 123-125], T_{2e} can be related to the spectral density functions of the system (the Fourier transformations of the correlation function) [121].

2.3 Quadrupole echo

The quantum mechanical treatment of the quadrupole echo is conveniently done in terms of the evolution of the density matrix [119, 117] following the two pulses. An operator space can be introduced which contains, for spin $I = 1$, a set of nine orthonormal operators. One particular choice, in the rotating frame, is [117, 126]

$$Q_1 = \frac{1}{\sqrt{2}}I_x, \quad Q_2 = \frac{1}{\sqrt{2}}I_y, \quad Q_3 = \frac{1}{\sqrt{2}}I_z, \quad Q_4 = \frac{1}{\sqrt{6}}(3I_z^2 - 2),$$

$$Q_5 = \frac{1}{\sqrt{2}}(I_xI_z - I_zI_x), \quad Q_6 = \frac{1}{\sqrt{2}}(I_yI_z - I_zI_y), \tag{2.14}$$

$$Q_7 = \frac{1}{\sqrt{2}}(I_x^2 - I_y^2), \quad Q_8 = \frac{1}{\sqrt{2}}(I_xI_y - I_yI_x), \quad Q_9 = 1, \quad .$$

Following the notation of Davis [117], the quadrupole Hamiltonian can be expressed as

$$H_Q = \sqrt{\frac{2}{3}}\hbar\omega_Q Q_4, \tag{2.15}$$

and the Hamiltonian during a pulse of strength ω_1 is

$$H_1 = -\sqrt{2}h\omega_1 Q_1. \tag{2.16}$$

Here ω_1 is the frequency of precession about the transverse magnetic field in the rotating frame. The total Hamiltonian in the absence of the r.f. pulse is

$$\begin{aligned} H_0 &= H_z + H_Q \\ &= -\sqrt{2}h\omega_0 Q_3 + \sqrt{\frac{2}{3}}h\omega_Q Q_4. \end{aligned} \tag{2.17}$$

The density matrix can be expressed in terms of these as

$$\rho(t) = \sum_q c_q(t) Q_q. \tag{2.18}$$

As discussed earlier, the quadrupole interaction can be treated as a small perturbation to the Zeeman Hamiltonian, and at equilibrium, the density matrix is

$$\rho(0) = \sum_q c_q(0) Q_q = c_3(0) Q_3, \tag{2.19}$$

where

$$c_3(0) = \frac{\sqrt{2}h\omega_0}{3kT} \tag{2.20}$$

and all other coefficients are zero.

During the first pulse of duration t_{w1} and strength ω_1, along the x-axis, the coefficient c_2 is also nonzero. The time evolution of each is described by the corresponding Liouville equations. A pair of solutions for c_2 and c_3,

$$\begin{aligned} c_2(t_{w1}) &= \frac{\sqrt{2}h\omega_0}{3kT}\sin(\omega_1 t_{w1}) \\ c_3(t_{w1}) &= \frac{\sqrt{2}h\omega_0}{3kT}\cos(\omega_1 t_{w1}), \end{aligned} \tag{2.21}$$

describes a precession of the vector magnetization about the component of the radio frequency (r.f.) field in the rotating frame. If the pulse is of magnitude and direction

such that $\omega_1 t_{w1} = \pi/2$, the z-component of the magnetization at the end of the r.f. pulse is rotated into the y-axis.

Following the $\pi/2$ pulse the only nonzero coefficient is

$$c_2(t_{w1}) = \frac{\sqrt{2}h\omega_0}{3kT} \tag{2.22}$$

and all other coefficients are zero. The system evolves for a time τ under the influence of the quadrupole Hamiltonian, Equation 2.15. The nonzero coefficients during this time period are c_2 and c_5. The solution of the corresponding Liouville equations for c_2 and c_5 at time τ takes the form of a precession in the (Q_2, Q_5) plane:

$$\begin{aligned} c_2(\tau) &= \frac{\sqrt{2}h\omega_0}{3kT}\cos(\omega_Q\tau) \\ c_5(\tau) &= -\frac{\sqrt{2}h\omega_0}{3kT}\sin(\omega_Q\tau). \end{aligned} \tag{2.23}$$

The coil in a NMR experiment is perpendicular to the magnetic field $\mathbf{H}_0$ and can detect the transverse magnetization M_x and M_y. Thus, after the first $\pi/2$ pulse the signal (in the rotating frame) is $\langle M_y \rangle$, which is proportional to $\langle I_y \rangle$:

$$\langle I_y(t) \rangle = \sqrt{2}c_2 = \frac{\sqrt{2}h\omega_0}{3kT}\cos(\omega_Q\tau). \tag{2.24}$$

This is the signal at the beginning of the free induction decay, (FID), following the pulse.

A second $\pi/2$ pulse, of strength ω_2 and duration t_{w2} along the y-axis, results in the formation of quadrupole echo. In this case, again, ω_2 is the frequency of precession about the transverse magnetic field in the rotating frame. During the pulse, c_2 is unaffected by the transverse field, because the r.f. Hamiltonian commutes with Q_2. If $\omega_Q \ll \omega_2$, the evolution under H_Q can be neglected. The effect of H_2 on c_5, at the end of the pulse, is given by

$$c_5(t_{w2}) = \frac{\sqrt{2}h\omega_0}{3kT}\sin(\omega_Q\tau)$$

$$\frac{1}{2}\left[\sqrt{3}c_4(t_{w2}) - c_7(t_{w2})\right] = 0. \tag{2.25}$$

After the pulse the system evolves under the quadrupole Hamiltonian 2.15. The solutions for c_2 and c_5, respectively, are

$$\begin{aligned} c_2(t) &= \frac{\sqrt{2}\hbar\omega_0}{3kT}\cos(\omega_Q[t-2\tau]) \\ c_5(t) &= -\frac{\sqrt{2}\hbar\omega_0}{3kT}\sin(\omega_Q[t-2\tau]). \end{aligned} \tag{2.26}$$

The quadrupole echo signal can be obtained from the expression for c_2:

$$\langle I_y(t)\rangle = \sqrt{2}c_2 = \frac{\sqrt{2}\hbar\omega_0}{3kT}\cos(\omega_Q[t-2\tau]). \tag{2.27}$$

The signal is symmetric about $t = 2\tau$ and has a maximum at this time. If relaxation is neglected, the amplitude is equal to the amplitude of the FID immediately following the first pulse. Quadrupole echo, in this way, recovers the FID completely a time 2τ after the first pulse, well beyound the recovery time of the receiver and after the ringing of the transmitter has ended.

Another interesting aspect of this technique is that, if the sign of the first pulse is changed, the quadrupole echo occurs with opposite sign. On the other hand a change in sign of the second pulse has no effect on the echo. These features prove very useful in eliminating various artifacts resulting from pulse imperfection and receiver recovery transients. A phase delay of $\pi/2$ in both pulses results in magnetization refocusing in the x-direction, which can be used for averaging of asymmetry in the quadrature section.

2.4 Relaxation

Molecular motions which contribute to the time-dependent part of the Hamiltonian result in phase accumulation in the rotating frame which, in turn, gives rise to a

decay in the quadrupole echo. If the decay is assumed to be exponential, the average relaxation rate, $1/T_{2e}$, may be obtained. This can be related to the reduction in the apparent second moment, ΔM_2, due to the motion.

The limiting cases of fast and slow motion are defined in terms of the relationship between ΔM_2 and the correlation time for the motions, τ_c. The resulting relaxation rate is a sum of the contributions from the individual relaxation mechanisms.

For fast motion, $\Delta M_2 \cdot \tau_c^2 \ll 1$, the general theory of motional averaging gives

$$\frac{1}{T_{2e}} = \Delta M_2 \cdot \tau_c. \tag{2.28}$$

This is essentially independent of the details of motion [127].

In the case of slow motion, $\Delta M_2 \cdot \tau_c^2 \gg 1$, the result depends on the character of motion and on the way relaxation is measured. When a two pulse sequence is used, in which the separation τ between the pulses is large enough that $\Delta M_2 \tau^2 \gg 1$, then, for large rotational jumps of the molecule [127],

$$T_{2e} = p \cdot \tau_c, \tag{2.29}$$

where $p \geq 1$. This means that during the time 2τ characteristic of the echo experiment, some deuterium nuclei acquire random phase from molecular jumps, which changes the frequency by an amount $\geq \sqrt{\Delta M_2}$. As a result, the second pulse at time τ does not refocus all of the magnetization at time 2τ. Only a fraction $\exp\left[-2\tau/(p\tau_c)\right]$ of the spins, which do not undergo large jumps, contribute to the echo. In the case of a symmetric two site jump, $p = 2$ [127]. For rotational diffusion the situation is more complex. Nonetheless T_{2e} still increases with increasing τ_c for long correlation times.

For fast motions $T_{2e} \sim \tau_c^{-1}$ while for slow motions $T_{2e} \sim \tau_c$. Therefore, in the intermediate motion situation, $\Delta M_2 \cdot \tau_c^2 \approx 1$, T_{2e} must go through a minimum. Pauls and coworkers [127] propose, for the region of intermediate τ_c, an expression of the

form

$$\frac{1}{T_{2r}} = \frac{\Delta M_2 \cdot \tau_c}{1 + p\Delta M_2 \cdot \tau_c^2}, \tag{2.30}$$

which is reduced to expressions 2.28 for short τ_c and 2.29 for long τ_c. At the minimum

$$T_{2r}(min) \approx 2\frac{p}{\Delta M_2} \quad \text{and} \quad \tau_c \approx \sqrt{p\Delta M_2}. \tag{2.31}$$

Deviations from the exponential character of the decay may result from a dependence of the decay rate on the orientation of the molecular axis and for correlation times far from the fast motion regime.

Chapter 3

Equipment Details and Sample Preparation.

3.1 The spectrometer

Deuterium NMR was performed in a 3.5 T superconducting magnet (Nalorac Cryogenics, Martinez, CA), using a locally constructed solid state spectrometer [128]. The spectrometer consists of a slave computer for data storage and initial pulse sequence programming, a 1 kW radiotransmitter and a quadrature detection section with a 12 bit digitizing oscilloscope. A deuterium NMR probe was designed for measurements between -20°C and 80°C at pressures up to 2.7 kbar.

A quadrupole echo pulse sequence ($\pi/2_x$ - τ - $\pi/2_{-y}$ - τ) was used [122]. The parameters of the sequence were adjusted before each series of experiments and are presented in the corresponding chapters. The total number of scans, collected per point, is also shown there, together with the effective dwell time after two or four times oversampling [129].

3.2 The high pressure probe

A high pressure probe was designed for these experiments. An assembly drawing is shown in Figure 3.1. The pressure chamber (1) is made of annealed beryllium copper. The chamber is calculated to operate at pressures of up to 3.5 kbar with a safety factor of 3. The sealed sample (2) is placed in the NMR coil and both are immersed in the pressure transmitting medium, hydraulic oil (AW ISO grade 32). The pressure chamber is suspended by means of three thin wall stainless steel tubes (3), which

also serve as thermal insulators, from a suspension plate (4). Three solid brass rods (5) provide the backbone for the whole internal structure of the probe. The brass rods are attached to the top plate (6). The top plate, hosting connectors for the excitation pulse and signal cables, is attached by three bolts (7) to a counter-ring (8). An aluminum tube (9) houses all elements of the probe. Upper (10) and lower (12) adjustment rings, separated by three brass studs, provide an adjustable support for the probe. Long threads on rods (8), studs (11) and tube (9) allow for an easy adjustment of the sample position in the volume of highest magnetic field homogeneity. The whole probe is rested, through ring 12 and a PTFE separator (not shown in the illustration), on top of the magnet (13).

The excitation pulse cable and signal cable, as well the heater and the thermocouple wires, enter through the top plate (6) (not shown in Figure 3.1). A diode array, separating the transmitter from the detection section, is situated atop the upper insulator plate (18). Coupling (16) and tuning (17) capacitors are placed between the top (18) and bottom insulator plates. Both capacitors are cylindrical with moving inner conductors and quartz insulators. Tuning is done by adjusting the inside conductors by turning insulated rods (20). A thin wire (14), connecting the tuning circuit to the NMR coil, enters the pressure chamber through the feed-through (15). The NMR coil is grounded through the chamber and the supporting frames to the outer conductors of the pulse and signal cables.

The pressure chamber is surrounded with Styrofoam insulation (21). Cold nitrogen gas is used as a coolant. It is carried down tube C and back up tube B (Figure 3.1). Pressure is applied to the sample via line A.

Figure 3.2 shows an exploded view of the chamber. The body (1) is made of brush alloy BERYLCO25 (ASA Alloys Inc.Concord, ON). Celazole U-60 (Hoechst Celanese Corp., Houston, TX) is used for the electrical feed-through (2). A pin (3)

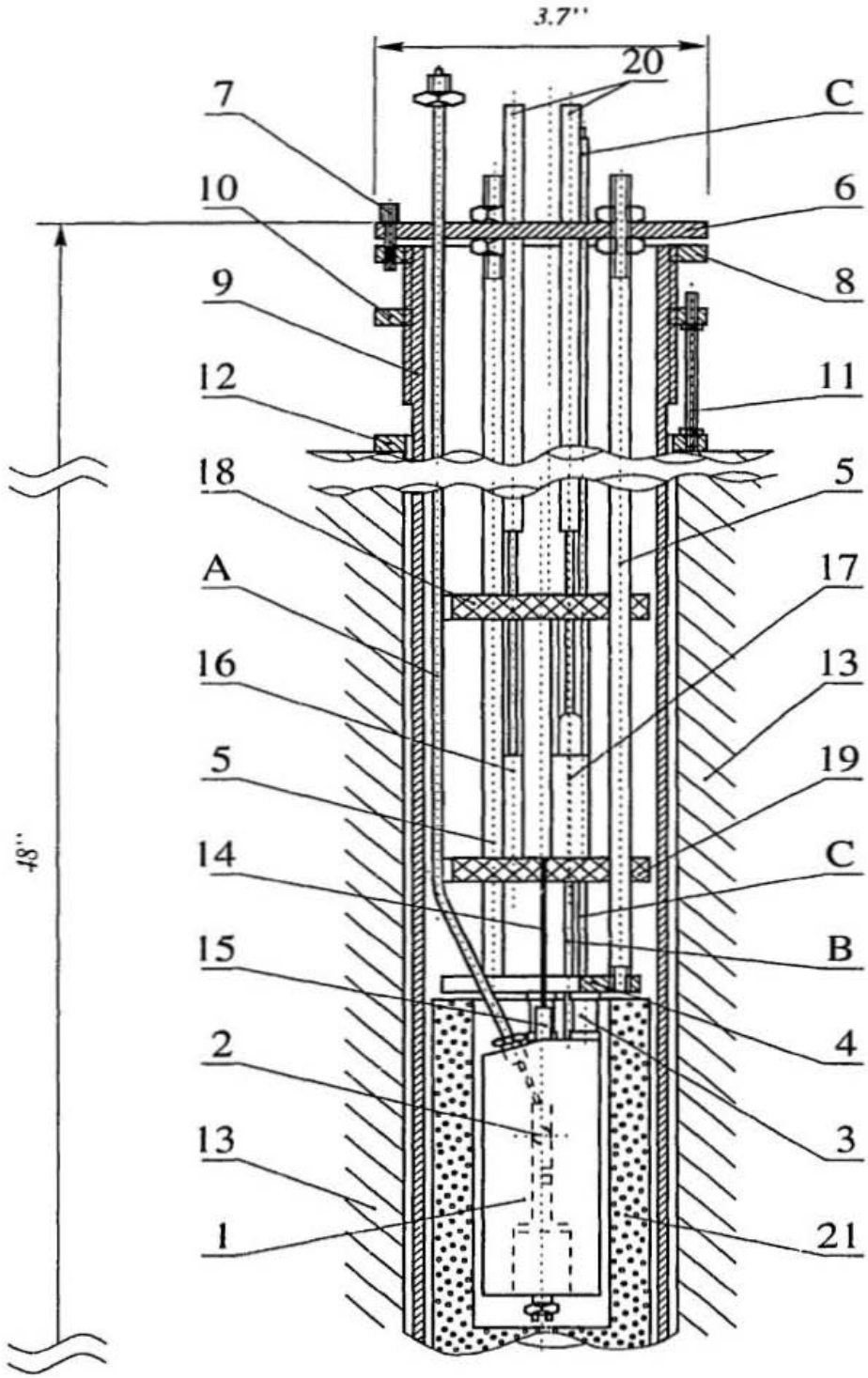

Figure 3.1: High pressure probe.

connects the high voltage wire (4) to the NMR coil. An insulator cap (5) is used to prevent arcing around the top of the chamber. Coolant is supplied through inlet C, circulated down channels (7) and released up tube B. The heater (8) is wound on the outer surface of the chamber. It is powered down wire D. Thermocouple E is attached to the top of the chamber. A dedicated computer controls the temperature with an accuracy of 0.1°C.

Pressure in the chamber is applied through inlet F. A Bridgman seal closes the compression volume and, at the same time, allows for easy access to the pressure compartment. A modular coil-holder, containing the sample (6), is easily inserted once the seal is removed. The seal consists of a beryllium copper plug (9), two quenched copper gaskets (10), PTFE gasket washer (11), spacer (12) and a beryllium copper support nut (13). A counter-nut (15) allows for initial compression of the seal through a washer (14).

The enlarged coil holder is shown in Figure 3.3. It consists of PTFE body (1), DELRIN lock screw (3), NMR coil (4), coil compression plug (7), counter-bar (9) and a coil compression screw (10). The NMR coil (4) is connected to the electrical feed-through pin (Figure 3.2, part 3) via pin 2. Ground is established between the coil terminal (8) and the wall of the chamber. The fluid sample (5) is heat sealed in a flexible polyethylene container (6) and placed in the coil. An 8 mm 12 turn tightly wound coil is used (wire gauge 28). A thin brass shim separates the coil from the chamber walls (not shown).

A schematic diagram of the pressure setup is shown in Figure 3.4. Hydraulic oil (AW ISO grade 32) is used as a pressure transmitter. The oil reservoir (7) is connected to the supply/bypass line at the entrance of the hydraulic jack (6). Valve 10 allows for the pressurized system to be decoupled from the compressor and valve 8 is the release pressure/bypass valve. The pressure gauge 4 is permanently connected

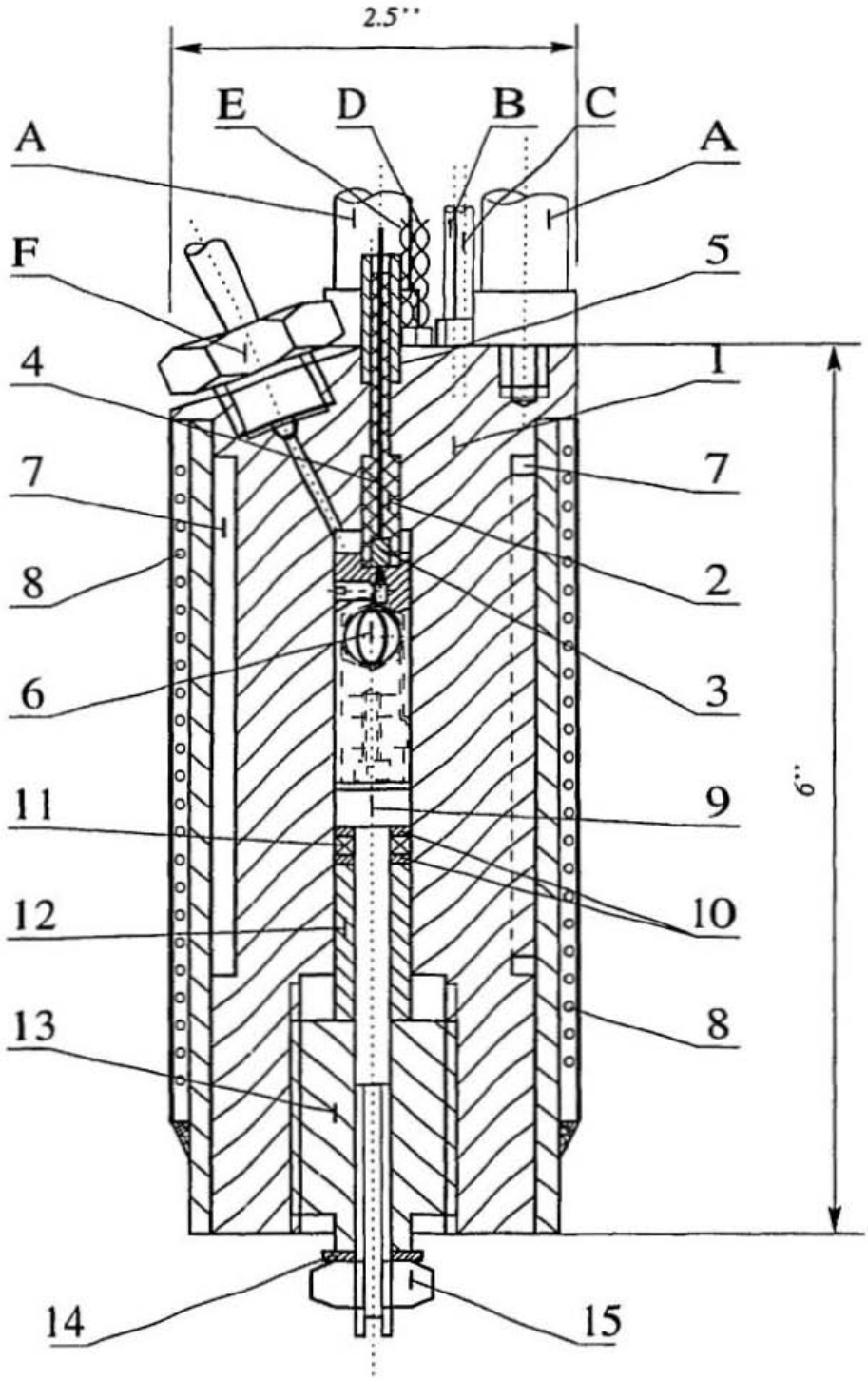

Figure 3.2: High pressure chamber.

to the high pressure line. It is of Bourdon type, covers a range of 2758 kbar with precision of ±14 bar and was calibrated against a dead weight gauge to better than 1% accuracy. Gauge 5 is for low pressure measurements. It is normally disconnected from the pressure line by valve 8. It is also of Bourdon type with an operating range of 207 kbar with precision of ±0.8 bar. Valve 11 is used for closing the pressure line when disconnecting the probe 1. All high pressure tubing and valves are rated for pressures not exceeding 4.137 kbar.

A pressure stabilizer (2) with a temperature regulator (3) is designed for maintaining constant pressure in the system when the temperature of the sample is changed. This is necessitated by the fact that all experiments are carried out at fixed volume of the pressurizing medium. The operation of the device is very simple. As the temperature is decreased (increased) in the sample chamber (1), the temperature of the stabilizer chamber (2) is increased (decreased). Chamber 2 has twice the volume of chamber 1 and the necessary temperature corrections in regulator 3 are half of the temperature changes in the sample chamber 1. Ultimately the gauge pressure is monitored and other adjustments are made as required. Therefore the pressure is stabilized within the accuracy of the pressure gauge.

3.3 Sample preparation

Both DMPC [11] and DPPC [23] are in the form of MLV suspensions above 40% wt. hydration. Some properties of DLPC are a function of water concentration up to 50% wt. [32] and these samples were studied at higher levels of hydration (see below).

Perdeuterated lipids (DLPC, DMPC and DPPC) were synthesized by acylation of glycerophosphocholine with the corresponding fatty acid anhydride, using the method of Gupta et al. [130]. Perdeuterated acids were prepared by the method

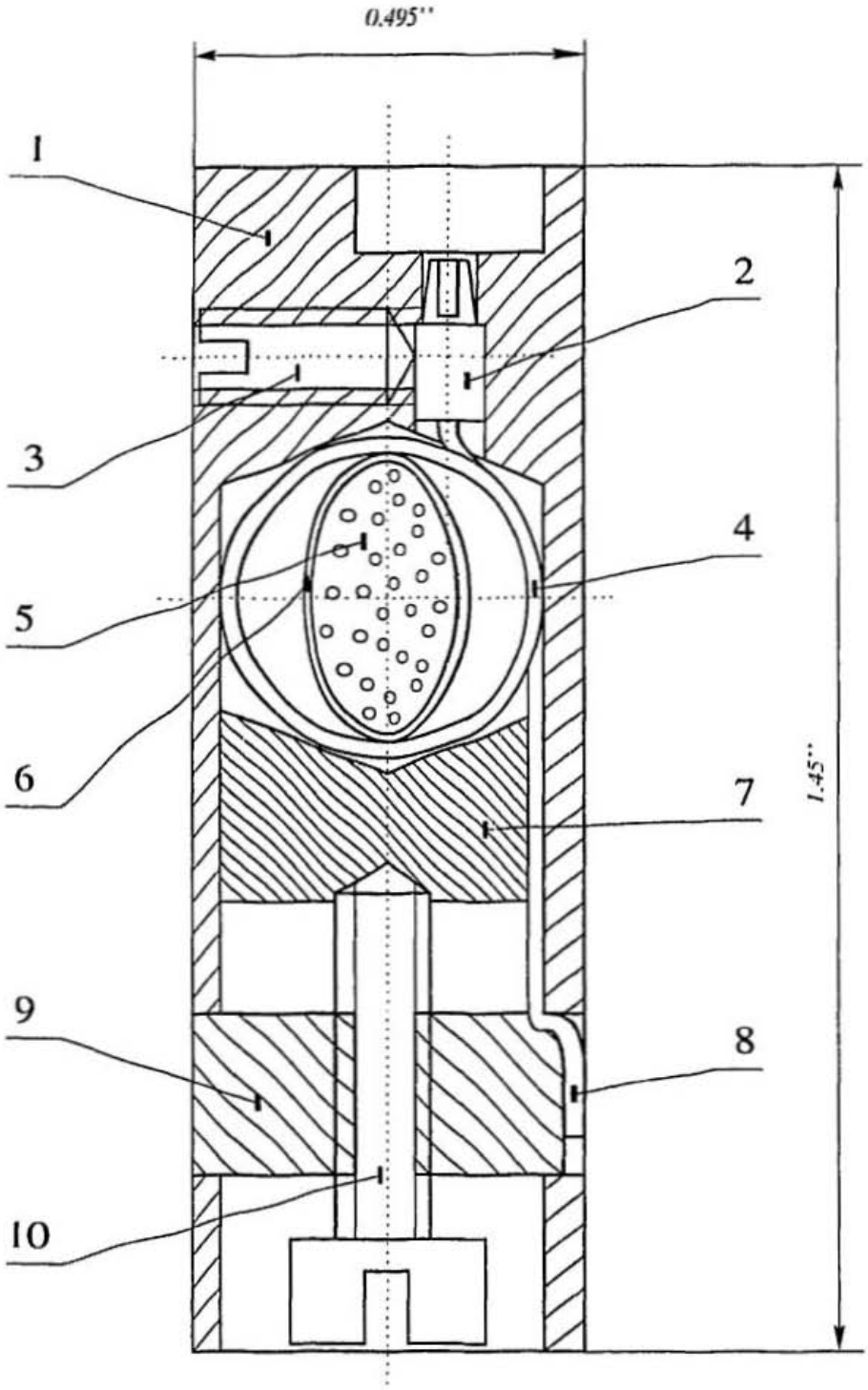

Figure 3.3: Coil and sample holder.

of Hsiao et al. [131]. Specific α-labeling of lauric acid was obtained by exchange with KOD at 200°C in excess HDO. The final products were purified on a 1.5 m Sephadex LH-20 (Pharmacia Biotech, Baie d'Urfé, PQ) liquid chromatography column and eluted with 100% ethanol redistilled before use. The purity of the lipids was checked with thin-layer chromatography. All were found to migrate as single spots. Headgroup deuterated DMPC-d_4 and DPPC-d_{13} were purchased from Avanti Polar Lipids (Alabaster, AL). Cholesterol was obtained from Sigma Chemical Co. (St. Louis, MO).

Phosphatidylcholine-cholesterol mixtures were obtained by dissolving both lipids in chloroform. The solvent was subsequently removed under a stream of dry nitrogen, followed by 6-8 hours vacuum dessication.

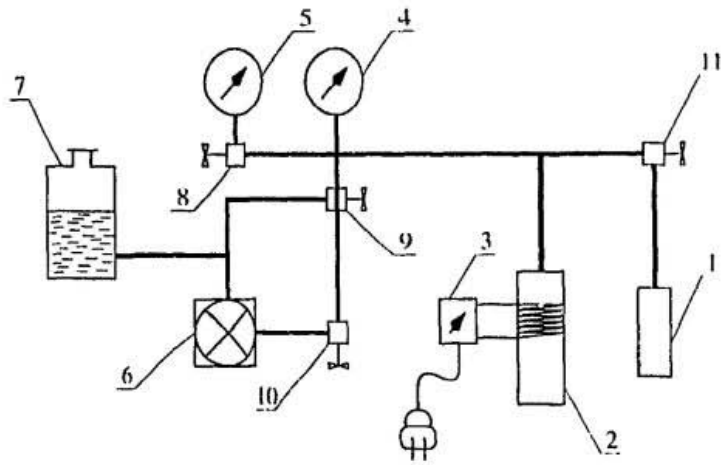

Figure 3.4: Schematic diagram of the high pressure equipment.

Before hydration all lipids were vacuum-dried for 5-8 hours. Hydration was done in excess 0.1 M phosphate buffer (pH 7.2) for DMPC and DPPC and to approximately 110 water molecules per DLPC molecule. To obtain multilamellar vesicles (MLV) the samples were stirred thoroughly with a fine glass rod above the main transition. After preparation the MLV suspensions were transferred into a

flexible polyethylene tube and heat-sealed.

Chapter 4

Pressure Effects on the Main Transition - DMPC.

The work described in this chapter was initially motivated by a systematic study of the chain length dependence of the discontinuity of properties like bilayer thickness and area per lipid at the main transition [22]. Of all saturated diacyl PC's with an even number of chain carbons, DMPC is the shortest chain length lipid that still displays a phase change from liquid crystal to gel under ambient conditions. The discontinuity in the area per lipid in DMPC is also the smallest in the homologous series.

The question initially addressed in this work was: In what way does pressure affect the discontinuity in the mean orientational order parameter across the transition?

For the study of pressure effects on the main transition, DMPC is an appropriate choice for other reasons. This lipid displays all essential features of the longer chain homologs and the temperature ranges of the phases of interest are easily accessible both at low and high pressure. The phase behaviour of DMPC at high pressure is also much simpler than, for example, that of DPPC (chapter 7 offers a detailed description of the phase behaviour of DPPC).

The main transition in diacylphospholipids is generally considered to be of first order [1, 20, 21, 132], although some properties inherent to a second order transition, have also been reported. Some of the first order features include a finite change in the transition enthalpy with an associated sharp peak in the heat capacity and

discontinuous changes in bilayer volume, bilayer area per lipid molecule, etc. Characteristics, typical of a second order transition include, for example, rather broad peaks or depressions, on the order of 10-20°C wide, in some fluorescence constants [133] and ultrasonic velocities [134]. The bilayer main transition has been thought of as occurring close to a critical point and the broad temperature features observed have been attributed to the presence of thermodynamic fluctuations. The magnitude of these fluctuations increases as the transition is approached [22, 24-26, 135-138]. For a thermodynamic system undergoing a first order transition close to a critical point, the two minima in the free energy, corresponding to the stable states at or close to the transition, are rather broad and the transition can be referred to as being "weakly first order". A large change in the order parameter corresponds to a relatively small energy change. This permits the magnitude of the fluctuations in such states to grow exponentially and essentially to reach macroscopic dimensions [139-142].

In this chapter, the main transition in DMPC is studied it is taken from the liquid crystal to gel phase by lowering the temperature at constant pressure, and when it is taken from the gel to liquid crystalline phase by reducing pressure at constant temperature. The first spectral moments of chain-perdeuterated DMPC are recorded as the relevant thermodynamic quantity is varied. Relating M_1 to the chain extension allows the bilayer area per lipid molecule to be approximated in the vicinity of the transition. The data in the variable temperature case are also analyzed in terms of a phenomenological model, developed by Morrow and coworkers [22]. The variations of M_1 are followed along paths in M_1/temperature/pressure space and a sketch of the behaviour of DMPC in this space is proposed. In terms of acyl chain order, the first order nature of the main transition is viewed as being

enhanced by both elevated temperature and pressure. In other words, high pressure and temperature suppress thermodynamic fluctuations and the main transition in DMPC occurs closer to a critical point at ambient conditions than at elevated pressure and temperature.

DMPC-d_{54} samples were prepared in the form of MLV, as described in Chapter 3. In the ^{2}H NMR experiments a standard quadrupole echo technique was used. The $\pi/2$ pulse duration was 2.85 μs at 1.6 kbar and 2.9 μs at ambient pressure. The quadrupole echo pulse separation was 40 μs. Each spectrum was obtained by averaging between 4000 and 6000 transients in the liquid crystalline and the gel phase respectively. The effective dwell time used for data acquisition was 1 μs in the liquid crystalline and 2 μs in the gel phase.

4.1 Constant pressure results (isobaric thermal expansion)

At ambient pressure, a liposome suspension of DMPC in excess water (above 40 wt. %) is in the L_α phase above 22-24°C and in $P_{\beta'}$ below this temperature [11]. A lower transition temperature of approximately 19.5°C is observed in perdeuterated DMPC in excellent agreement with previous measurements [22]. The depression in transition temperature has been attributed to isotope substitution [20, 22].

Figure 4.1(a) shows DMPC-d_{54} spectra as temperature is varied at ambient pressure and at 1.6 kbar. The corresponding values of M_4 are shown in Figure 4.2. The main transition is seen by deuterium NMR as a change in the spectral lineshapes from a superposition of powder lines in the liquid crystalline phase to a broader line profile in the gel, where the contributions from the individual deuterons are indistinguishable. It is also observed as a discontinuous increase in the first spectral moments from liquid crystal to gel. When DMPC is compressed to 1.6 kbar, the transition temperature is elevated to approximately 49.5°C. The pressure coefficient

of the main transition temperature, determined this way, is about 20°C per kbar and is in accord with previous measurements [6, 52, 54, 87, 90].

Figure 4.2 shows the first spectral moments for DMPC-d_{54} as a function of temperature at ambient pressure and at 1.6 kbar. As discussed earlier, the discontinuity in M_1, seen at the main transition, occurs at higher temperature when pressure is raised. In addition to shifting the transition temperature, hydrostatic pressure produces an increase in the discontinuity of the first moment across the transition. At high pressure the gel phase is seen to persist to lower values of M_1, which suggests that pressure has a stabilizing effect on this phase. The M_1 values in the liquid crystalline phase, just above the main transition, are lower at elevated pressure. Therefore, at elevated pressure, the liquid crystalline phase of DMPC accommodates less chain order than at ambient pressure. An indication of the decreased effect of temperature on the liquid crystalline bilayer at high pressure is the lower rate of change in M_1 with temperature at the same relative temperature $T_r = T - T_m$, where T_m is the main transition temperature.

Application of hydrostatic pressure reduces the order parameter at the midpoint of the transition, suggesting that pressure favours the formation of gel phase over the liquid crystal at the same degree of chain order.

A linear relationship exists between the mean orientational order parameter in the liquid crystalline phase and the average extension of the acyl chains $\langle l \rangle$ along the molecular long axis. Following Seelig and Seelig [15] and Schindler and Seelig [143], Morrow, Whitehead and Lu [22] express the average methylene segment axial extension as

$$\langle l \rangle = 1.25\text{Å} \left(\frac{1}{2} + \frac{\sqrt{3}}{\pi \ 167 \ \text{kHz}} M_1 \right) \tag{4.1}$$

where 167 kHz is the deuterium coupling constant. The average acyl chain length per segment, calculated in this way, is shown as a function of temperature for DMPC at

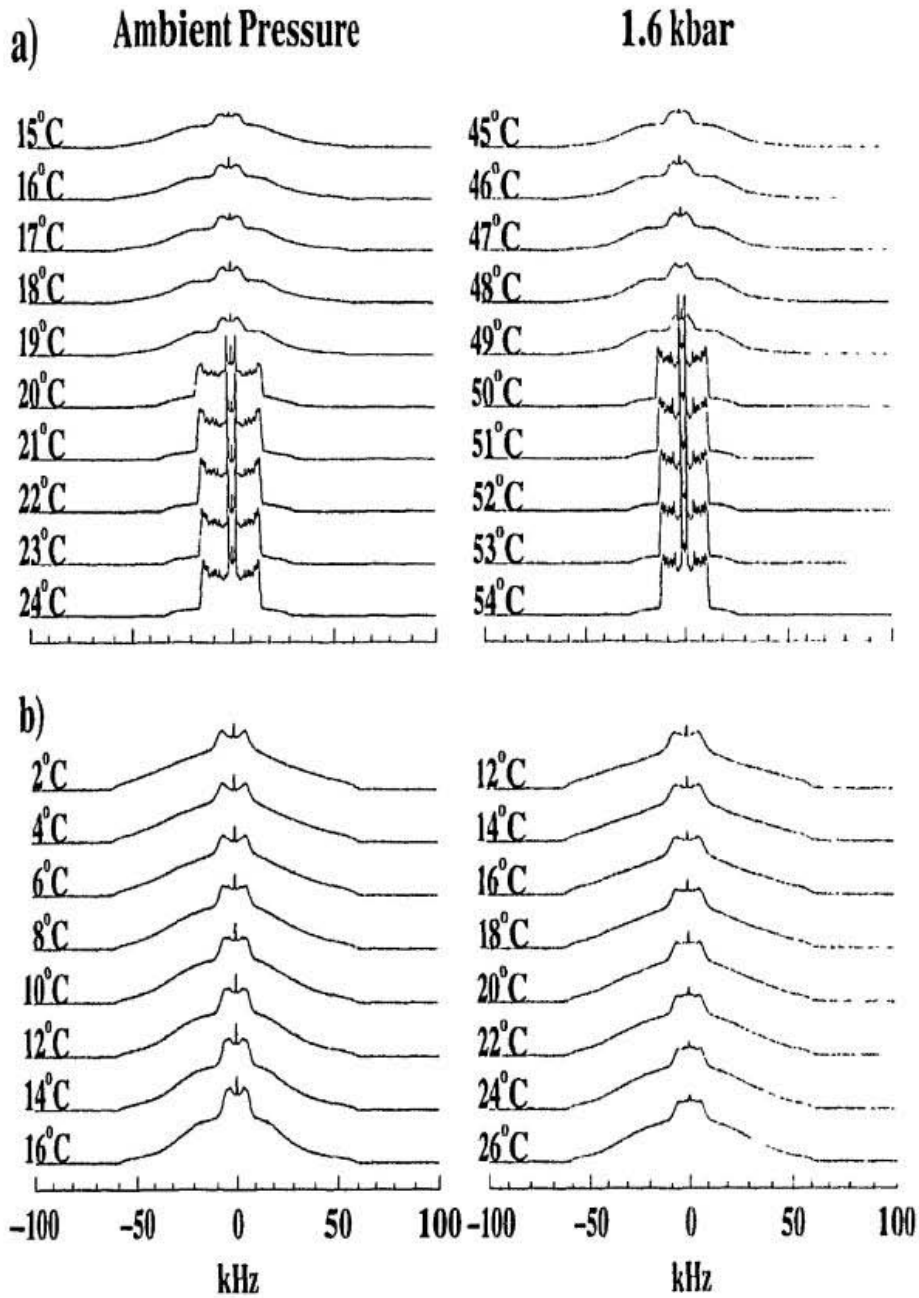

Figure 4.1: DMPC-d_{54} spectra around the main transition (a) and around the sub-transition (b) at ambient pressure (left) and at 1.6 kbar (right).

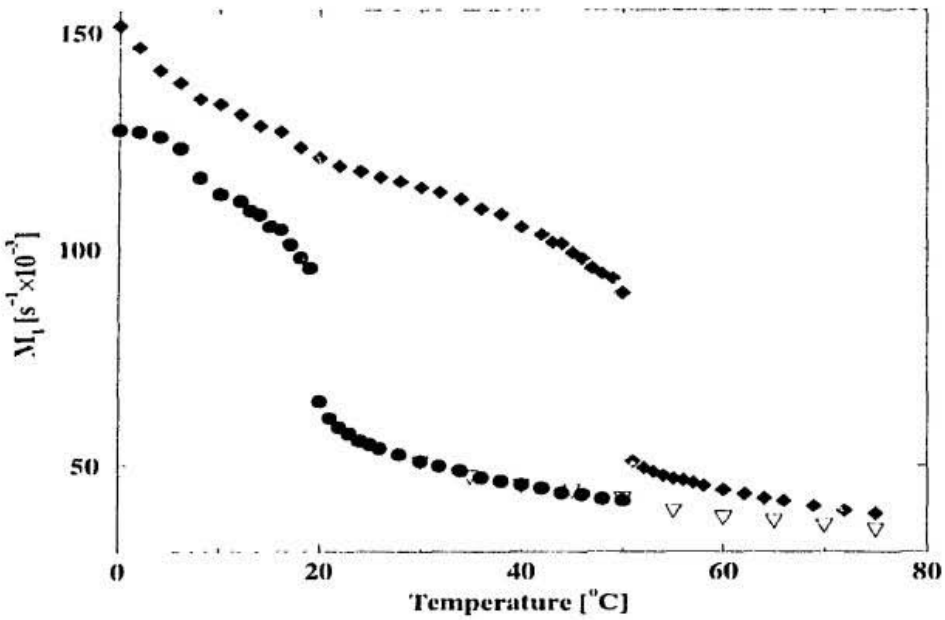

Figure 4.2: DMPC-d_{54} first moments vs. temperature at ambient pressure (circles) and at 1.6 kbar (diamonds). The inverted triangles show a second experiment at ambient pressure.

ambient pressure and at 1.6 kbar in Figure 4.3. The above expression has also been extended to the first moment results in the gel phase although a rigorous theoretical justification is presently lacking. It should be noted, though, that Morrow and coworkers [22] showed that the behaviour of $\langle l \rangle$, as seen by ^{2}H NMR, is consistent with the X-ray diffraction results [11, 144] for the change in bilayer thickness at the transition and in the gel phase.

As the temperature is lowered in the liquid crystalline phase, the average chain order, and thus the chain extension, increases both at ambient and elevated pressure. The strong anisotropy of the bilayer is manifested here in the isobaric increase in bilayer thickness with decreasing temperature. This is consistent with earlier

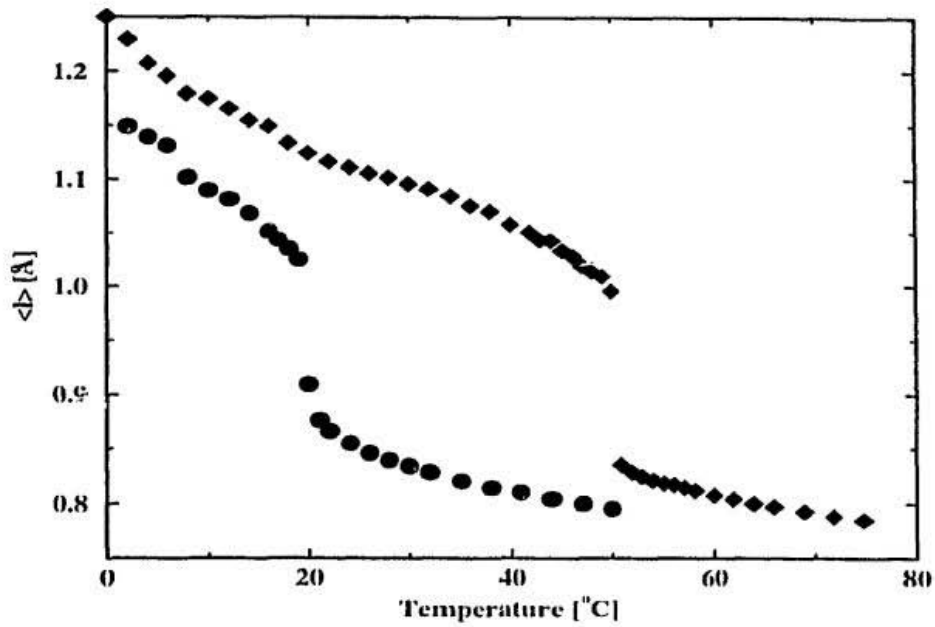

Figure 4.3: DMPC-d_{54} average chain extension per methylene vs. temperature at ambient pressure (circles) and at 1.6 kbar (diamonds).

neutron scattering measurements [90]. The response of average chain length to temperature at the same relative temperature T_r is weaker at high pressure, reflecting the decreased ability of the bilayer order to respond to changes in temperature. The transition occurs at low pressure when the acyl chains extend to over 0.87 Å per segment in the liquid crystalline phase. At high pressure the transition on cooling occurs when the liquid crystal chain extension is about 0.84 Å per methylene. This decrease in the maximum chain order in the liquid crystalline phase possibly reflects the reduced effect of fluctuations on the liquid crystalline phase at high pressure.

First spectral moments can also be used to obtain information on the changes in bilayer area per lipid molecule. Since the response of the volume of the bilayer to temperature is about two orders of magnitude weaker than that of the area per lipid

molecule in the bilayer [1, 113], the change in the bilayer volume with temperature away from the transition can be neglected as far as its effect on area per lipid is concerned (the volume change across the main transition is about 4% [145]). If the bilayer volume can thus be considered constant away from the transition, the inverse of the mean methylene extension $\langle l \rangle^{-1}$ is proportional to the average area per lipid molecule. The temperature dependence of $\langle l \rangle^{-1}$ is shown in Figure 4.4.

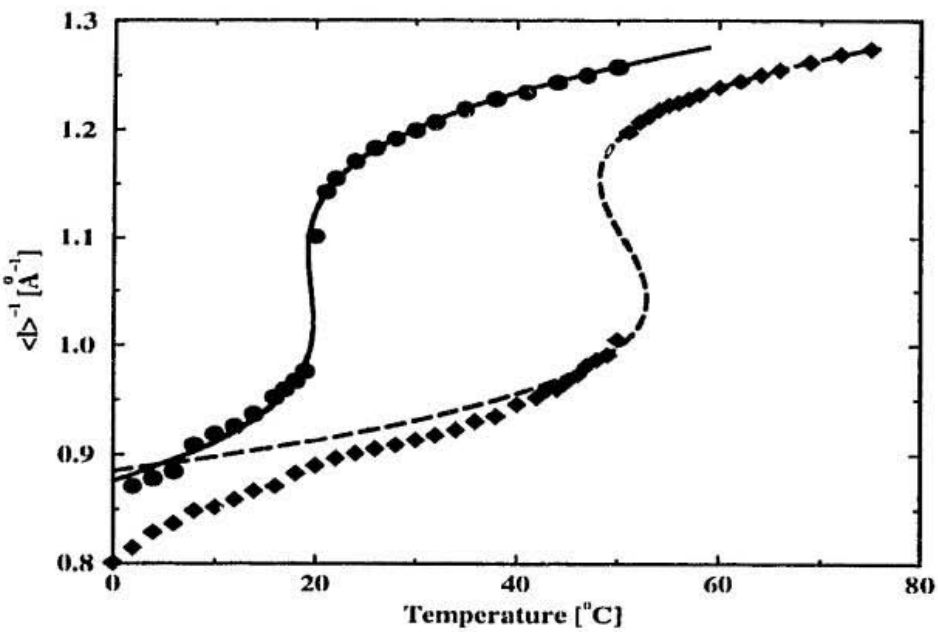

Figure 4.4: DMPC-d_{54} inverse methylene extension vs. temperature at ambient pressure (circles) and at 1.6 kbar (diamonds). The solid line is the model equation of state for s_+=0.03030 and T_+ = 19.25°C at ambient pressure (see section 4.4). The dashed line is the model equation of state for s_+=0.05065 and T_+ = 48.27°C at 1.6 kbar.

Pressure and temperature have different effects on the phospholipid bilayer. In Figure 4.1(a), the acyl chain order just above the transition can be compared at ambient pressure and at 1.6 kbar. The NMR spectrum at ambient pressure and

20°C, which is right above the main transition, has a pronounced unresolved group of lines at approximately the maximum splitting. This suggests that close to the main transition, the DMPC methylene orientational order is relatively constant along the acyl chains for carbons close to the glycerol backbone. When the pressure is increased to 1.6 kbar, DMPC enters the liquid crystalline phase at 50°C and the spectral lines corresponding to various methylene groups along the acyl chains appear well resolved. This reflects a relatively uniform variation of the methylene order with chain position.

At ambient pressure, DMPC undergoes another transition at about 7°C, to the L_c phase. This transition (the subtransition) is seen as a change in the methyl lineshapes (the spectral features narrower than 10 kHz in Figure 4.1(b)), a decrease in the intensity around ±20 kHz and by a small stepwise increase in M_1 with decreasing temperature (Figure 4.2).

Application of 1.6 kbar elevates the subtransition temperature to about 20°C implying a subtransition pressure coefficient for this temperature of approximately 8°C per kbar. This value is smaller than that for the main transition temperature, probably due to the higher chain order and hence lower compressibility of the bilayer at low temperatures.

4.2 Constant temperature results (isothermal compression)

When heated above the ambient pressure main transition temperature and then compressed isothermally, DMPC undergoes a transition from the liquid crystalline into a more ordered phase. Figure 4.5 shows selected deuterium NMR spectra around the pressure-induced main transition for 25, 35 and 45°C. From the deuterium NMR perspective, this higher order phase (Figure 4.5, top spectra) is identical with the low temperature gel phase observed at ambient pressure (Figure 4.1(a),

top spectra). Some spectra at the transition appear to be a superposition of liquid crystalline and gel spectra, which most probably reflects the fact that the studied system is actually an ensemble of smaller systems, namely the individual liposomes. Minor variations in vesicle size, lipid composition and hydration may result in slightly different transition pressures for the individual liposomes. In this sense, the measured transition pressure is an average over a very large number of subsystems (typically about 10^{11}). The fact that these mixed spectra are not seen in the temperature experiment is partly due to the temperature width of the main transition being slightly smaller than the one degree steps used, while the effectively smaller pressure steps are probably comparable to the main transition width in pressure.

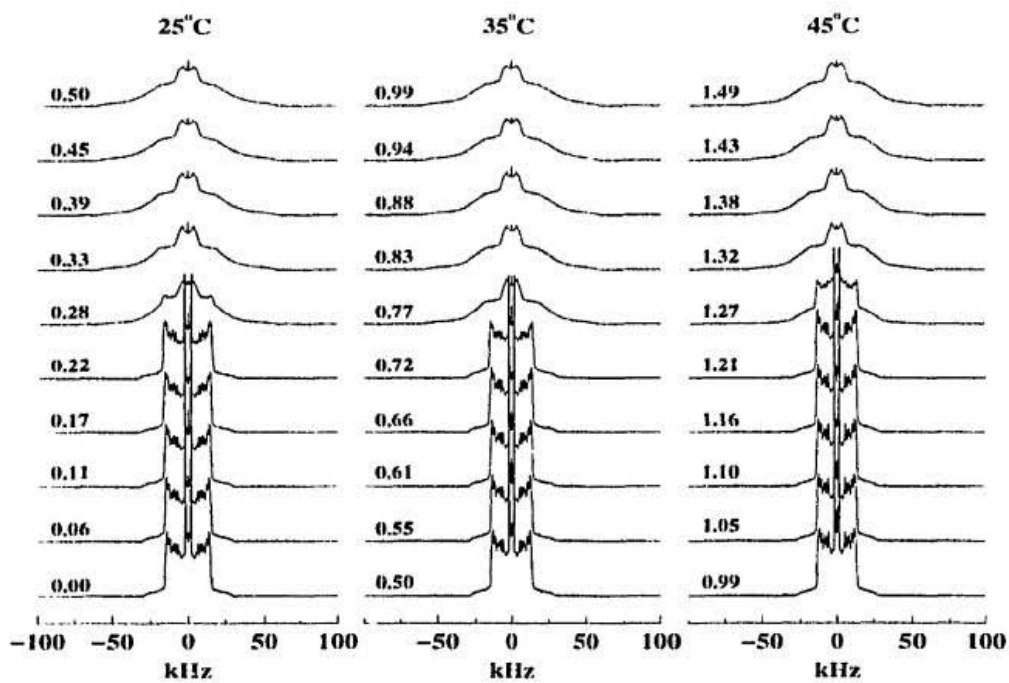

Figure 4.5: DMPC-d_{54} spectra at constant temperature for 25°C, 35°C and 45°C. Pressure in kbar is shown next to each spectrum.

Figure 4.6 shows DMPC-d_{54} M_1 as a function of pressure at 25, 35 and 45°C. For each temperature the main transition is seen as a discontinuous change in M_1. As the temperature is increased, the size of this change increases. M_1 is proportional to the mean acyl chain order in the liquid crystalline phase and, to a certain extent, reflects the mean molecular order in the gel phase. As the temperature is increased from 25 to 45°C, the order parameter at the center of the transition is observed to decrease slightly. This indicates that, at higher temperature, the formation of a gel phase is favoured over the liquid crystalline phase at the same degree of orientational order.

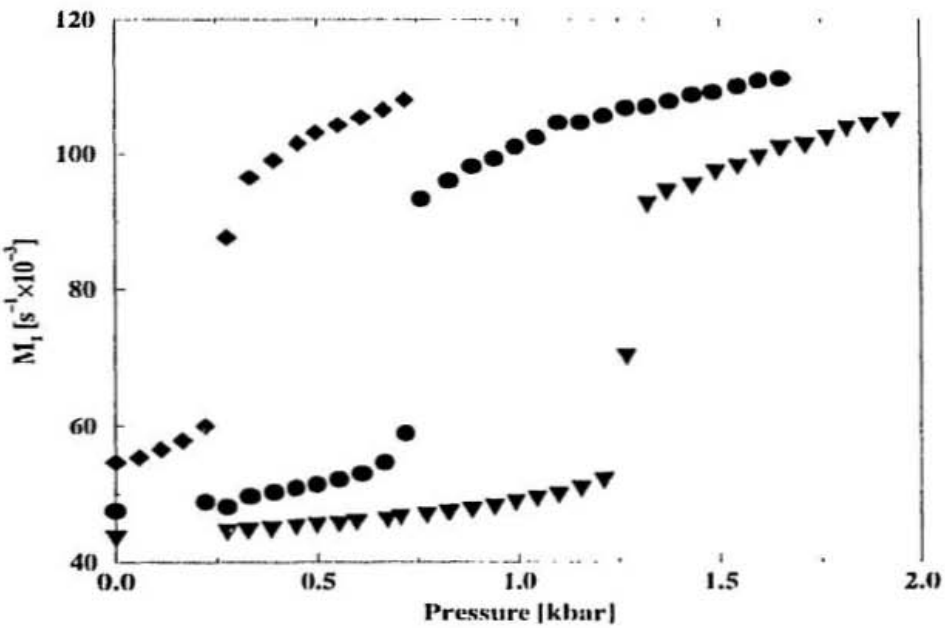

Figure 4.6: DMPC-d_{54} first spectral moments vs. pressure at 25°C (diamonds), 35°C (circles) and 45°C (inverted triangles).

At 25°C, M_1 below the transition appears to be changing faster with pressure than at 45°C. The increase in the M_1 discontinuity across the main transition with

temperature and the weaker dependence of M_1 on pressure in the liquid crystalline phase near the higher temperature transition suggest that, at lower temperature, liquid crystal DMPC can accommodate larger scale fluctuations, so that the main transition is of a "weaker first order" nature and closer to a critical point than at higher temperature.

In the liquid crystalline phase, the results for the M_1 curvature can be interpreted in terms of the mean axial chain extension per methylene group. Figure 4.7 shows mean extension per segment calculated by applying Equation 4.1 to both the liquid crystal and gel M_1 values of Figure 4.6. The apparent thickness of the hydrophobic region of the bilayer, calculated this way, increases with pressure for all the temperatures. A pressure-induced increase in the bilayer thickness has been experimentally observed by small angle neutron scattering [90, 19] and has been theoretically described (M.D. Whitmore, private communication). The increase in $\langle l \rangle$ and M_1 with pressure is smaller at 45°C than at lower temperature indicating a decrease in the axial compressibility of the DMPC bilayer with temperature.

The inverse of the axial chain length per methylene $\langle l \rangle^{-1}$ is shown in Figure 4.8 as a function of applied pressure for three different temperatures. Since the isothermal volume compressibility of the bilayer is much smaller than the isothermal area compressibility [1, 113], the volume changes can be neglected in comparison with the changes in area and $\langle l \rangle^{-1}$ can be considered to be proportional to the area per lipid molecule.

A closer look at the spectral changes in the liquid crystalline phase provides some useful information about the order of the acyl chains. In the liquid crystalline phase, for example, the spectra corresponding to pressures immediately below the main transition for the three temperatures studied (Figure 4.5) can be compared.

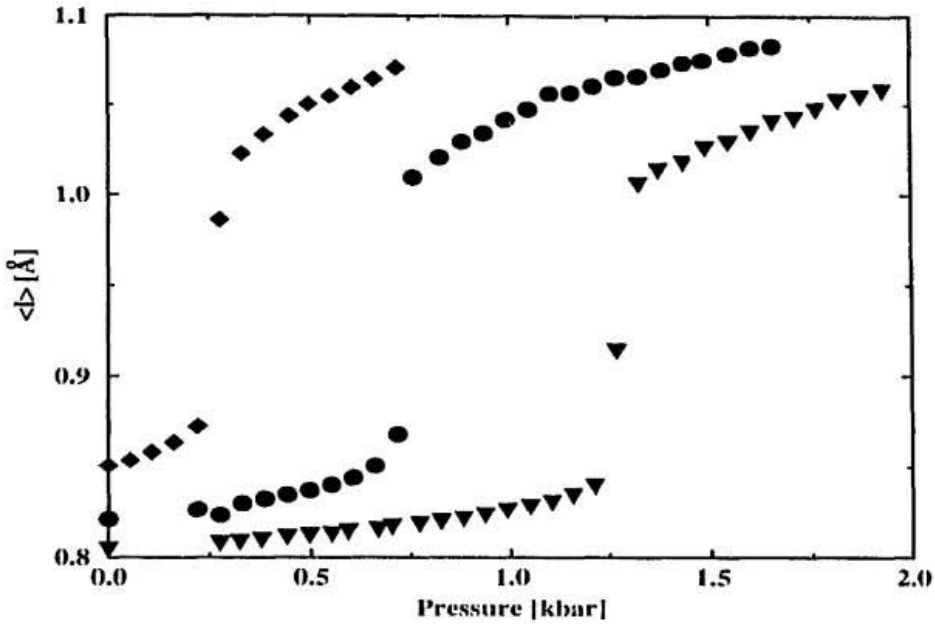

Figure 4.7: DMPC-d_{54} average chain extension per methylene vs. pressure at 25°C (diamonds), 35°C (circles) and 45°C (inverted triangles).

The spectrum at 25°C and 0.22 kbar reveals an unresolved group of lines at approximately maximum splitting. Such a grouping suggests that the order parameter of the methylene groups close to the glycerol backbone depends little on the carbon position along the acyl chains. In comparison the spectrum at 45°C and 1.21 kbar has a relatively uniform distribution of methylene deuteron splittings over the whole plateau region.

4.3 DMPC M_1 in the pressure and temperature space

The results from both isothermal and isobaric measurements of M_1 are shown together in Figure 4.9 as a function of pressure and temperature. The discontinuity in

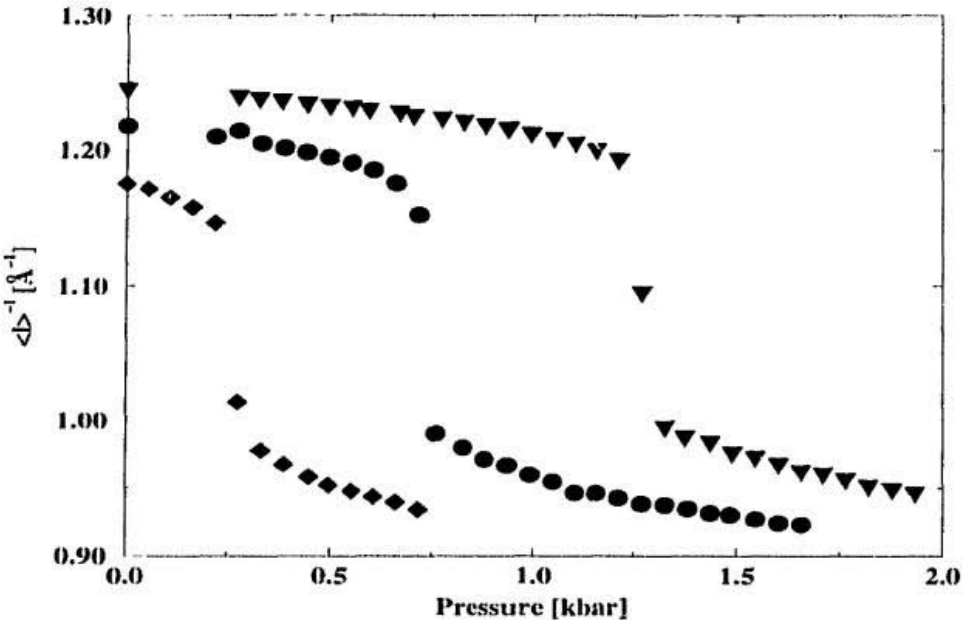

Figure 4.8: DMPC-d_{54} inverse chain extension per methylene vs. pressure at 25°C (diamonds), 35°C (circles) and 45°C (inverted triangles).

M_1 across the main transition is seen to increase with both pressure and temperature. The differences between the liquid crystalline and the gel phases are enhanced and the main transition becomes better pronounced, or "more first order", at both higher pressure for isobaric experiments and higher temperature for isothermal experiments. Figure 4.9 also suggests that the differences between the liquid crystal and the gel should vanish at low temperature and some hypothetical negative pressure. Therefore the first order character of the phase transition between L_α and $L_{\beta'}$ phases in hydrated DMPC cannot be removed by hydrostatic compression. The system appears to approach a critical point from "above" in hydrostatic pressure and temperature space.

It is interesting to note that, in some ways, hydrostatic pressure affects the bilayer

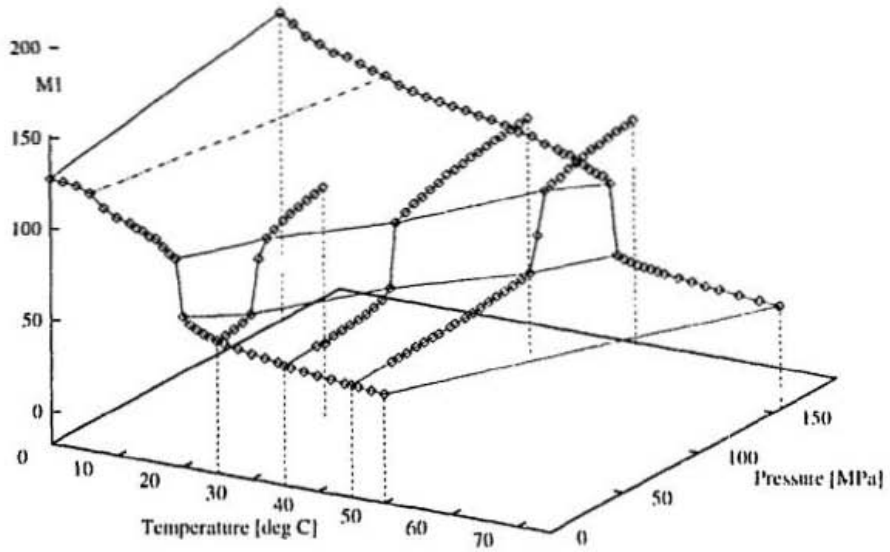

Figure 4.9: DMPC-d_{54} M_1 vs. pressure and temperature. M_1 is shown in $s^{-1} \times 10^{-3}$; diamonds represent experimental points at ambient pressure and 1.6 kbar, and at 25°C, 35°C and 45°C. Solid lines are an extrapolation at the main transition and at the borders of the experimental region. The dash-dotted line shows the subtransition.

in a way similar to an effective chain length increase. For example, the application of pressure elevates the transition temperature of the DMPC suspension to a value which matches the transition temperature for the homologous lipid with chains two methylenes longer (DPPC). The change in the orientational order parameter across the main transition in DPPC is larger than that in DMPC [22]. Pressure is observed to increase the M_1 discontinuity at DMPC transition as well. Also, the curvature in M_1 versus temperature in the immediate vicinity of the main transition is smaller in DPPC than in DMPC and is lowered by pressure in DMPC. Briefly, as Morrow and coworkers point out [22] for ambient pressure, DMPC undergoes a phase change

closer to a critical point than does DPPC. Hydrostatic pressure produces changes in DMPC which correspond to an increase in separation between the transition and the critical point. In this sense, compressed DMPC approaches the state of ambient pressure DPPC.

Figure 4.9 also gives an indication of the trend in the pressure behaviour of the subtransition temperature. The dash-dotted line indicates the appearance of some L_c phase as the pressure is elevated from 0 to 1.6 kbar. The subtransition temperature is determined by the little step, observed in M_1 temperature dependence and by the spectral changes occurring at the same temperatures. The pressure coefficient of the subtransition is obviously different from that of the main transition. In the case of DLPC the different dependence of various transition temperatures to pressure results in separation of the liquid crystalline phase (or its modified region L_x [36]) and the crystalline phase, as discussed later in chapter 5.

4.4 Modeling of the transition

A number of statistical mechanical models have been developed to discuss the phenomena associated with the transition from liquid crystalline to gel phase in phospholipids. Both microscopic [25, 138, 146, 147] and phenomenological [22, 24, 26, 135-137, 148] approaches have been used to address changes in membrane compressibility, ion permeability, elasticity, etc.

A Landau-type phenomenological model, [22, 137], can be used for comparison of DMPC temperature behaviour at ambient and elevated pressure. The model is based on a free energy expansion in terms of area per lipid in the vicinity of the main transition. All terms in the expansion higher than the fourth order term, have been discarded. The remaining leading terms have been shown to describe adequately all essential features of the bilayer main transition [22, 26, 137]. In

principle, the gel and liquid crystal coexistence temperature, T_m, can be changed by varying some environmental parameters, such as the membrane composition [137], its ionic environment [24], etc., in such a way that the discontinuity in the physical properties of the bilayer at the main transition vanishes at some temperature T_c. Beyond this temperature the bilayer is in a single phase.

An order parameter can be defined as [22]

$$s = \frac{\langle l \rangle^{-1} - \langle l_c \rangle^{-1}}{\langle l_c \rangle^{-1}}. \tag{4.2}$$

Here $\langle l_c \rangle^{-1}$ is the inverse of the average methylene extension at $T = T_c$. It is identified as the value of $\langle l \rangle^{-1}$ at the midpoint of the transition. The order parameter is positive and increasing with temperature in the liquid crystalline phase, following the temperature behaviour of the area per lipid molecule, as shown in Figure 4.10. The expression for the free energy in terms of powers of this order parameter is [22]

$$G = G_0 \left[\frac{s^4}{4} + \alpha(T - T_c)\frac{s^2}{2} + \beta(T_m - T)s \right], \tag{4.3}$$

where $\beta > 0$ and $\alpha > 0$. G_0 is a constant giving the overall scale of the free energy.

For the lipid to be in equilibrium, the free energy must have a minimum, hence an equation of state can be obtained by minimizing the free energy to give

$$\frac{dG}{ds} = G_0[s^3 + \alpha(T - T_c)s + \beta(T_m - T)] = 0. \tag{4.4}$$

The points (T_+, s_+) and (T_-, s_-), defined as the extrema of the equation of state (Equation 4.4), are the spinodals. Assuming $|T_\pm - T| \ll |T_c - T_m|$, their location can be determined by an iterative procedure which begins with obtaining an initial estimate of $\langle l_c \rangle^{-1} = (\langle l_l \rangle^{-1} + \langle l_g \rangle^{-1})/2$, the inverse methylene extension midway across the transition, and of

$$s_\pm \approx \pm \frac{\Delta}{\sqrt{12}}, \tag{4.5}$$

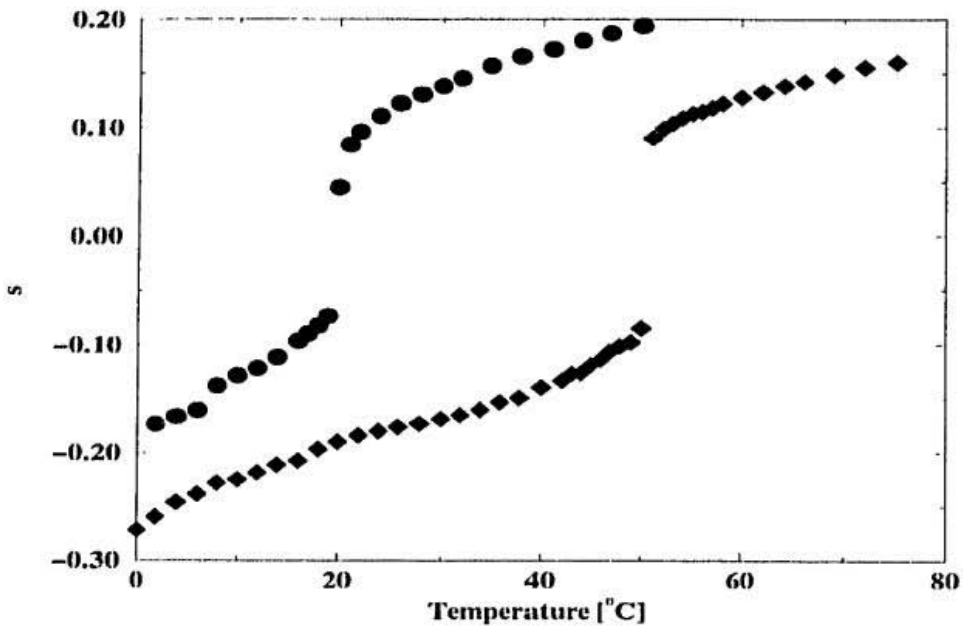

Figure 4.10: DMPC-d_{54} order parameter $s = (\langle l \rangle^{-1} - \langle l_c \rangle^{-1})/\langle l_c \rangle^{-1}$ vs. temperature at ambient pressure (circles) and 1.6 kbar (diamonds).

where $\Delta = s_l - s_g$ is the change in order parameter across the main transition. The values initially determined in this way are then used for fitting the data from Figure 4.10. The equation of state can be rewritten in the form [22]

$$T = T_+ + \frac{(T_m + T_+)}{2}\left[3\left(\frac{\delta}{s_+}\right)^2 + \left(\frac{\delta}{s_+}\right)^3\right], \tag{4.6}$$

where $\delta = s - s_+$. The temperature is first plotted versus $[3(\delta/s_+)^2 + (\delta/s_+)^3]$. In these coordinates the experimental points fit on a straight line. Then s_+ is adjusted and re-entered in the coordinate transformation, Equation 4.6, until the values of T_+ determined from the slope and the intercept agree.

The temperature, plotted versus $[3(\delta/s_+)^2 + (\delta/s_+)^3]$, is shown in Figure 4.11. The final values for s_+ and $\langle l_c \rangle^{-1}$ can be used for determination of the parameters

in the equation of state. The solid lines in Figure 4.4 are the equations of state for ambient pressure and 1.5 kbar, obtained for $s_+ = 0.03030$ and $\langle l_c \rangle^{-1} = 1.053$ Å^{-1}, and $s_+ = 0.05065$ and $\langle l_c \rangle^{-1} = 1.098$ Å^{-1}, respectively. The spinodal temperatures, T_+, in these cases are 19.25°C and 48.27°C for transition temperatures T_m of 19.5°C and 50.5°C. Once s_+ and T_m are determined, the parameter β, which is related to the curvature of s vs. T near the spinodal, can be calculated from [22]

$$\beta = \frac{2s_\pm^3}{(T_m - T_\pm)}. \tag{4.7}$$

The values of β for ambient pressure and 1.5 kbar are 2.23 and 1.17 respectively. The lower value at high pressure indicates a higher curvature at the spinodal and reflects the reduced lateral compressibility of the bilayer at 1.5 kbar. A summary of the parameters, determined by means of the model of Morrow, Whitehead and Lu [22], is presented in table 4.1.

	0 kbar	1.6 kbar
T_m(°C)	19.5	50.5
$\langle l_c \rangle^{-1}$(Å^{-1})	1.053	1.098
$\langle l_+ \rangle^{-1}$(Å^{-1})	1.085	1.154
T_+(°C)	19.3	48.3
$(T_m - T_+)$(°C)	0.2	2.2
$\beta \times 10^4$(°C^{-1})	2.23	1.17
$\Delta\langle l \rangle^{-1}$(Å^{-1})	0.111	0.193
$\Delta\langle l \rangle$(Å)	0.100	0.161

Table 4.1: Some thermodynamic and phenomenological parameters for DMPC at ambient pressure and 1.5 kbar.

Strictly speaking the procedure described above is justified for the liquid crystalline phase only. The results of Morrow, Whitehead and Lu [22], though, show that fits, obtained using data from the liquid crystalline phase can be extrapolated successfully to the gel phase of DMPC over a relatively broad temperature interval vicinity of the transition. This leads to the conclusion that the bilayer phase behaviour in the vicinity of the main transition is largely dominated by thermodynamic

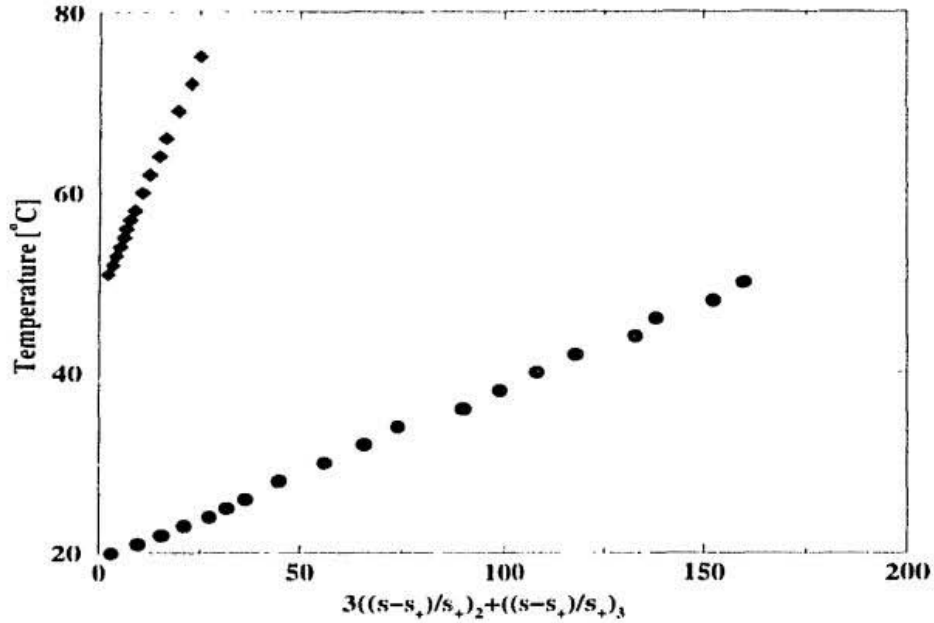

Figure 4.11: Temperature versus $3((s-s_+)/s_+)^2+((s-s_+)/s_+)^3$ at ambient pressure (circles) and 1.6 kbar (diamonds).

fluctuations [26, 134], both in the fluid and in the gel phases. The ambient pressure results for both β and the temperature behaviour of the gel phase, discussed here, agree well with the measurements by Morrow and coworkers [22]. At high pressure, though, the equation of state obtained from the liquid crystalline data does not describe the gel phase well. In determination of $\langle l \rangle^{-1}$, $s_\pm$, and $T_\pm$, an equation of state is sought such that the immediate vicinity of the transition on the gel side is matched, as originally intended in the model. It is clearly seen from Figure 4.4 that there are two equations of state - one for the liquid crystalline and one for the gel phase. The pressure-induced flattening of $s(T)$ in the liquid crystalline phase results in a modeled gel phase branch with smaller temperature expansion coefficient than observed experimentally.

Another manifestation of the fundamental differences between the effects of temperature and pressure on the phospholipid behaviour is the different functional dependence of the order parameter s on pressure. Figure 4.12 shows the order parameter as defined in Equation 4.2. A coordinate transformation of the form $(s/s_+ - 1)^3$ linearises the experimental equations of state for 25, 35 and 45°C. A plot of pressure as a function of $(s/s_+ - 1)^3$ is shown in Figure 4.13. The straight lines suggest a different functional dependence exists between s and pressure than that between s and temperature.

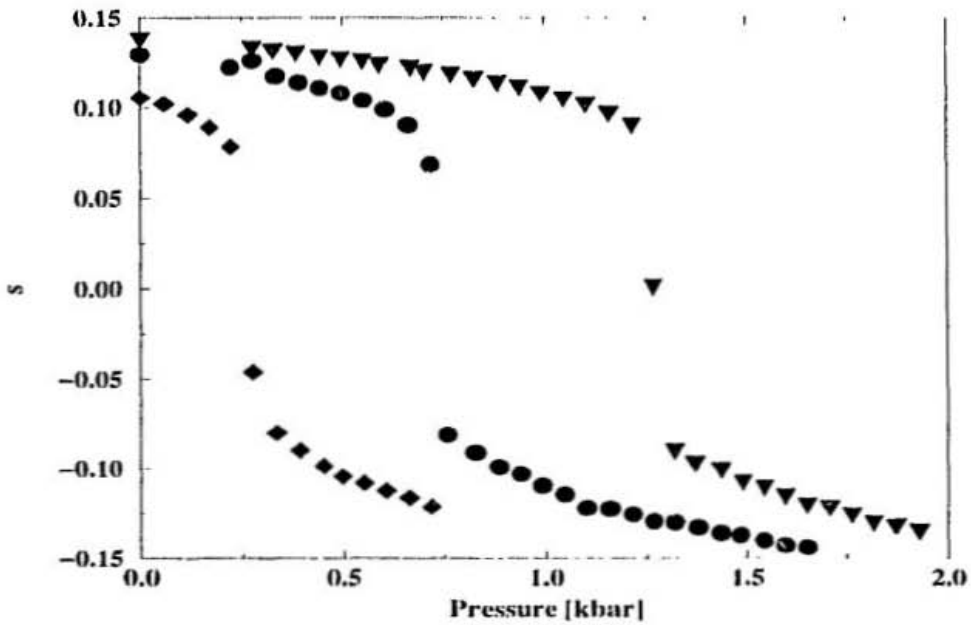

Figure 4.12: DMPC-d_{54} order parameter $s = (\langle l \rangle^{-1} - \langle l_c \rangle^{-1})/\langle l_c \rangle^{-1}$ vs. pressure at 25°C (diamonds), 35°C (circles) and 45°C (inverted triangles).

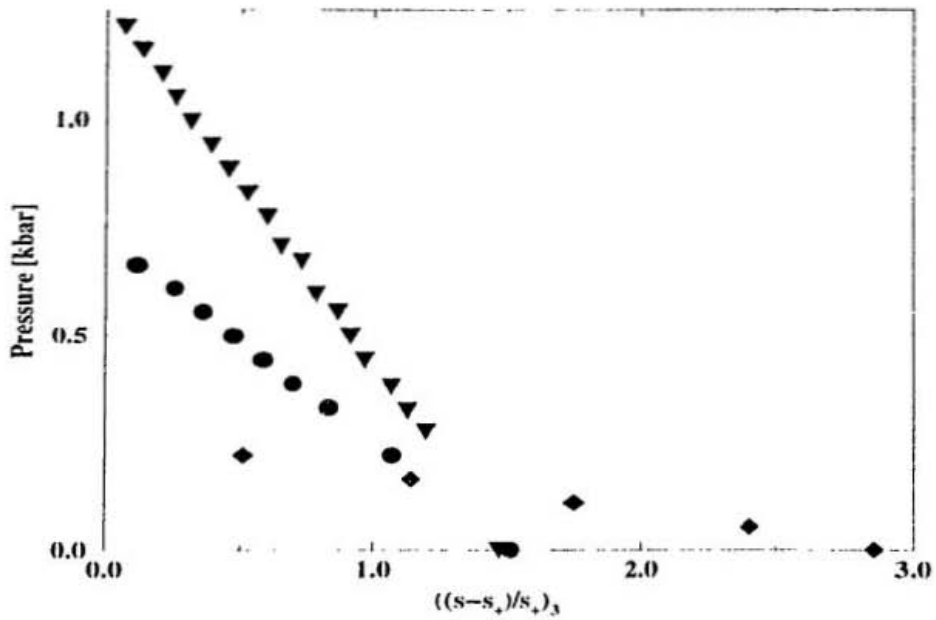

Figure 4.13: Pressure versus $((s - s_+)/s_+)^3$ plot at 25°C (diamonds), 35°C (circles) and 45°C (inverted triangles).

4.5 Summary

The main transition in DMPC-d_{54} was studied by varying temperature at ambient and at elevated pressure and by varying pressure at fixed temperature. When temperature was varied the discontinuity in the first spectral moments was found to increase with pressure. M_1 was used as an indicator of the thickness of the bilayer hydrophobic region and of the inverse of the bilayer area per molecule. The thickness of the membrane hydrophobic region was found to increase as the temperature was decreased. This effect was less pronounced at high pressure. A phenomenological model was also used to compare the ambient and high pressure behaviour of DMPC. The distance between the transition temperature and the spinodal temperature, as determined from the model, was found to increase with pressure. These observations

led to the conclusion that the main transition at ambient pressure occurs closer to a critical point than at elevated pressure.

When pressure was varied at constant temperature the change in orientational order across the transition was found to increase at higher temperature. The thickness of the chain region was found to increase with increasing pressure. This increase was stronger at lower temperatures. It was concluded that the role of thermodynamic fluctuations is diminished by high temperature and that the bilayer phase transition occurs closer to a critical point at lower temperature.

The effects of pressure and temperature on DMPC-d_{54} were compared. The response of the bilayer to compression or heating was found to be weaker at high pressure and temperature than under ambient conditions. Pressure and temperature were concluded to enhance the first order characteristics of the DMPC main transition.

Chapter 5

DLPC - Phase Behaviour and Dynamics

Many physical properties within the family of disaturated diacyl PC's depend on the length of the hydrocarbon chains. In a recent deuterium NMR study, Morrow and coworkers [22] discussed the dependence of the main transition temperature, enthalpy and the discontinuity in the orientational order on the acyl chain length in saturated PC's with 18, 16, 14 and 12 carbons in the chains. A steady decrease in these parameters is reported as the chain length is decreased from 18 to 14 carbons. The 12 carbon homolog (DLPC) does not follow this trend since its main transition is obscured by the intervention of a transition into a more ordered crystalline phase [31, 32]. Calorimetric studies show a broad peak in excess heat capacity, associated with the ambient pressure transition in DLPC. This peak is sometimes resolvable into two steps: a narrow one at lower temperature and a broad, poorly defined higher temperature feature [31, 32, 35, 149]. In deuterium NMR the low temperature feature appears as a large discontinuity in the first spectral moment. The higher temperature feature cannot be clearly identified from the M_1 temperature behaviour. The broad feature in the excess heat capacity has recently been associated with the transition from the usual liquid crystalline phase into an unusual fluid phase labeled L_x [35]. X-ray results indicate a continuous variation of bilayer properties as DLPC enters the L_x phase from the L_α phase [36]. There is no evidence of positional ordering within the bilayer.

In the previous chapter, the effect of hydrostatic pressure on the phospholipid bilayer was shown to be analogous to an effective chain length increase. It is therefore

conceivable that DLPC at elevated pressure may display some phase features typical of a longer chain homolog. In particular, it is possible that the transition from liquid crystal to gel might be separated from the fluid to crystalline transition. If this is the case, an understanding of the crystalline phase stability, relative to the high pressure gel and the $L_{\beta'}$ phase would be of major significance to the interpretation of DLPC's unusual phase behaviour.

A very important question with bearing on the phase behaviour, passive permeability and other properties of the bilayer is the possible effect of thermodynamic fluctuations. This is related to the location of the lipid phase transition with respect to a critical point on the fluid-gel coexistence curve. In this respect DLPC occupies a place of particular interest in the disaturated phosphatidylcholines homologous series. An extrapolation of the transition properties of the longer chain homologs to a chain length of 12 carbons suggests that at the transition to the gel phase, a continuous change in the mean orientational order is to be expected provided such a phase can be observed. On the other hand, as shown in the previous chapter, pressure enhances the first order features of the liquid crystal to gel transition. It is conceivable that DLPC could be brought closer to a critical point by hydrostatic compression.

All experiments were performed on DLPC-d_{46} and DLPC-α-d_4 synthesized as described in Chapter 3. MLV suspensions were prepared by hydrating in phosphate buffer to approximately 110 water molecules per lipid. The $\pi/2$ pulse duration was between 2.5 μs and 3.1 μs. The pulse separation was held at 35 μs, except for the transverse relaxation measurements where it was varied between 20 μs and 600 μs in the disordered phase and between 20 μs and 160 μs for the phases with shorter T_2. Oversampling was used [129], resulting in effective dwell times of 4 μs and 2 μs in the fluid and in the lower temperature phases respectively. In the case of perdeuterated

lipid, 2000 scans were averaged in the disordered phase and up to 6000 in the other phases. For the specifically labeled DLPC, the number of scans was increased to 16000 and 32000 in the corresponding phases.

5.1 Results

5.1.1 DLPC-d_{46} chain order

Perdeuterated DLPC was studied at ambient pressure between 30°C and −13°C and at 1.5 kbar from 50°C to −20°C. Spectra near the phase transition, as well as representative spectra well into each phase region are shown in Figure 5.1. For both pressures, the spectra at high temperatures are typical of a liquid crystalline phase.

As the temperature is lowered below −2°C at ambient pressure, DLPC-d_{46} enters a highly ordered phase in which the lipid molecules appear to be almost completely immobilized. The presence of intensity out to ±63 kHz reflects severe restrictions on the motions of the acyl chains. The spectral contribution from the methyl deuterons appears as a feature with about a third of the maximum splitting. This is typical of fast methyl reorientation about an essentially immobilized three-fold axis. These spectral features are characteristic of the crystalline (L_c) phase.

The spectra just above the L_c phase, namely at 0°C, −1°C and −2°C, indicate axially symmetric reorientation. The spectral intensity, however, decreases more quickly with temperature for doublets with larger splittings than for those with smaller splittings. Such spectral distortion is a result of rapid transverse relaxation of the deuterons close to the glycerol backbone along with a decrease in relaxation rates with position along the acyl chains.

At 1.5 kbar, DLPC-d_{46} is in the liquid crystalline phase above 30°C. At temperatures between 28°C and 23°C, the spectra still reflect axially symmetric molecular

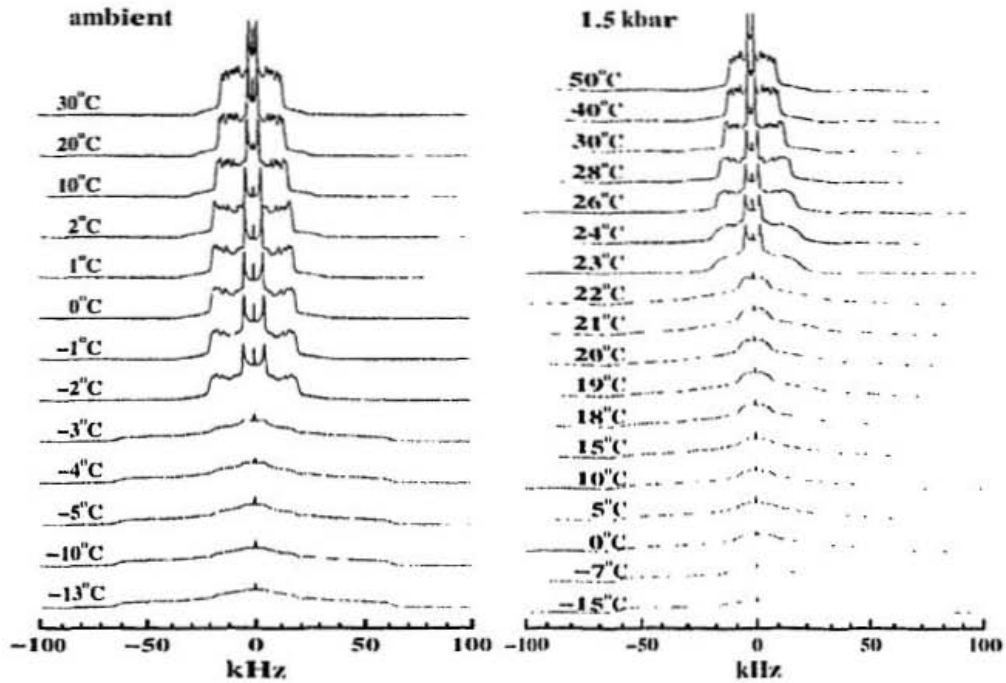

Figure 5.1: DLPC-d_{46} selected spectra at ambient pressure (a) and at 1.5 kbar (b).

motions although they are distorted by a severe intensity decrease at maximum splitting. At 22°C, the axial symmetry of the molecular motions is lost and the spectra become characteristic of a more ordered phase. Between 22°C and 20°C the spectral lineshapes closely resemble the spectra typically observed in the gel phases of longer chain diacyl PC's [88]. A temperature of 19°C marks the onset of a spectral intensity buildup at ±63 kHz as DLPC enters the L_c phase. It is interesting to note that, in contrast to the abrupt transition from a disordered phase into the crystalline phase that occurs at ambient pressure, the phase change from gel to L_c, observed at high pressure, is rather gradual. At elevated pressure and −15°C, essentially all molecular motions have stopped and the spectrum is typical of a diacyl PC crystalline phase.

In the liquid crystalline phase, the first spectral moment of perdeuterated lipids is directly proportional to the average orientational order parameter of the C-D bond [119], as discussed earlier. In the more ordered phases, the axial symmetry of the molecular motions is lost and a deviation from such proportionality is observed. Nevertheless M_1 remains a good indicator of the average molecular order even in the gel phase [22]. Figure 5.2(a) shows first spectral moments for DLPC-d_{46} as the sample is cooled from 30°C to −13°C at ambient pressure and from 50°C to −20°C at 1.5 kbar. Values of M_1 obtained at 1.5 kbar while heating the sample back to 40°C and while cooling again to −20°C are shown on Figure 5.2(b).

At ambient pressure M_1 increases continuously to approximately 63×10^3 s^{-1} and then suddenly rises to over 150×10^3 s^{-1} below −2°C [87]. The latter value exceeds the gel phase values typically observed with longer chain diacyl PCs. In gel-phase DPPC-d_{62}, for example, M_1 usually lies between 100×10^3 s^{-1} and 130×10^3 s^{-1} [22]. Values for M_1 above 150×10^3 s^{-1} are usually observed in the highly ordered crystalline phase of longer chain homologs. This further supports the identification of the DLPC low temperature phase with the L_c phase.

The temperature behaviour observed in DLPC-d_{46} at ambient pressure agrees with earlier studies [22, 32]. The decrease in the spectral intensity at maximum splitting, as well as the flattening in the M_1 temperature dependence in the region above the phase transition, results from an enhanced dependence, near the transition, of the transverse relaxation rate on the deuteron position along the acyl chains [128]. The anomalous behaviour of M_1 coincides with the observation of distorted spectra at 0°C, −1°C and −2°C in Figure 5.1. From the deuterium NMR perspective, it is difficult to identify the upper boundary of this unusual region because of the gradual transition from the 'traditional' liquid crystalline phase and because of the lack of abrupt spectral changes in this region. With the application of 1.5 kbar

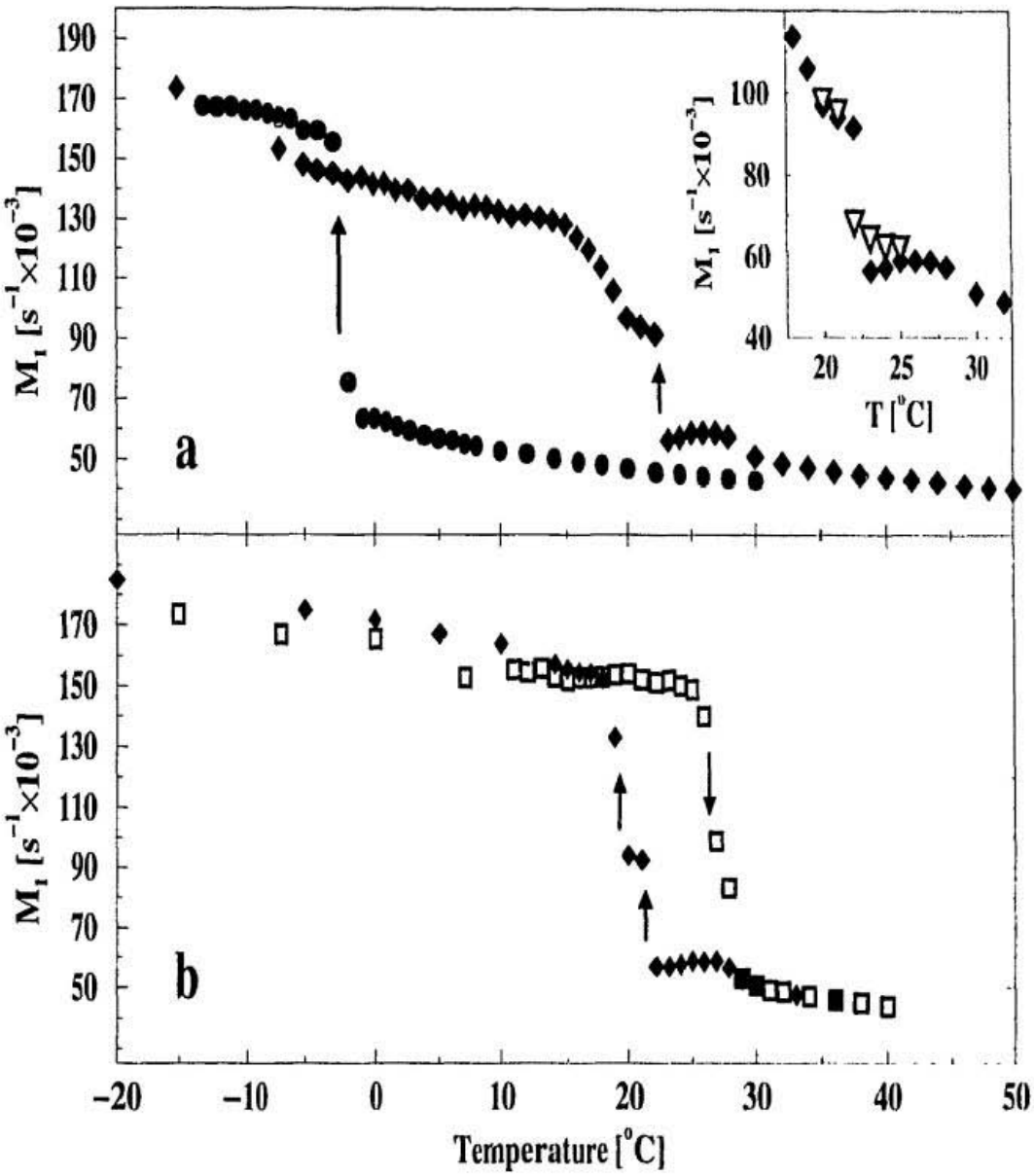

Figure 5.2: DLPC-d_{46} first spectral moments vs. temperature: cooling (a) at ambient pressure (solid circles) and at 1.5 kbar (solid diamonds); (b) 1.5 kbar second cooling scan (solid diamonds) and a heating scan (empty squares). The inset to (a) shows M_1 at the transition for a quadrupole pulse separation of 35 μs (solid diamonds) and 20 μs (open inverted triangles).

of hydrostatic pressure, the region of anomalous M_1 behaviour covers a broader temperature range, up to approximately 6°C, and the flattening of M_1 before the onset of a more ordered phase evolves into an actual decrease in M_1. The effect of position dependent transverse relaxation times on M_1 is illustrated in the inset to Figure 5.2(a) where the first spectral moments are shown for a $\pi/2$-pulse separation $\tau = 20$ μs (empty triangles) together with the M_1 values obtained with $\tau = 35$ μs, as throughout the rest of the experiment (solid diamonds). The use of shorter pulse separation reduces the loss of signal prior to acquisition. As a result the spectral distortions are reduced and, therefore, higher values for M_1 are obtained in the vicinity of the transition.

Between 23°C and 22°C, the first spectral moment at 1.5 kbar increase from 56×10^3 s^{-1} to 91×10^3 s^{-1}. The M_1 values at 22°C, 21°C and 20°C, as well as the corresponding spectra, are similar to corresponding values and spectra seen in the gel phase of longer chain diacyl PCs. The sample was cooled in this region at an effective rate of 0.4°C/h. Below 19°C, M_1 is observed to increase more quickly with decreasing temperature. At 15°C, M_1 approaches values characteristic of the ambient pressure crystalline phase. The corresponding spectra also undergo changes which suggest increasing motional restrictions.

The cooling series was terminated with the sample well into the L_c phase. The pressure was then held at 1.5 kbar and spectra were collected as the sample was warmed back to 40°C. The first spectral moments as a function of temperature for this warming series are shown in Figure 5.2(b) (empty squares). A rather small decrease in M_1 is observed as the temperature is raised up to 26°C, at which point DLPC-d_{46} enters the liquid crystalline phase. M_1 values in the L_α phase match closely the ones measured during the initial cooling cycle. In view of some previous observations of an unusual (L_x) ambient pressure fluid phase [35, 36] it is interesting

to note that DLPC re-enters the liquid crystalline phase above the unusual region where transverse relaxation rates depend on the position along the acyl chain. A striking aspect of this temperature cycling is the strong hysteresis in the DLPC phase behaviour at 1.5 kbar, observed upon comparison between the cooling and the heating scans (Figure 5.2(a) and 5.2(b)).

Spectra were then recorded during a second cooling series, at 1.5 kbar, from 40°C to −20°C. The corresponding values for M_1 are shown in Figure 5.2(b) (solid diamonds). The second cooling experiment reproduces the first one well in the disordered phase and in the gel phase down to 20°C. Below 19°C M_1 abruptly increases to 152×10^3 s^{-1} and then slowly increases to reach 185×10^3 s^{-1} at −20°C. The two cooling experiments differ mainly in that the L_c phase is established faster in the second scan than in the first one.

The behaviour observed between 29°C and 23°C when DLPC-d_{46} is cooled at 1.5 kbar is atypical of diacyl PCs. The strong spectral distortion, due to position-dependent transverse relaxation time, is noticeable at ambient pressure, although it is much less pronounced than at 1.5 kbar. To obtain a better understanding of the phase behaviour of DLPC-d_{46}, a second sample was prepared and studied at pressures of 0.55 kbar, 1.1 kbar, 1.65 kbar and 2.21 kbar. The lipid was cooled at 1°C (2°C for 2.21 kbar case) intervals away from the transition and at 0.5°C steps near the transition. The results are shown in Figure 5.3. The cooling rate throughout the region of 0.5°C temperature decrements was approximately 0.6°C/h.

A close examination of the pretransitional regions above the transitions in Figure 5.3 reveals an increase in the temperature range over which the anomalous behaviour is observed as the pressure is increased. Pressure appears to enhance spectral distortions which give rise to deviations of M_1 from the behaviour expected for diacyl PCs. These observations support the notion that the anomalous region,

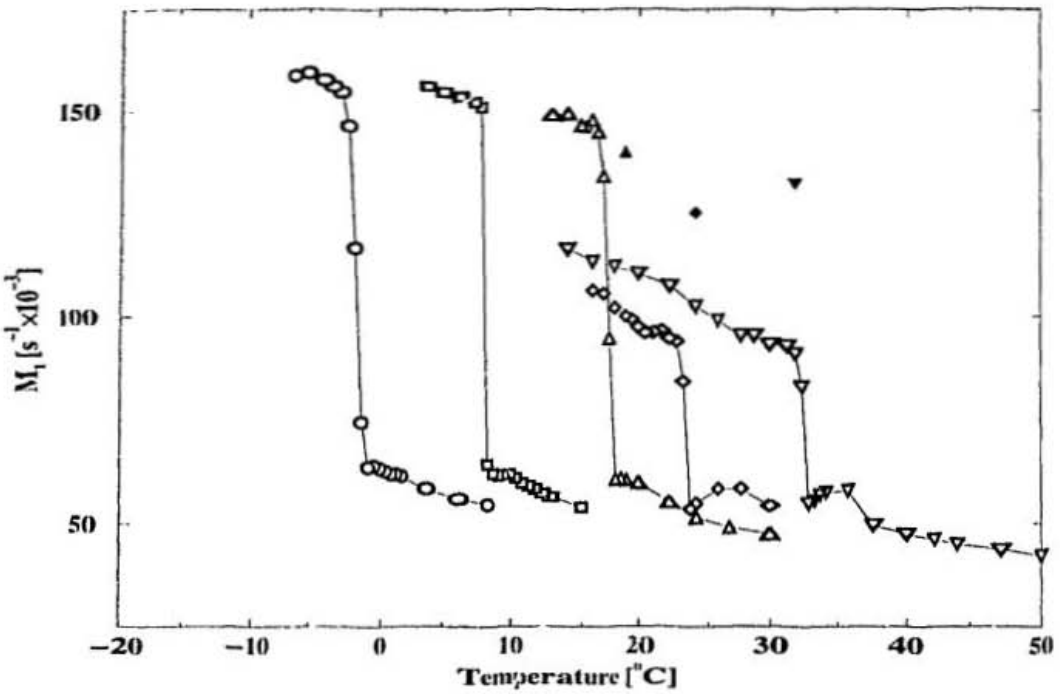

Figure 5.3: DLPC-d_{46} first spectral moments vs. temperature at ambient pressure (circles), 0.55 kbar (squares), 1.1 kbar (triangles), 1.65 kbar (diamonds) and 2.21 kbar (inverted triangles). The solid symbols result from annealing of the system after temperature cycling (see text).

observed above the L_c–L_α transition at ambient pressure, as well as the unusual fluid region observed at elevated pressure above the transition into the gel phase, might be related to the L_x phase, reported recently by Hatta and coworkers [35, 36]. Elevated pressure appears to enhance the distinction between the anomalous region and the liquid crystalline phase.

Another question, in light of the hysteresis seen in Figures 5.2(a) and 5.2(b) and the differences in the way L_c phase is established, concerns the relative stability of the various DLPC bilayer phases. The data in Figure 5.3 show that, below 1.1 kbar, DLPC undergoes a cooling transition from a disordered (possibly L_x phase) directly into a crystalline phase. At 1.65 kbar and 2.21 kbar the transition proceeds through

a gel phase which, compared to the behaviour seen in Figure 5.2, persists to lower temperatures. The latter observation raises the possibility that the establishment of the crystalline phase is dominated by kinetic effects. If the sample is quickly overcooled, the molecular mobility may become low and it may take a long time for the L_c molecular arrangement to occur. A similar dynamics-dominated phase metastability is observed, for example, in the longer chain homolog DPPC where the formation of L_c phase from $L_{\beta'}$ phase is very slow and proceeds over periods of the order of days [37, 150]. To address this issue, limited temperature cycling experiments were carried out at 1.1 kbar, 1.65 kbar and 2.21 kbar. The samples were cooled into the region where the crystalline phase was previously observed then heated and equilibrated at a temperature within the gel or the unusual fluid phase region. After a few hours of annealing, the system was always found in L_c phase.

After the cooling experiment at 1.1 kbar, the sample was warmed from 13°C to 19°C and allowed to anneal for three hours. The resulting value of M_1 (Figure 5.3, solid triangle) appeared as an extrapolation of the crystalline phase behaviour into the temperature range in which the unusual fluid phase was observed during the initial cooling. The corresponding spectrum was also typical of the L_c phase suggesting that this is the stable phase in this temperature region.

The 1.65 kbar cooling scan was ended at 15°C and the sample was warmed to 24°C, which is slightly above the L_x-gel transition temperature. The spectrum, acquired three hours later, was again typical of a crystalline phase and the first spectral moment (Figure 5.3, solid diamond) had a much higher value than was initially observed at 15°C while cooling. The observation of a transition from gel to crystalline phase, rather than from gel to L_x phase under these circumstances suggests that the crystalline phase is stable in this region.

During the experiment at 2.21 kbar, cooling was initially stopped at 24°C and

the sample was warmed to 30°C, just below the observed cooling transition from L_x to gel phase. Heating under these conditions appeared to recover both the spectral lineshape and the value of M_1 to their values observed during the initial cool-down. Under these conditions the system displayed no hysteresis, suggesting that the temperature behaviour of M_1 is reversible down to 24°C. The sample was subsequently cooled further to 14°C and then warmed back to 35°C, well into the L_x region observed during the initial cooling. The observed spectrum appeared to be a distorted liquid crystalline spectrum. The system was then cooled to 30°C where a gel spectrum was obtained. The first moment at this point, though, was a bit higher than M_1 at 30°C before heating to 35°C. The sample was then heated to 31.5°C, and equilibrated for ten hours. The features of the resulting spectrum were characteristic of a crystalline phase (the corresponding M_1 is shown as a solid inverted triangle on Figure 5.3). As the temperature was increased further, DLPC-d_{46} underwent a transition to a regular liquid crystalline phase between 33°C and 38°C.

Below the L_α region the crystalline phase appears to be relatively more stable than the L_x and gel phases, once nucleation has occurred. At elevated pressures, though, such nucleation seems to proceed slowly and even when such a process has begun, slow molecular reorganization essentially prevents the growth of the L_c phase unless the temperature is not much below the L_x phase range.

5.1.2 Specific label observations

One way of circumventing the spectral distortion associated with position-dependence of the transverse relaxation time is the use of specifically labeled lipids. In order to gain further insight into the chain dynamics, experiments were performed using DLPC labeled at the first lauric methylene adjacent to the carbonyl groups

on both chains (DLPC-α-d_4). Transverse relaxation rates ($1/T_{2e}$) determined from the quadrupole echo decay were recorded as a function of temperature at ambient pressure and at 1.5 kbar, together with the corresponding quadrupole spectra. Methyl quadrupole lines of DLPC-d_{46} are easily distinguishable on the perdeuterated spectra and were also used for monitoring the dynamics of the acyl chains ends.

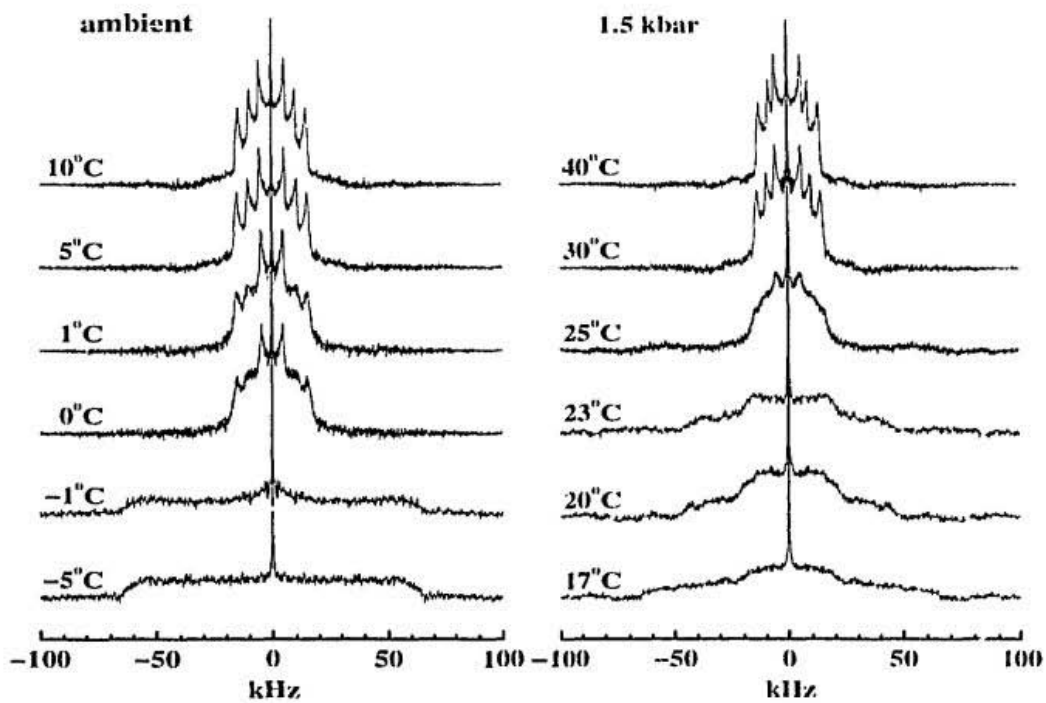

Figure 5.4: DLPC-α-d_4 spectra at selected temperatures; (a) ambient pressure; (b) 1.5 kbar.

The phase changes, observed with the perdeuterated as compared to the specifically labeled lipids, occur at slightly lower temperatures, as a result of the isotope substitution [32]. Selected spectra of DLPC-α-d_4 at ambient pressure and 1.5 kbar are shown on Figure 5.4. The spectrum at 1.5 kbar and 25°C has a width which is comparable to the width of the liquid crystalline spectrum at 30°C and the same

pressure, although the lineshape is distorted as a result of inequivalent relaxation rates among the α-deuterons. The high pressure spectra at 23°C and 20°C reflect axially asymmetric motions and most likely represent a gel phase. Intensity buildup at ± 63 kHz in the spectrum at 17°C (Figure 5.1(b)) is indicative of crystalline phase growth.

The temperature dependence of the mean transverse relaxation time, $\overline{T_{2r}}$, for DLPC-α-d_4 is shown in Figure 5.5(a) for ambient pressure and 1.5 kbar. For comparison, M_1 values for perdeuterated DLPC are presented as a function of temperature in Figure 5.5(b). The ambient pressure value of $\overline{T_{2r}}$ decreases from 590 μs to 190 μs as the temperature is lowered from 8°C to 0°C. Between 0°C and -10°C, $\overline{T_{2r}}$ undergoes a slight increase to approximately 260 μs. The transverse relaxation time at 1.5 kbar in the liquid crystalline phase is lower than that at ambient pressure and between 40°C and 30°C it is of the order of 400 μs. Hence, the correlation times for motions contributing to transverse relaxation in the L_α phase increase at elevated pressure. As the temperature is lowered through the region where the L_x phase is observed, $\overline{T_{2r}}$ decreases dramatically from 400 μs at 30°C to 54 μs at 24°C. The transverse relaxation time has a minimum at the L_x to gel transition and then increases slightly to about 140 μs as the temperature is lowered to 17°C. Below 17°C, where the transition from gel to L_c phase is completed, $\overline{T_{2r}}$ remains approximately constant.

The terminal methyl groups provide additional information on the molecular order of the acyl chains in the disordered phase. Methyl deuteron splittings for DLPC-d_{46}, extracted from the spectra of Figure 5.1 at 1.5 kbar, are shown on Figure 5.6 as a function of temperature. Although a discontinuity in the methyl splittings at the onset of the L_x phase at 30°C is not observed, there is a change in the slope of the methyl splittings with temperature at that point. Such behaviour is atypical

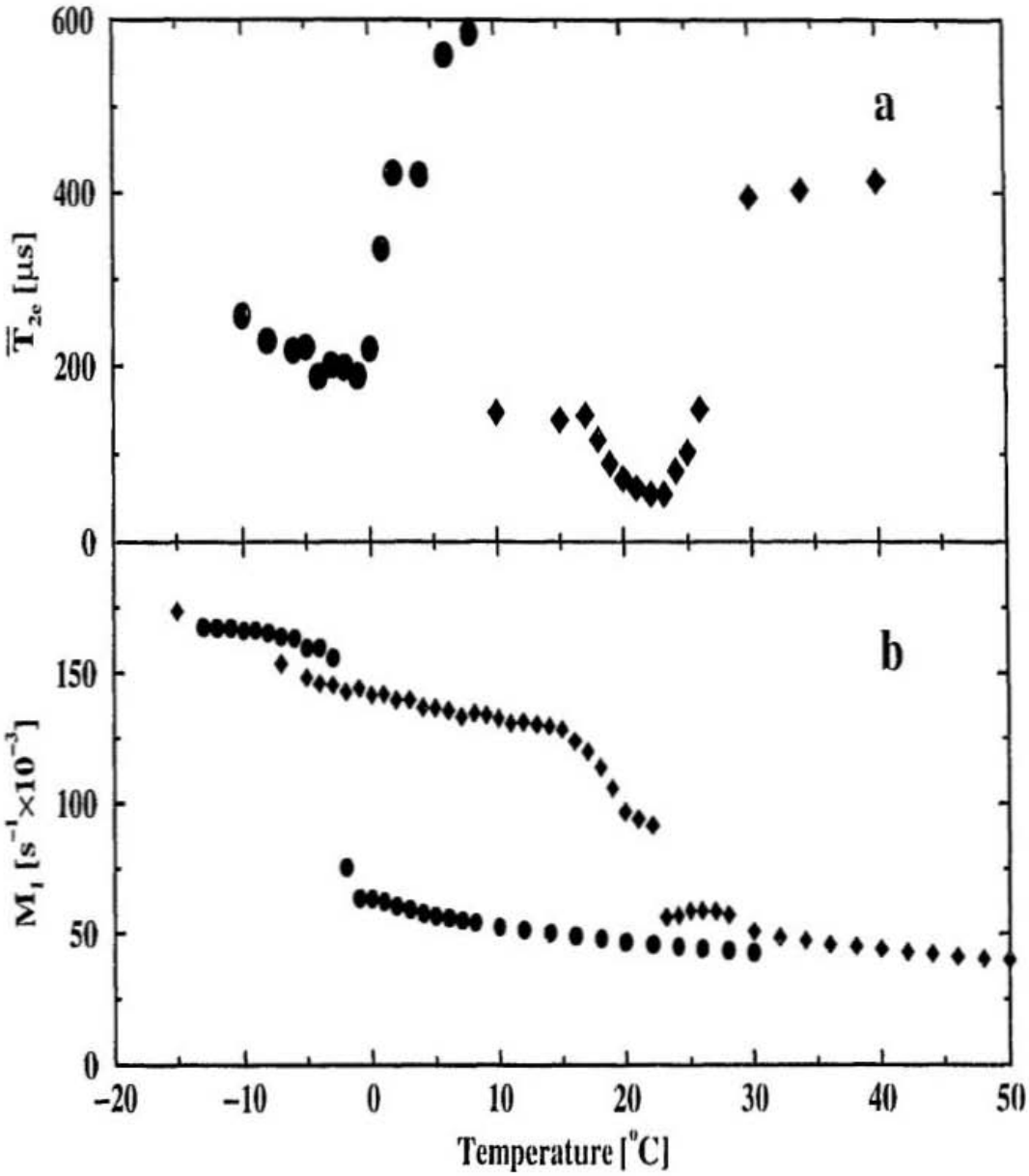

Figure 5.5: Mean transverse relaxation time $\overline{T_{2e}}$ for DLPC-α-d_4 (a) and first spectral moments for DLPC-d_{46} as a function of temperature at ambient pressure (circles) and 1.5 kbar (diamonds).

of the phospholipid main transitions as viewed by deuterium NMR.

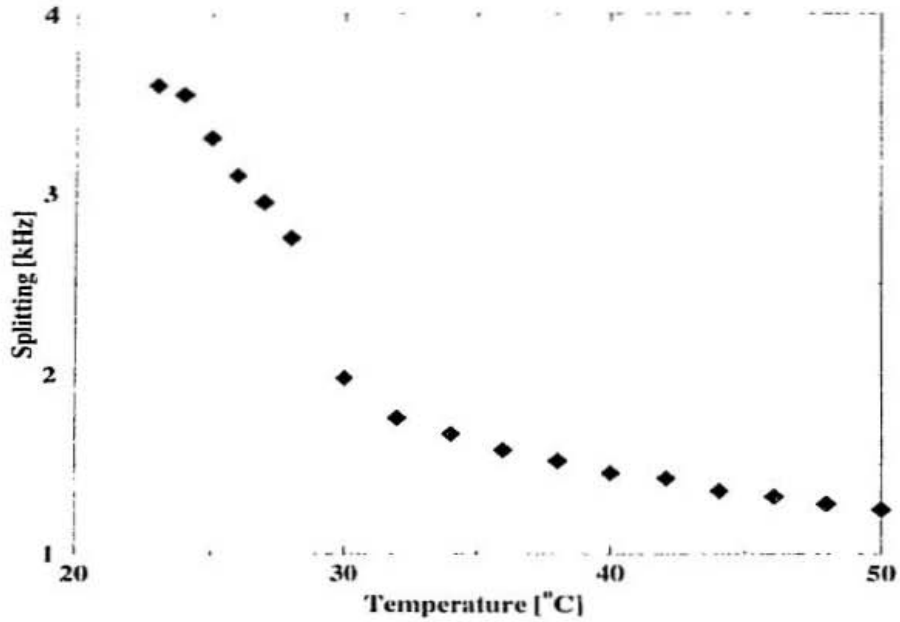

Figure 5.6: DLPC-d_{46} methyl splittings as a function of temperature at 1.5 kbar.

5.2 Discussion

The hydrocarbon chains in DLPC are close to the minimum length necessary for the formation of stable bilayers, and the unusual phase behaviour of this lipid [31, 32, 35, 36, 149] probably reflects a balance between the interactions in PC headgroup and in the hydrocarbon region which is different from that typical of the longer chain homologs. The high pressure results, discussed in the previous section, elucidate some of the unusual aspects of DLPC ambient pressure phase behaviour. They also contribute to the understanding of its place in the diacyl PC homologous series.

Calorimetric studies of the DLPC ordered to disordered phase change show that

it proceeds in two stages [31, 32, 35, 149]. In the region, a few degrees wide, between the two excess heat capacity peaks, DLPC is in a state labeled L_x [35, 36]. This state is characterised by axially symmetric molecular motions, which can be inferred from the powder lineshapes. The relaxation times, observed in this state, are very short and depend on the deuteron position along the acyl chain. These relaxation measurements suggest that the motional rates are much reduced and possibly affected by interactions in the headgroup region. From the deuterium NMR results presented here, pressure is seen to affect both the width, in temperature, and the prominence of this region of unusual properties. The spectra in this region are characteristic of fast axially symmetric motions with high transverse relaxation rates which are strongly dependent on position along the acyl chains. The changes in the temperature dependence of M_1 with pressure, shown in Figure 5.3 as well as the similarity in the NMR spectra at ambient and elevated pressure, in the unusual fluid region, allow this region of unusual behaviour at high pressure to be identified with the ambient pressure L_x phase observed by Finegold and coworkers [35] and by Hatta and coworkers [36]. The upper boundary of this L_x phase is effectively impossible to identify from the M_1 temperature dependence, shown in Figure 5.2, due to the smooth variation of first moments as DLPC enters the L_α phase from the liquid crystalline phase. This absence of a discontinuity between the liquid crystalline phase and the region of unusual fluid behaviour suggests a continuous change in the amplitude of the molecular motions, which is in accord with the report of Hatta and coworkers [36] of a continuous variation of the bilayer thickness between the L_α and the L_x phase. Transverse relaxation rates, on the other hand, undergo a rather abrupt increase upon entrance into the L_α phase from the L_x phase. This indicates a decrease in the chain motional rates in the L_α phase.

The observation of an unusual fluid phase between the gel and liquid crystal

phases of DLPC raises some interesting questions about the nature of the main phase transition in lipid bilayers.

The transition from liquid crystalline to gel phase in longer chain diacyl homologs involves two aspects: the acyl chain conformational order increases discontinuously and intermolecular positional order is established. In longer chain lipids the two aspects are strongly coupled. In the case of DLPC, it is possible to speculate that the decreased motional rates observed in the L_x phase indicate an increase in the intermolecular order without a concomitant change in the conformational order of the chains. High pressure seems to enhance this decoupling by shifting the onset temperature of lateral ordering further above the onset temperature for the chain ordering, at which the transition to gel phase occurs. A reason for this might be sought in the relative strengthening of the headgroup interactions with respect to the intrachain interactions due to the relatively small chain length. Another effect, which might bear relevance to the role of the headgroups in this transition is the observed dependence of the higher temperature calorimetric feature on sample hydration [32].

The temperature cycling experiments illustrated on Figure 5.3 show strong hysteresis, suggesting that both gel (when present) and L_x phase are metastable. Reversible cycling through these phases is possible as long as nucleation of the L_c phase has not begun. For example, during the initial cooling experiment, samples were equilibrated for a few hours in the L_x phase without evidence of ordered phase formation. Pressure appears to hamper L_c phase nucleation as well as crystalline domain growth. The latter effect can be seen, for example, in the cooling experiments where the gel phase persists to lower temperatures when the sample is cooled faster. After initial nucleation of the crystalline phase, the growth of its domains is very slow if the temperature is more than a few degrees below the transition from

L_x to an ordered phase.

In an earlier study of diacylphosphatidylcholines, Morrow, Whitehead and Lu [22] discussed the observed decrease with chain length of the mean orientational order discontinuity at the fluid-gel transition in terms of a decreasing difference between the transition temperature and a critical temperature on the fluid gel coexistence curve. As far as the main transition is concerned, DLPC at ambient pressure cannot be compared to the longer chain phospholipids due to the intervention of a transition into a more ordered L_c phase, which renders the gel phase unobservable. High pressure is shown here to suppress the onset of this ordered phase and to allow for the observation of a true gel phase. The interpretation of the main transition in terms of change in the order parameter is further complicated, though, by the presence of the region of unusual dynamics, L_x. As a result of the abrupt decrease in the rates of molecular motions in the L_x region, the discontinuity in M_1 cannot be used directly since the M_1 values in the immediate vicinity of the transition are strongly reduced by fast transverse relaxation. Nonetheless, the first spectral moments in this region can provide the necessary information about the temperature behaviour of the chain order. As shown on the inset of Figure 5.2(a), the discontinuity in M_1 decreases as the separation between the 90° pulses is reduced from 35 μs to 20 μs. If a simple exponential decay is assumed, the pulse separation can be easily extrapolated to zero. Such an approximation is justified for the region of very small pulse separation discussed here. The M_1 values obtained in this way are shown as a function of temperature in Figure 5.7(a), (empty downwards triangles), together with the values of M_1 for 35 μs (solid diamonds) and 20 μs (solid downwards triangles) pulse separations. For comparison Figure 5.7(b) shows the relaxation time for DLPC-α-d_{46}. The M_1 values obtained by extrapolation to zero pulse separation reveal essentially no discontinuity at the fluid to gel phase transition. The results

shown in Figure 5.7(a), appear to illustrate the expected near-second order character of the transition in DLPC. This suggests that, in principle, a second order phase transition in pure disaturated diacylphosphatidylcholine may be observable.

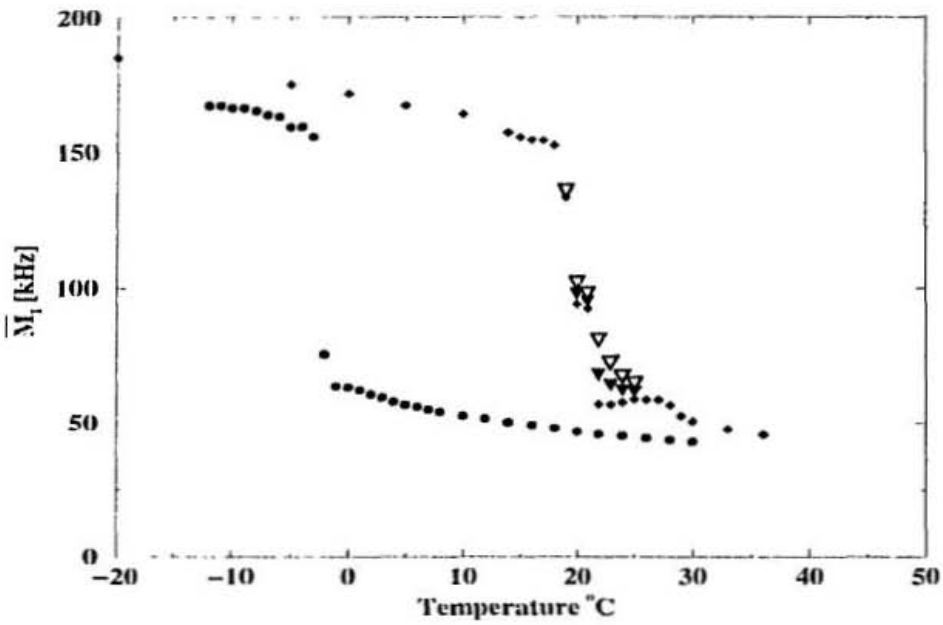

Figure 5.7: DLPC-d_{46} first spectral moments as a function of temperature (a) at ambient pressure (circles) and at 1.5 kbar at pulse separation of 35 μs (diamonds), 20 μs (solid inverted triangles) and extrapolated to zero pulse separation (empty inverted triangles).

5.3 Summary

The phase behaviour of DLPC at ambient pressure is substantially different from that of its longer chain homologs. Since pressure affects the different phase transitions in different ways, it was possible to separate the disordered phase to gel transition from the transition between gel and the crystalline phase and to obtain

a true gel phase in DLPC. The unusual region in the fluid phase was found to be enhanced by the application of hydrostatic pressure and was identified with the ambient pressure L_x phase, observed by Finegold and coworkers [35] and by Hatta and coworkers [36]. In experiments where the temperature was increased, a single transition was observed from crystalline to liquid crystalline phase. An extrapolation of the orientational order parameter to zero pulse separation suggests the transition from a disordered to a gel phase in DLPC proceeds without a discontinuity in the chain order, as implied by the ambient pressure trends in longer chain diacyl PC's [22]. It appears that the unusual dynamical properties of DLPC might result from enhanced headgroup interactions in a region of finite temperature width above the transition to an ordered phase, while the transition itself is associated with a change in the chain order.

Chapter 6

Pressure Effects on PC Headgroups

The previous two chapters focused on the hydrocarbon region of the bilayer. In this chapter, the focus is on the perturbing influence of pressure on the PC polar headgroups, which, as they form the interface between water and the bilayer interior, influence important bilayer properties including the structure and stability. Deuterium NMR has been used extensively as a nonperturbing method for the study of phospholipid headgroups at various membrane and water subphase compositions, levels of hydration, etc. [39, 41, 42, 45, 47, 49, 50, 151]. It is currently accepted that, in the fluid phase, the average orientation of the polar headgroup dipole is roughly parallel (within 30°) to the plane of the bilayer [38, 39]. When various charged membrane or water subphase constituents are added to the lipid suspension, the phosphorylcholine headgroup tilts towards, or away from, the bilayer normal depending on the sign of the membrane surface charge. From the deuterium NMR perspective, this is seen as a counterdirectional change in the quadrupole splittings of the deuterons at the α and β choline carbons [41, 42].

Application of hydrostatic pressure leads to a reduction of the bilayer area per lipid molecule, as discussed in chapter 4. The phospholipid headgroups are expected to respond to the reduced molecular area by adopting a new conformation, possibly a more upright position. Pressure can be changed in a continuous manner, allowing for the headgroup conformation to be varied in a (presumably) continuous fashion as well, without any alterations in the lipid-water system composition. In this chapter, the isothermal response of DMPC-d_4 and DPPC-d_{13} headgroups to pressure

is discussed in terms the relative changes in deuteron quadrupole splittings at the α and β choline carbons. A scenario for the effect of temperature on the headgroup is proposed, based on isobaric measurements at ambient and elevated pressure.

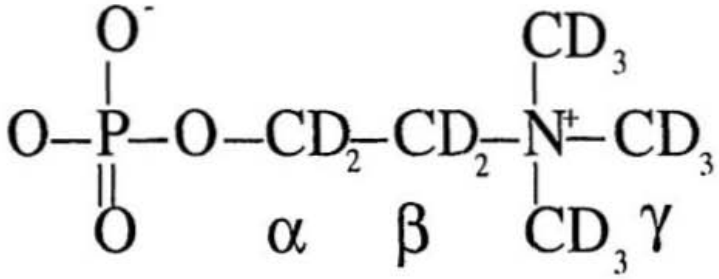

Figure 6.1: Structure of phosphatidylcholine headgroup.

Lipid samples were in the form of MLV, prepared by hydration in excess phosphate buffer (pH 7.2) above the main transition temperature. Quadrupole echo $\pi/2$ pulses between 2.2 μs and 2.4 μs were used with a pulse separation of 75 μs. Digitizing with a dwell time of 5 μs was used with 4 times oversampling [129, 152] to result in an effective dwell time of 20 μs. Quadrupole splittings were determined in the liquid crystalline phase from the 90° edges of the powder lines.

6.1 Results and discussion

Two disaturated PCs were studied, the 14 and 16 carbon homologs DMPC-d_4, deuterated at α and β choline positions, and DPPC-d_{13} with a perdeuterated headgroup. Spectra were collected for a series of pressures at 65°C in the liquid crystalline phase. This temperature allowed for the observation of a fluid phase over a conveniently broad pressure range (ambient - 2 kbar for DMPC and ambient - 1 kbar for DPPC) without overheating the samples. Figure 6.2 shows representative spectra for DMPC-d_4 and DPPC-d_{13} in the liquid crystalline phase. All spectra in the liquid crystalline phase are a superposition of axially symmetric powder patterns.

The outer peaks on the ambient pressure spectra of both DMPC-d_4 and DPPC-d_{13} correspond to the α choline deuterons while the inner peaks are produced by more freely reorienting β choline deuterons. All γ deuterons in DPPC-d_{13} produce a single, narrow (approximately ± 1 kHz) doublet of high intensity. The spike at zero frequency is due to some naturally present HDO in the water subphase.

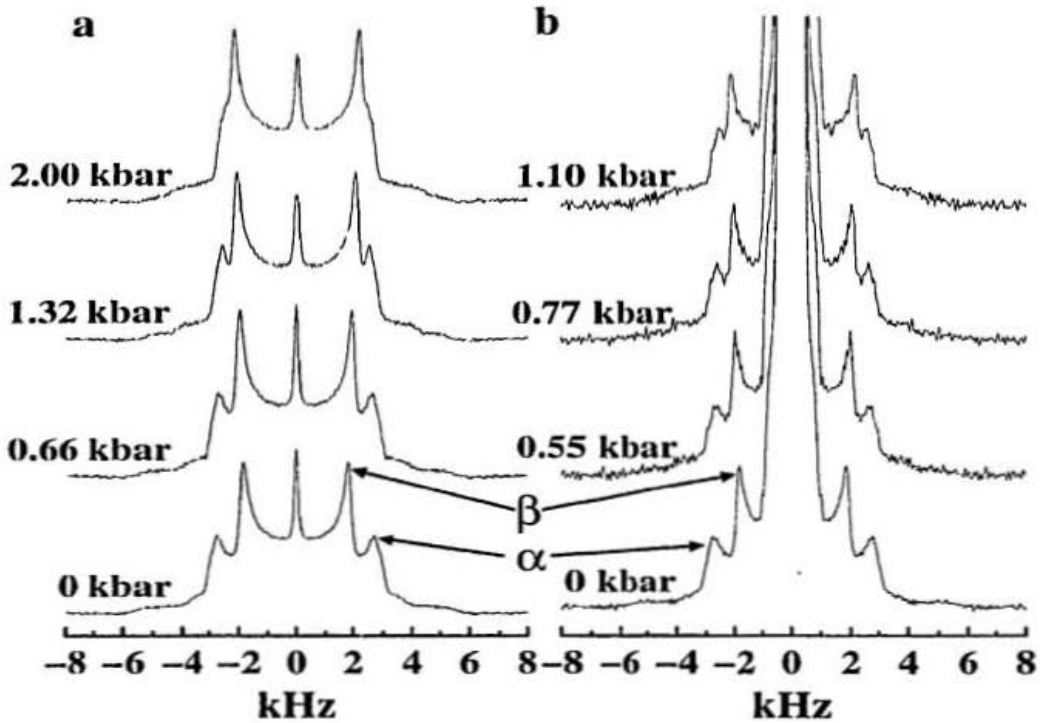

Figure 6.2: Deuterium NMR spectra of DMPC-d_4 (a) and DPPC-d_{13} (b) at 65°C and different pressures. Pressure is indicated in kbar next to each spectrum.

The α doublet in DMPC-d_4 with splitting of 5.44 kHz actually consists of two doublets. Under decoupling conditions these are observed with a separation of about 300 Hz in DPPC [41]. This is due to a slight inequivalence of the two α-carbon deuterons, resulting from reduced motional freedom in the immediate vicinity of the glycerol backbone [40]. All α splittings in these experiments are determined from the observed single, slightly broadened doublet and thus represent an effective

average of the two doublets.

Figure 6.3 shows the pressure dependence of the α (circles) and β (diamonds) deuteron quadrupole splittings for DMPC-d_1 (solid symbols) at 65°C. The α splitting decreases approximately linearly with a slope of −270 Hz per kbar in an approximately linear fashion, while the β splitting increases with a slope of 350 Hz per kbar. The pressure dependence of the α (circles) and β (diamonds) deuteron quadrupole splittings for DPPC-d_{13} at 65°C is also shown in Figure 6.4 (open symbols). A linear decrease in the α quadrupole splittings is observed with a slope of −580 Hz per kbar. The β deuteron splittings increase at 870 Hz per kbar [87]. All nine methyl (γ) deuterons appear to be equivalent due to a rapid reorientation about the C_γ N and the N–C_γ bonds. A single line results from their superimposed contributions with a splitting increasing with pressure by 130 Hz per kbar at 65°C.

The application of hydrostatic pressure is seen to produce a counterdirectional change in the α and β quadrupole splittings. Analogous changes in the choline α and β splittings have been observed previously in response to perturbations in the bilayer surface charge density [39, 42-46, 48, 49]. In contrast to changes in orientational order, which affect all methylene splittings in the same way, a counterdirectional change is generally indicative of a conformational change in the headgroup. Decreasing α and increasing β quadrupole splittings are also observed in conjunction with the presence of metal ions in the water subphase [40, 41], positively charged amphiphiles [42, 45, 49] and polypeptides [47]. At present such behaviour of the choline α and β deuteron splittings is believed to be associated with a concerted tilt of the whole headgroup away from the bilayer plane. This conformational change is most likely a result of torsion about the bond between the glycerol number one carbon and its adjacent phosphocholine oxygen [48] or about the C(1) C(2) glycerol bond

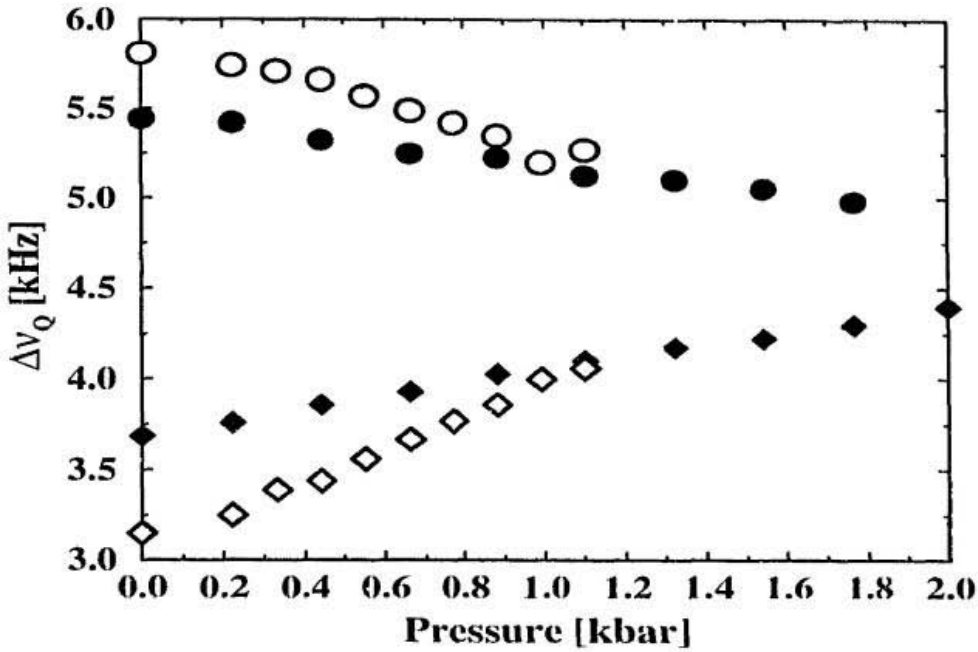

Figure 6.3: Choline α (circles) and β (diamonds) splittings as a function of pressure for DMPC (solid symbols) and DPPC (open symbols) at 65°C.

[13]. *Ab initio* calculations of the corresponding torsional energies in glycerophosphocholine [153] suggest that such deformations are essentially unobstructed, due to minimal variations of these energies over a broad range of bond dihedral angles. The headgroup tilt is assumed to result from a torque produced by the interaction between the phosphocholine P^-–N^+ dipole and the positive surface charge of the cations adsorbed at the bilayer surface, or by the presence of positively charged membrane constituents.

A negative surface charge tilts the headgroup in the opposite direction, away from the bilayer normal. The effect of this tilt, from a deuterium NMR perspective, is an increase in the α and a decrease in the β quadrupole splittings as the surface charge is increased [39]. A tilt of the phosphorylcholine moiety towards the membrane

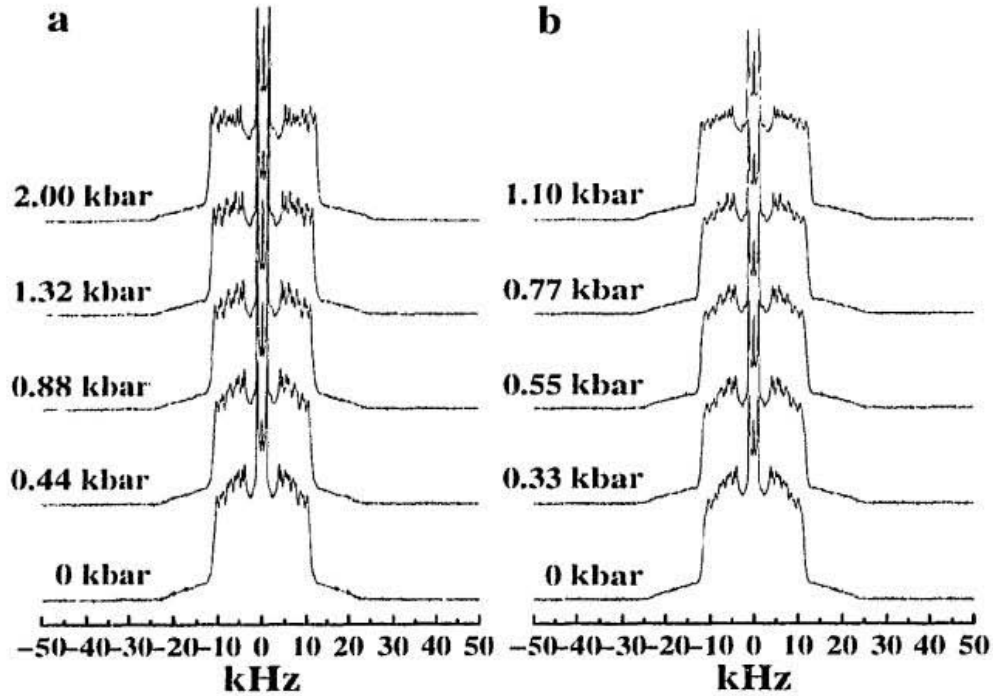

Figure 6.4: Deuterium NMR spectra of DMPC-d_{54} (a) and DPPC-d_{62} (b) at different pressures. Pressure is indicated in kbar next to each spectrum.

surface is also observed with reduced hydration of the bilayer headgroup region [50, 51].

Hydrostatic pressure produces a highly anisotropic deformation in a fluid phospholipid bilayer. In the lateral direction the bilayer is compressed easily in response to hydrostatic pressure, while small angle neutron diffraction data [19, 90] show an increase in the overall bilayer thickness with pressure. As was illustrated in chapter 4, a similar result can be inferred for the axial extension of the hydrocarbon chains from deuterium NMR measurements. Additional pressure experiments were carried out on chain perdeuterated DMPC-d_{54} and DPPC-d_{62} at 65°C in order to obtain a better understanding of the response of the molecular area in the two lipids to pressure. The corresponding spectra are shown in Figure 6.4(a) and Figure 6.4(b).

The first spectral moments in perdeuterated chains can be related to the mean axial extension of the whole chain as described in chapter 1. Figure 6.5 shows M_1 as a function of pressure from 1 kbar to ambient pressure for DPPC-d_{62} and from 2 kbar to ambient pressure for DMPC-d_{54}. The increase in M_1 with pressure reflects an increase in the hydrocarbon chain order and, subject to the constant volume approximation made in chapter 4, a decrease in the bilayer area per molecule in the liquid crystalline phase. The approach adopted in chapter 4 [22, 143] gives an increase in the acyl chain axial extension of approximately 2.5% per kbar for DPPC and of 3.5% per kbar over 2 kbar in the case of DMPC. This can also serve as an estimate for the reduction in the bilayer area per molecule. A decrease in the area per lipid molecule with pressure is very likely to result in the observed tilt in the polar headgroup towards a more upright position, where the headgroup spans a smaller bilayer area. It is interesting to note that the pressure induced changes in the α and β quadrupole splittings are in directions which are opposite to those for dehydration-induced headgroup tilt reported by Bechinger and Seelig [50]. This argues against the possibility that the observed headgroup tilt results from a pressure-induced water exclusion.

The response of the headgroup deuteron quadrupole splittings (Figure 6.3) as well as the first spectral moments of perdeuterated lipids (Figure 6.5) to pressure is stronger in DPPC than in DMPC. In the light of the proposed headgroup tilting in response to area reduction, it is natural to attribute this difference to a stronger response in the DPPC bilayer to lateral compression than in the DMPC bilayer. To understand such behaviour, it is important to remember that the transition temperature at ambient pressure for DMPC-d_{54} is approximately 19°C, while in DPPC-d_{62} it is about 38°C ([22], Chapter 7). It is helpful to consider the isothermal experiments on DMPC-d_{54}, described in chapter 4. An increase in temperature of 20°C was seen to substantially reduce the sensitivity of M_1 to pressure in the

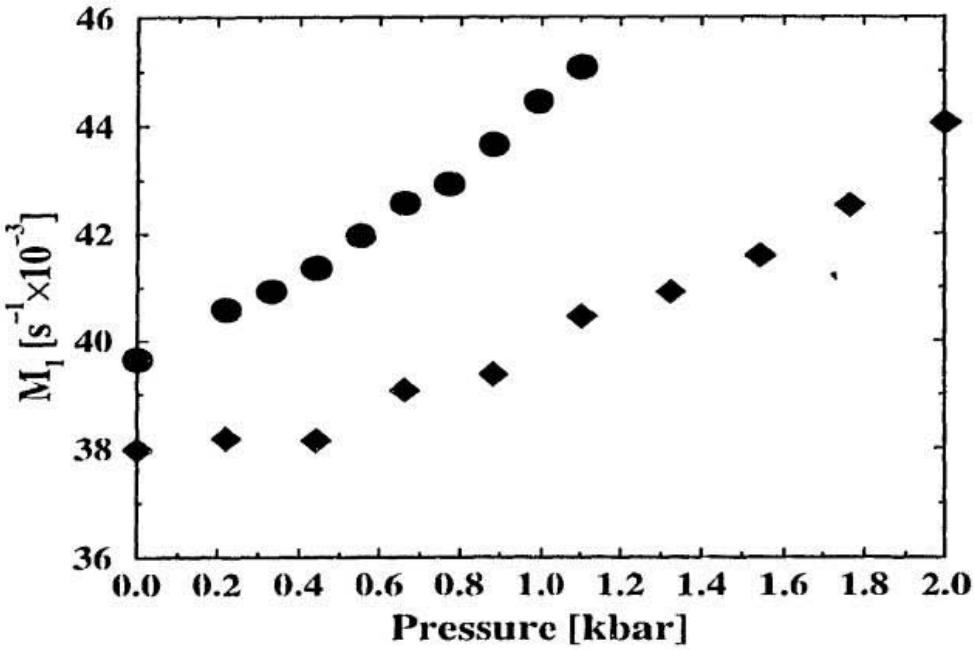

Figure 6.5: First spectral moments vs. pressure for DMPC-d_{54} (diamonds) and DPPC-d_{62} (circles).

liquid crystalline phase. Presumably, the lateral bilayer compression in response to applied hydrostatic pressure is similarly reduced at increased temperature. Thus at 65°C the slower variation of the DMPC headgroup deuteron quadrupole splittings with pressure can probably be accounted for by the reduced lateral response to hydrostatic pressure far above the ambient pressure transition temperature.

A convenient way of comparing the conformational changes in the phosphocholine headgroup, produced by various perturbants, is to plot the β splittings versus the α splittings as the magnitude of the perturbation is varied [41, 45-48, 50, 154-155]. These plots are typically linear with slopes grouped around -1 when the headgroup tilt is produced by the presence of a negative surface charge, -0.6 when the surface charge is positive [45] and about -0.76 when the headgroup is

tilted by dehydration of the membrane surfaces [50]. The negative slope reflects the opposite direction of the changes in the α and β quadrupole splittings and serves as an indication that a headgroup conformational change rather than a change in the orientational order takes place. The magnitude of the slope illustrates the different nature of the interactions between the headgroup and the corresponding perturbing agent [45]. The correlation between the α and β quadrupole splittings of DMPC-d_4 and DPPC-d_{13} from ambient pressure to 2 kbar and 1 kbar, respectively, at 65°C, are shown in Figure 6.6. The dependence is approximately linear with slopes of -1.31 and -1.46 for the cases of DMPC and DPPC, respectively [87]. These results show that the observed variations in the headgroup quadrupole splittings with pressure reflect conformational changes rather than changes in orientational order. The magnitude of the slope is larger than that observed for both charge-induced and hydration-induced tilt, suggesting that a different mechanism is responsible for the pressure-induced change in the headgroup conformation.

The effect of temperature on the α and β quadrupole splittings makes an additional contribution to the understanding of phosphatidylcholine headgroup behaviour. At ambient pressure, the choline β splitting is observed to decrease with temperature over a broad temperature range, while the α splitting remains essentially unaffected [41]. This behaviour has been attributed to the effect of temperature on headgroup motion. An increase in the torsional freedom about the C_α, C_β σ-bond has been proposed to account for the decrease in the β splitting with increasing temperature [41]. Proximity to the bulky phosphate group is thought to result in an essentially temperature independent α splitting. To better understand the effects of pressure on headgroup behaviour, variable temperature experiments were carried out at ambient pressure and at 1.5 kbar. Selected spectra are shown in Figures 6.7(a) and (b). The temperature dependences of DMPC-d_4 α and β quadrupole

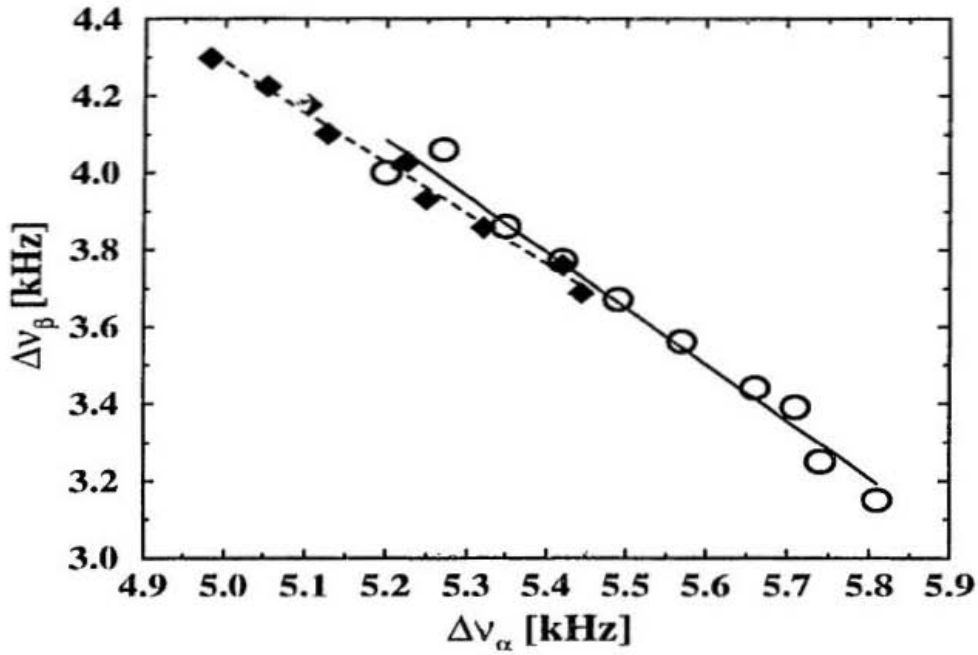

Figure 6.6: Choline β ($\Delta\nu_\beta$) vs. α ($\Delta\nu_\alpha$) splittings for DMPC-d_4 (solid diamonds) and DPPC (open circles).

splittings are shown in Figure 6.8 for ambient pressure and 1.5 kbar. Application of 1.5 kbar is seen to have a relatively small effect on the temperature dependence of both splittings. Nonetheless, the temperature sensitivity of the β splitting decreases slightly at 1.5 kbar in comparison to the ambient pressure situation and a weak, yet nonzero, temperature dependence of the α splitting appears.

The difference in the response of the α and β quadrupole splittings to temperature may reflect the combined effect of temperature and area per lipid on headgroup orientational order. Increasing temperature is expected to increase area per lipid and decrease orientational order. A tilt of the headgroup towards the bilayer in response to increased area per lipid would increase the α splitting and decrease the

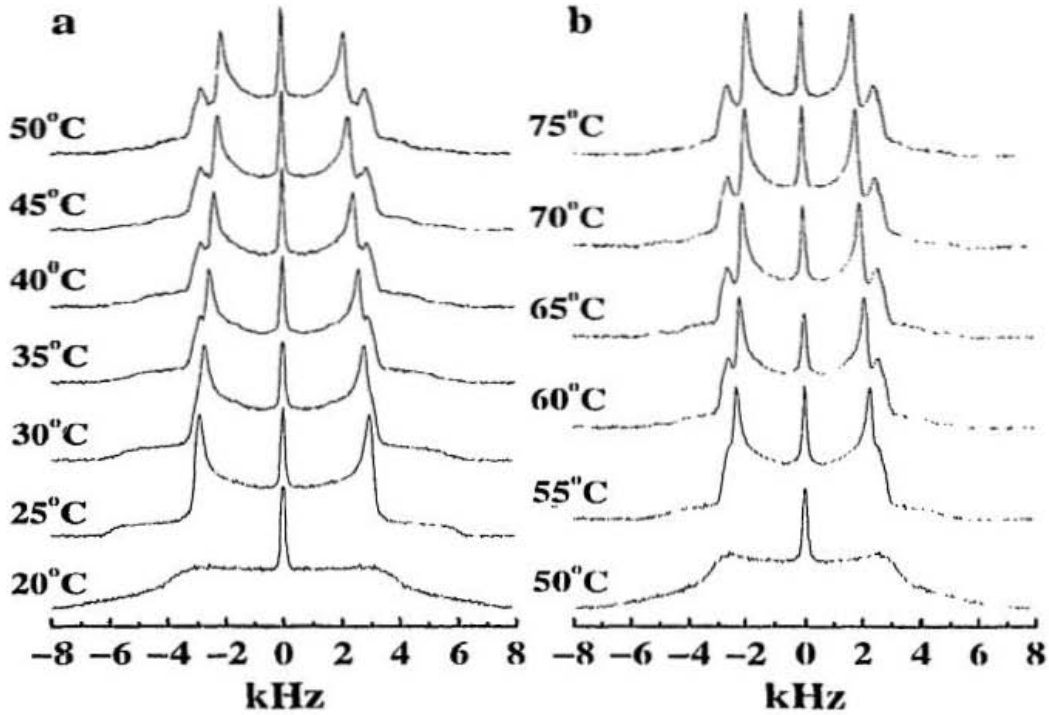

Figure 6.7: Choline deuterium NMR spectra for DMPC-d_4 as a function of temperature at ambient pressure (a) and at 1.5 kbar (b).

β splitting. The decrease in orientational order would reduce both splittings. Competition between these two effects could reduce the response of the α splitting to temperature. For the β splitting the two effects would be additive. It is possible that at ambient pressure the two trends in the α splitting exactly offset each other so that the α splitting appears to be independent of temperature. At elevated pressure though, as discussed in chapter 4, the bilayer area thermal expansivity is reduced. Under these circumstances, the increase in α deuteron splitting arising from the headgroup conformational change would be smaller and might no longer compensate for the decrease in orientational order resulting in the observed overall decrease in α splitting with temperature. The β splitting would become less dependent on temperature.

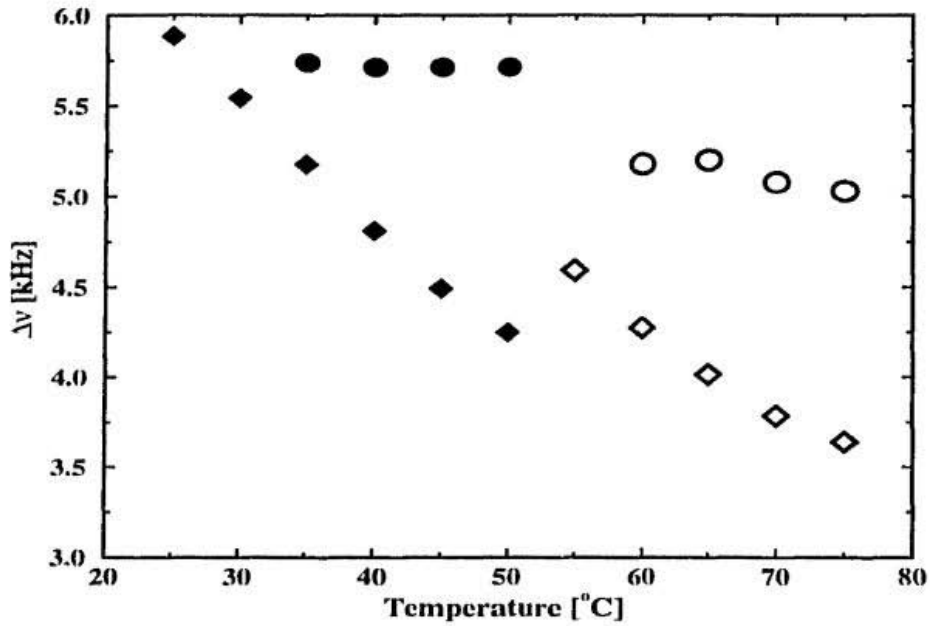

Figure 6.8: DMPC-d_4 α (circles) and β (diamonds) splittings as a function of temperature at ambient pressure (solid symbols) and at 1.5 kbar (open symbols).

6.2 Summary

Application of hydrostatic pressure to MLV suspensions of DMPC and DPPC results in a reduction of the headgroup choline α deuteron splittings and an increase in the β deuteron quadrupole splitting. The counterdirectional change in choline deuteron splittings indicates a conformational change of the headgroup in response to pressure rather than a change in headgroup orientational order. The headgroup choline deuteron quadrupole splittings change in a way similar to that of the changes induced by positive membrane surface charge, which reflects a headgroup tilt towards the bilayer normal. It was concluded that the reduction in the bilayer area per lipid molecule with pressure, deduced from the isothermal pressure dependence of the mean orientational order in chain perdeuterated DMPC and DPPC, is the reason

for the observed headgroup conformational changes. On the basis of isobaric experiments, it is proposed that the temperature behaviour of the headgroup is dominated by two parallel temperature-dependent factors, i.e. headgroup tilt and orientational disorder. Volume compression as a method of varying the headgroup orientation in a continuous, nonperturbing way within a single sample may prove useful in obtaining information on the mechanical properties of the headgroup region of the bilayer and on the mechanisms of surface charge-induced conformational changes in the phosphatidylcholine headgroup.

Chapter 7

Other Results

7.1 Ordered phases in DPPC

The most extensively studied of all saturated diacyl PCs is the 16 carbon homolog DPPC. The special interest in this lipid stems from its biological importance as the major constituent of the higher animal pulmonary surfactant and as a component of the cell membranes. Another intriguing property of this lipid is its immunoinertness, with relevance to liposomal drug delivery. DPPC is also relatively easy to prepare synthetically, store and handle, and it displays most of its interesting physical properties over a convenient range of experimental parameters.

At ambient pressure, protcated DPPC is in the liquid crystalline (L_α) phase above its main transition at 41.5°C [1, 5, 9, 10, 23, 132, 156] and in the rippled ($P_{\beta'}$) phase down to approximately 35°C [5, 157]. Chain perdeuteration lowers the main transition temperature to approximately 37°C (see subsection 7.1.1 below, also [20, 22]). Below the pretransition, the lipid is in a tilted lamellar ($L_{\beta'}$) phase and below approximately 21°C (the subtransition), the stable phase in DPPC is the crystalline (L_c) phase. The subtransition temperature of 21°C is determined from DSC heating scans [18, 37]. The observed transition enthalpy depends on the duration and temperature at which the sample is equilibrated prior to thermal scanning. Because of the unusual properties of the crystalline (subgel) phase, it has been subject to investigation by a number of experimental methods, including DSC (DTA) [31, 33, 37, 157-159], NMR [159-161], EPR [150], FTIR [34] and X-ray

diffraction [157, 159]. Initiation of this phase upon cooling involves a fast stage of subgel seed formation from germ nuclei and a slower process of subgel domain growth [150].

Phosphatidylcholine systems display a rich barotropic behaviour [19, 56, 60-62, 65, 70, 82, 83, 85, 90, 97, 102, 103]. As many as seven phases have been suggested in DPPC at different pressures and temperatures [83, 86, 102]. The liquid crystalline phase observed at ambient pressure exists at high pressure as well, although the transition temperature into more ordered phases increases with pressure by approximately 21°C per kbar [61, 83, 87, 90, 97]. Six ordered phases have been reported. Three, also seen at ambient pressure, are $P_{\beta'}$ (or GI), $L_{\beta'}$ (GII) and the crystalline phase (L_c, or C). Those seen only at high pressure include an interdigitated gel, which is lamellar [90] with intercalated chains and is most appropriately labeled L_i in the spirit of Luzzati's nomenclature [8], and two low temperature phases, $GIII$ and a highly ordered phase X.

In the current study, the phase behaviour of DPPC-d_{62} was studied as a function of temperature at 2.20 kbar, 1.00 kbar and ambient pressure. These are the first reports of constant pressure results on such systems. They became possible after the implementation of the pressure stabilizer, described in chapter 3. Isothermal decompression experiments were also carried out, allowing for a two dimensional study of the DPPC-d_{62} phase diagram. Various phase boundaries were investigated together with some aspects of the formation of the ordered L_c and X phases.

Samples were prepared in the form of MLV suspensions of synthetic DPPC-d_{62} in excess 0.1M phosphate buffer (pH 7.2) which were heat sealed into flexible polyethylene tubes. A quadrupole echo sequence was used with a duration of the $\pi/2$ pulse between 2.35 μs and 2.55 μs, and a pulse separation of 35 μs. For each spectrum, between 8000 and 64000 transients were averaged. Free induction decays

were digitized at 2 μs per point in the liquid crystalline phase and at 1 μs per point in the ordered phases. Two times oversampling was performed [129, 152] to result in effective dwell times of 4 μs in the liquid crystalline phase and 2 μs in the gel phases. The temperature regulator was calibrated against a differential copper-constantan thermocouple and was found to be accurate to within 0.25°C. Pressure was measured with a Bourdon type gauge with a precision of 0.014 kbar and when checked against a dead weight gauge was found accurate to within 1%. All experiments were carried out as the temperature or the pressure were decreased in a stepwise fashion.

7.1.1 Results and discussion

The main transition in DPPC-d_{62} at ambient pressure was found to occur at around 37°C, in good agreement with previous measurements [22]. It is appropriate to mention that Morrow, Whitehead and Lu [22] used temperature equipment, thermocouple and ice-point compensated thermocouple amplifier different from the ones used in these experiments. The transition temperatures determined this way, are therefore not equipment dependent. Spectra obtained as the temperature is lowered from 40°C to 30°C through the ambient pressure main transition in 1°C steps are shown in Figure 7.1. Above 37°C, the spectra consist of superimposed Pake doublets and reflect fast axially symmetric molecular motions. Below this temperature, DPPC-d_{62} is in a $P_{\beta'}$ phase and the corresponding spectra between 36°C and 30°C are taken as being characteristic of this phase. The corresponding first spectral moments are shown in Figure 7.2. The spectrum at 37°C is a superposition of the two types of spectra, resulting from some local inhomogeneities of the samples. The central isotropic spike, seen in essentially all spectra, is produced by traces of HDO, present in the buffer, or by minute quantities of small nonvesicular lipid aggregates in the suspension.

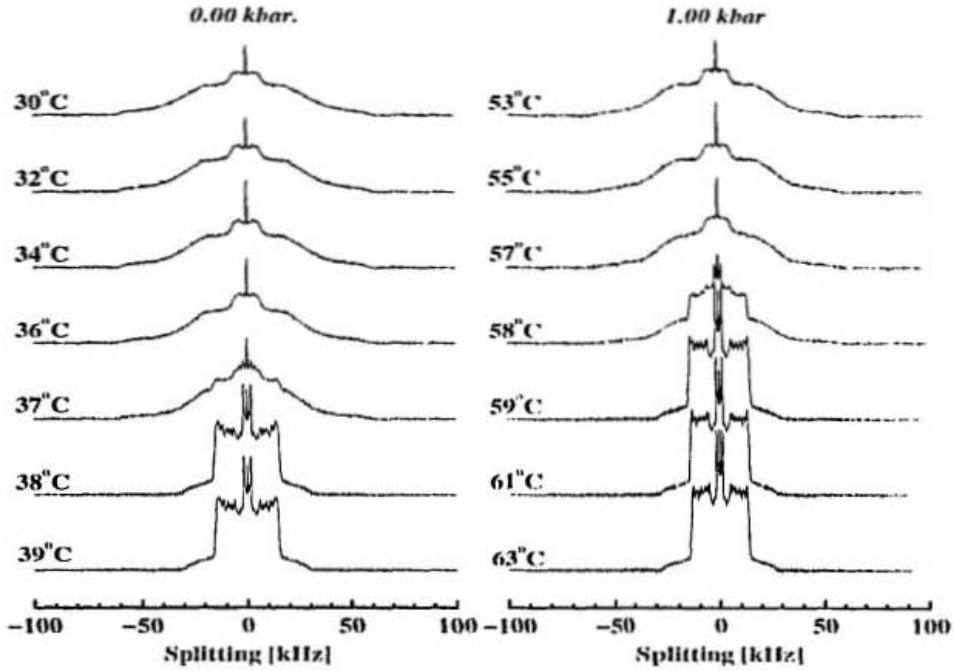

Figure 7.1: DPPC-d_{62} spectra around the main transition at ambient pressure (a) and 1 kbar (b).

Representative spectra from a cooling experiment around the main transition at 1 kbar are shown in Figure 7.1. The spectra above the transition, which occurs at 58°C for this pressure, are typical of the L_α phase. The maximum deuteron splittings are smaller than at ambient pressure, indicating the bilayer is less ordered at this pressure just above the transition, in analogy to the case of DMPC-d_{54}, discussed in chapter 5. This is also reflected in the lower M_1 value of about 50×10^3 s^{-1} in the liquid crystalline phase just above the 1 kbar transition as compared to almost 60×10^3 s^{-1} at the corresponding temperature for ambient pressure (Figure 7.2). The spectra below the transition at 1 kbar (Figure 7.1) are very similar to the ambient pressure $P_{\beta'}$ spectra of Figure 7.1, suggesting that DPPC-d_{62} at this pressure still undergoes a transition from L_α to $P_{\beta'}$. In Figure 7.4, each experiment is represented

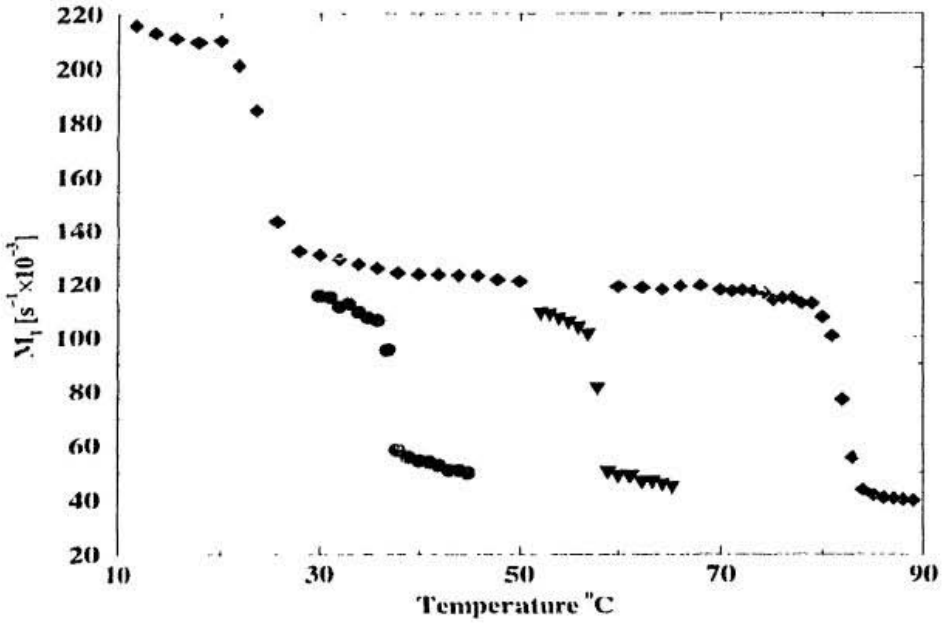

Figure 7.2: DPPC-d_{62} first moments vs. temperature at ambient pressure (circles), 1.00 kbar (inverted triangles) and 2.20 kbar (diamonds).

by an empty triangle pointing in the direction of temperature change for this series of spectra.

The thermotropic behaviour of DPPC-d_{62} at 2.2 kbar is more complex. Four phases are observed as the lipid is cooled down to 22°C. Spectra on both sides of each ordered phase to ordered phase transition are shown in Figure 7.3. The liquid crystalline phase persists down to 82°C. The transition from liquid crystal into an ordered phase is clearly seen as an increase in M_1 from approximately 45×10^3 s^{-1} to over 100×10^3 s^{-1} (Figure 7.2) at about 80°C. At 81°C the lipid enters an unusual phase with axially asymmetric motions and well pronounced spectral features at approximately ±25 kHz, as well as broad methyl splittings at almost ±10 kHz. This phase is suggested to be an interdigitated gel on basis of the close similarity between

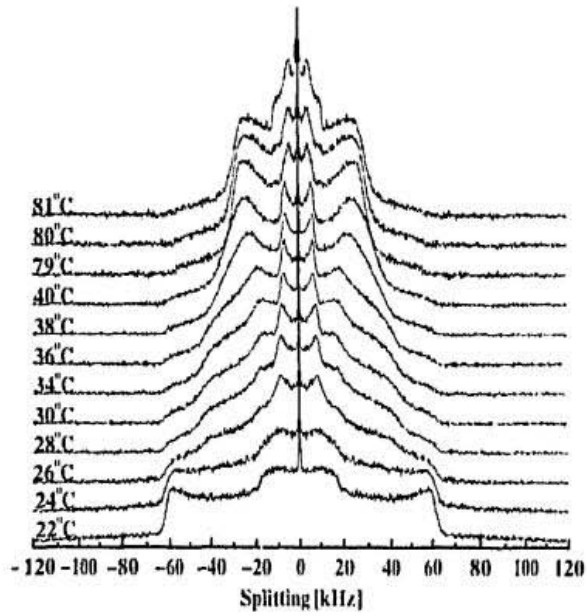

Figure 7.3: DPPC-d_{62} representative spectra at 2.2 kbar.

the spectra observed from 81°C to 38°C and spectra observed under conditions of alcohol-induced interdigitation in DPPC (M. Lafleur, private communication). Further confidence in such identification is provided by a comparison between the spectral features in this phase and the spectra obtained by isothermal compression of DPPC by Driscoll and coworkers [83]. Interdigitation is also observed in this region of the phase diagram by neutron diffraction [19, 90], FTIR spectroscopy [70, 72] and deuterium NMR of specifically labeled lipid [86].

At approximately 37°C, the DPPC-d_{62} spectral lineshape undergoes substantial changes. The intensity at ± 25 kHz decreases, giving rise to an unusual, generally triangular lineshape (Figure 7.3). Although the first spectral moments are continuous at this temperature, an upwards kink in their temperature dependence marks the transition (Figure 7.2). Isothermal measurements in this region of the DPPC

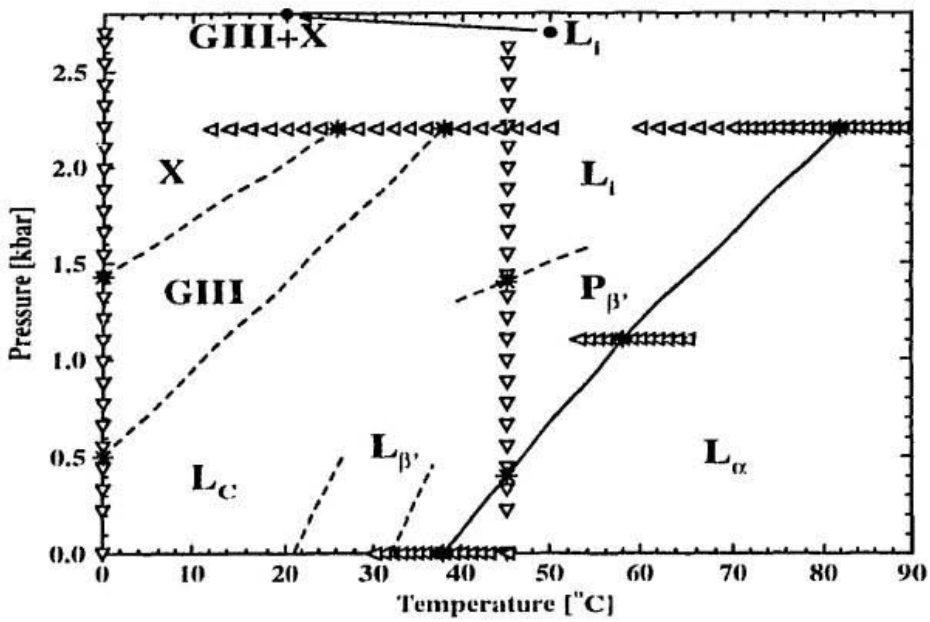

Figure 7.4: Transitions in the pressure/temperature phase space of DPPC. Experimental points are shown with triangles pointing in the direction of the change in the corresponding parameter. The solid line is the main transition. The individual transitions are shown with asterisks.

phase diagram allow us to identify the new phase as *GIII* [61, 83, 86]. It is interesting to note that the transition into the *GIII* phase occurs at about 8°C below the temperature extrapolated from constant temperature experiments with protcated DPPC [90]. At 24°C the first spectral moments undergo a major stepwise increase from about 130×10^3 s^{-1} to almost 210×10^3 s^{-1} (Figure 7.2), accompanied by a spectral change from the *GIII* lineshape to a fully ordered rigid lattice spectrum (Figure 7.3). This low temperature, high pressure phase appears in the same phase region as the *X* phase, observed in isothermal experiments [83, 86] or *GIV* phase [102, 97] (observed but unlabeled by Utoh and Takemura [56]). It displays the same deuterium NMR spectral features as the *X* phase [83]. Although little is know

about the exact nature, or indeed the distinctness, of the proposed ordered phases in DPPC, it has been suggested that they differ mainly in the type of packing of the almost fully extended acyl chains [103].

In addition to the isobaric experiments at ambient pressure, 1 kbar and 2.2 kbar, DPPC-d_{62} was studied under isothermal decompression at 0°C and 15°C. Selected spectra at the borders of the various phases are shown in Figure 7.5 and the corresponding first spectral moments are plotted as a function of pressure in Figure 7.6. Each of the isothermal experiments is represented by a downwards empty triangle on the DPPC-d_{62} phase diagram (Figure 7.4). The experiment at 45°C was started by isothermal compression to 2.62 kbar, well into the interdigitated phase. Spectra were collected as the pressure was lowered in a stepwise fashion to ambient pressure. At approximately 1.43 kbar the L_i spectra change to the kind of lineshape, typical of the $P_{\beta'}$ phase, observed at ambient pressure below 37°C. This phase transition is also indicated by the change in slope of M_1 vs. pressure (Figure 7.6). Extrapolation from constant temperature experiments on protcated DPPC [90] at the same pressure shows a transition approximately 8°C higher than is observed here. This is probably due, in part, to the isotope substitution in the present study. An abrupt drop in M_1 at 0.4 kbar marks the onset of a liquid crystalline phase. The spectral lineshape below this pressure is typical of a fast axially symmetric molecular motion (Figure 7.5).

Another section of the phase diagram was sampled as the pressure was lowered from 2.7 kbar to ambient at 0°C. Under these conditions, DPPC-d_{62} undergoes two phase transitions. Representative spectra around the phase transitions are shown in Figure 7.5 and the corresponding first moments are plotted in Figure 7.6. The high edges at ±63 kHz in the spectrum at 2.7 kbar (Figure 7.5), as well as the very high values of M_1, indicate that the lipid system is in a highly ordered phase with

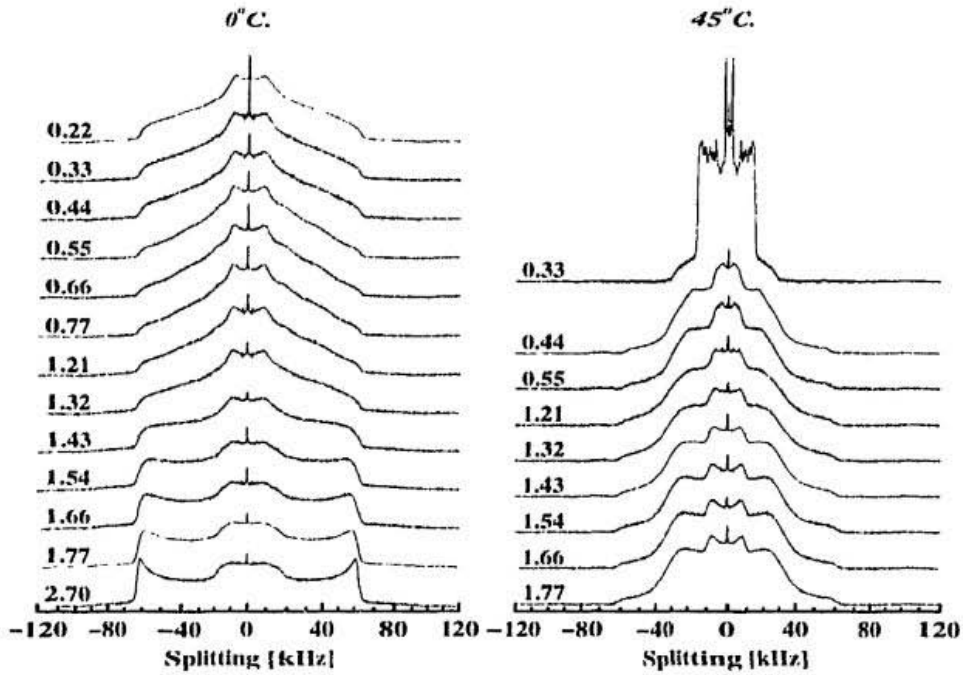

Figure 7.5: DPPC-d_{62} spectra as a function of pressure at 0°C and 45°C. Pressure is indicated in kbar next to each spectrum.

essentially completely frozen molecular motions. Spectra in this phase resemble very much the spectra observed by Driscoll and coworkers [83] in the X phase. This high pressure, low temperature phase has been previously observed by other methods as well [56, 97, 102].

As the pressure is lowered through 1.43 kbar, at 0°C, the DPPC-d_{62} spectra acquire features typical of the $GIII$ phase discussed in connection with the isobaric experiment at 2.2 kbar. The various steps in the spectral lineshape reflect differences in the local environment of the deuterons along the acyl chains [86]. A substantial reduction in M_1 at this pressure also indicates the onset of the $GIII$ phase (Figure 7.6).

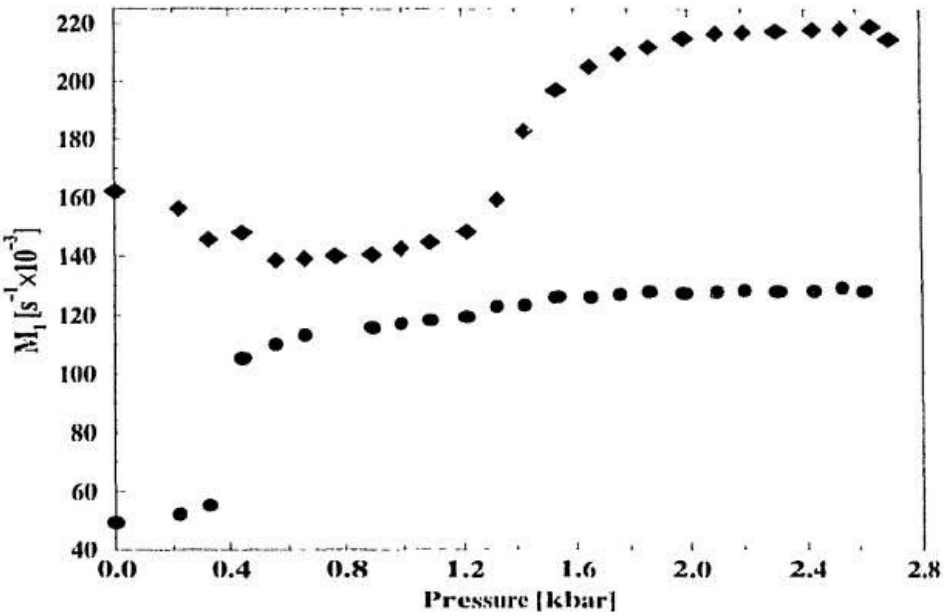

Figure 7.6: DPPC-d_{62} M_1 as a function of pressure at 0°C (diamonds) and 45°C (circles).

At approximately 0.5 kbar the lipid enters the crystalline (L_c) phase. The spectral lineshape in this phase is roughly trapezoidal with shoulders, extending to relatively high intensity edges at ±63 kHz. It is interesting to note that intensity at maximum splitting actually increases as pressure is decreased. A concomitant increase in M_1 below the transition also reflects the intensity increase at maximum splitting (Figure 7.6). In light of the discussion of DLPC-d_{46} crystalline phase metastability (chapter 6) and the ambient pressure metastability of the crystalline phase [18], exceptional caution must be exercised in assigning phase boundaries to this phase. At ambient pressure, formation of the crystalline phase requires incubation at low temperatures for more than a day. The observed increase in M_1 with decreasing pressure may thus reflect a kinetic process, rather than changes between

equilibrium states. Another interesting observation is that it is possible to obtain the crystalline phase as a result of a relatively fast compression-decompression cycle through the $GIII$ (and possibly the X) phase as an alternative to the lengthy low temperature annealing at ambient pressure. The phase identification is based on the observation that the spectrum at ambient pressure and 0°C following the pressure scanning experiment is essentially indistinguishable from the spectrum obtained from a DPPC-d_{62} sample after a prolonged ambient pressure incubation at sub-zero temperature.

An interesting way of following the changes in the spectral lineshape as the pressure is lowered from 2.7 kbar to ambient is illustrated in Figure 7.7. The spectra of Figure 7.5(a) are overlapped, allowing the most prominent spectral changes to stand out. The most dramatic spectral changes across the transitions $X \rightarrow GIII$ and $GIII \rightarrow L_c$ take place in the frequency regions between 40 and 63 kHz and between 10 and 20 kHz. Spectral intensity decreases from the sharp cusp-like features at $\pm$63kHz in the X phase to a minimum in the $GIII$ phase, with a subsequent increase in the L_c phase. Intensity around 20 kHz increases from a minimum in the X phase until reaching its highest value in the $GIII$ phase, then it decreases in the crystalline phase. This type of plot proves very useful in tracing subtle changes in the spectral lineshapes.

At ambient pressure the L_c phase is the most ordered DPPC phase detected in these experiments. The roughly trapezoidal lineshape suggests, though, that some residual motional freedom is still present in this phase. In contrast, the X phase at high pressure and low temperature is distinguishable by very high intensity at maximum splitting. This resembles the behaviour expected from completely immobilized deuterons in a powder sample. One possibility is that this phase results from a pressure-induced partial dehydration of the bilayer. Spectra with features,

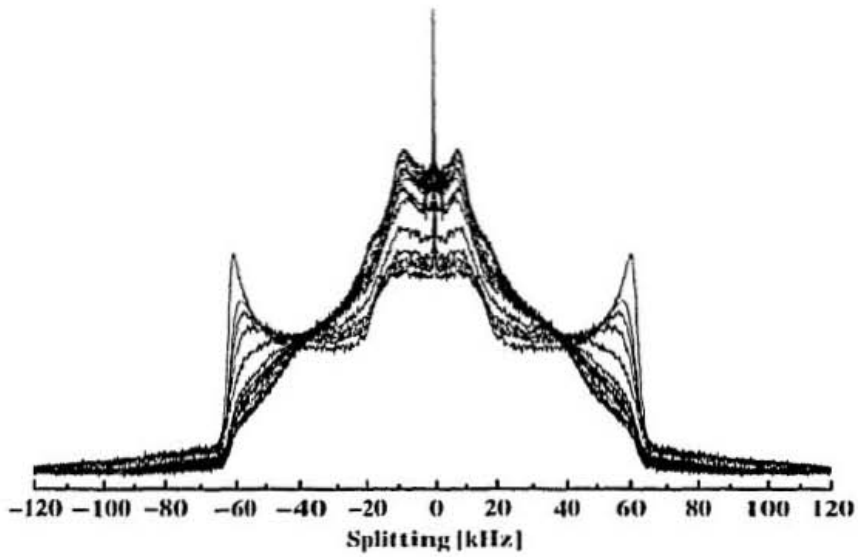

Figure 7.7: Overlapped DPPC-d_{62} spectra during decompression at 0°C. Pressure was decremented in steps of 0.11 kbar.

resembling these of the X phase spectra, have also been observed at ambient pressure and low temperature [20].

All experiments are summarized schematically in a phase diagram-type plot (Figure 7.4). Figure 7.8 shows representative spectra from all phases. In its general appearance this phase diagram agrees with earlier observations [19, 56, 61, 83, 86, 90, 97]. The individual experiments at a fixed value of either temperature or pressure are shown as triangles, pointing in the direction of variation of the corresponding parameter. Different phases are labeled in boxes, located approximately in the middle of the phase region according to the nomenclature used in this text. The phase transitions, identified as described earlier, are shown as asterisks on the tracks of the individual experiments. The arrows next to the transitions show the direction

of the phase change, together with identification of the initial and the final phases. Linear extrapolations are used to schematically represent the topology of the phase boundaries. The low temperature border of the L_α phase is rather well defined and is thus shown with a solid line. The slope of this line as the pressure is increased from ambient to 1 kbar appears to be slightly different from the slope above 1 kbar. This may reflect the fact that DPPC-d_{62} undergoes a transition into the $P_{\beta'}$ phase up to at least 1 kbar, while at 2.2 kbar it enters the L_i phase directly.

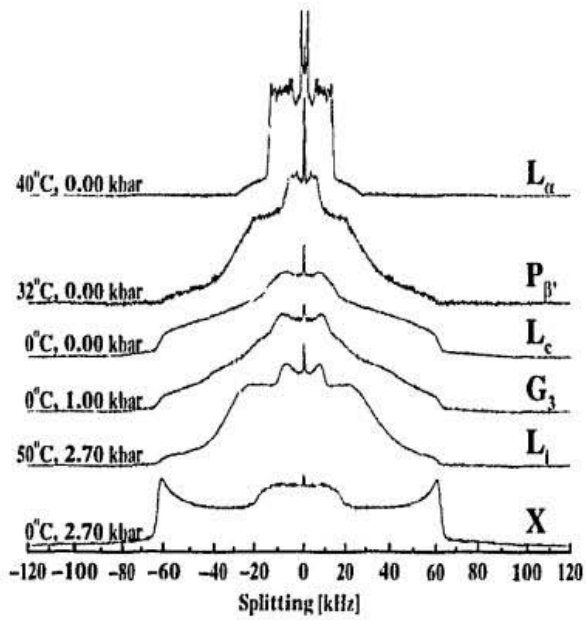

Figure 7.8: Representative deuterium NMR spectra in the various DPPC phases identified in this experiment.

Two additional transitions from the L_i phase, one isobaric into the $GIII$ phase and one isothermal into the $P_{\beta'}$ phase, are used to obtain a general idea about the extension of the interdigitated gel. Additional measurements are necessary for a reliable description of the phase boundary, which may possibly contain triple points

L_i, $P_{\beta'}$, $L_{\beta'}$, or L_i, $L_{\beta'}$, *GIII* [61, 97, 83].

The phase boundary between the *GIII* and the L_c phases is also unclear as a consequence of the observation that, at 2.2 kbar, DPPC-d_{62} enters the *GIII* phase via a temperature transition from the L_i phase, while the lipid leaves the *GIII* phase into a different phase, the L_c phase, upon decompression at 0°C. Moreover, as a result of the L_c phase metastability, a transition into the *GIII* phase is observed under isothermal compression from the $L_{\beta'}$ phase [61, 97, 83, 86]. Nevertheless, the high temperature boundary of the *GIII* phase is in reasonable agreement with previous measurements [56, 97].

The last phase boundary in this diagram separates the *X* phase from the *GIII* phase. It is described by two transition points, one at 2.2 kbar from the *GIII* phase into the *X* phase and one at 0°C from the *X* phase into the *GIII* phase. The use of a dashed line in Figure 7.4 reflects the fact that the transition into the *X* phase is probably largely dominated by the kinetics of the phase conversion rather than reflecting the relative stability of the two phases. This may, as well, be the reason behind some differences between these and previous results [83]. To illustrate the effect of transition kinetics, the lipid suspension was rapidly brought well into the expected *X* phase region in an additional experiment (Figure 7.4, solid circles). Initially the sample was equilibrated in the liquid crystalline phase at 45°C and ambient pressure for 30 minutes. Then it was compressed isothermally to 0.44 kbar in the $P_{\beta'}$, where it was annealed for an additional hour. A subsequent compression to 2.75 kbar and heating to 50°C resulted in an interdigitated gel phase after the lipid was equilibrated for approximately two hours. A subsequent cooling to 20°C over approximately two hours was followed by equilibration for 45 minutes. The pressure was increased to 2.82 kbar. The spectrum collected under these conditions revealed features suggesting an overcooled *GIII* phase. Over a period of 8 hours,

no substantial changes in the spectrum were observed, suggesting that under these pressure and temperature conditions, lipid reorganization is slow.

7.1.2 Summary

The effect of high pressure on DPPC-d_{62} bilayer phase behaviour was studied under isothermal decompression conditions, and for the first time, under isobaric cooling. Besides the ambient pressure thermotropic phases, a number of high pressure phases were observed. The temperature of the transition from fluid into more ordered phases was found to increase with pressure at approximately 21°C per kbar. At 2.2 kbar the lipid underwent an isobaric transition from L_α directly into an interdigitated L_i phase. Upon further cooling, DPPC was converted into a high pressure gel $GIII$ phase, which in turn underwent a transition into a completely ordered X phase. Partial decompression restored the $GIII$ phase. Complete removal of pressure resulted in a crystalline (L_c) phase, otherwise achievable by long term incubation at low temperature. This suggested a fast way of obtaining the crystalline phase via a compression-cooling-decompression cycle. The X and the L_c phases were characterized by very slow molecular dynamics, dominating the transitions into these phases.

7.2 Membrane Cholesterol

Cholesterol is a polycyclic alcohol, found in most higher animal cell membranes. It plays an important role as a precursor to a number of hormones and bile salts in mammals [132]. The physical properties of diacyl PC/cholesterol mixtures, in the form of model membranes, have been studied extensively by a variety of methods [162-174]. A phase diagram of eutectic [173, 175] type for the system DPPC/cholesterol has been determined from NMR, DSC and EPR experiments

[165, 167, 170, 171, 173, 175] and has also been predicted theoretically [176 180]. The liquid disordered phase at zero cholesterol concentration coincides with the high temperature phase of the pure lipid (l_α). Upon increasing cholesterol concentration at temperatures close to and above the pure lipid main transition temperature, the lipid system presumably crosses a two phase coexistence region as it enters a fluid ordered (l_o) phase. In the l_o phase, the molecular motions are axially symmetric, but the width of the powder pattern is substantially increased as are the deuteron first spectral moments for the lipid. Below the pure lipid transition temperature the bilayer exists in its gel phase up to about 5 mil % cholesterol. From 5 mol % to 25 mol % the lipids are in a two phase gel l_o coexistence region. Beyond 25 mol %, the bilayer is in the l_o phase.

At 30 mol % cholesterol in DPPC-d_{62}, the system is in a liquid ordered phase over a very broad range of temperatures [175]. Application of hydrostatic pressure has been observed to have an ordering effect on a DMPC/cholesterol system [72, 89]. The main issues addressed in the present study are: firstly, what effect does pressure have on the DPPC/cholesterol phase behaviour; secondly, does cholesterol, under high pressure, remain in the DPPC bilayer, which is known to be more ordered than the DMPC bilayer at corresponding temperatures [22]; and thirdly, does cholesterol impede the formation of an interdigitated gel, which is more easily formed in DPPC in comparison to DMPC.

Samples of 28.5 mol % cholesterol in DPPC were prepared by mixing the two lipids in chloroform solution, then evaporating the solvent under dry nitrogen flow over approximately 10 hours. After the solvent was removed the lipid mixture was vacuum-dried for 4-5 hours. Suspensions of MLV were prepared by hydration in 0.1 M phosphate buffer (pH 7.2). The lipid-buffer compositions were subsequently transferred into polyethylene tubes and heat-sealed. A standard quadrupole echo

sequence was used with $\pi/2$ pulse duration between 2.35 and 2.4 μs. The pulse separation used throughout all experiments was 35 μs, except for the relaxation measurements. Transverse relaxation times, T_{2e}, were extracted from the decrease of the spectral area as the pulse separation was varied between 20 μs and 600 μs. The decay time of the quadrupole echo amplitude gave very similar results. Each spectrum was obtained by averaging of between 8000 and 72000 free induction decays. Oversampling was used [129], resulting in effective dwell time of 2 μs.

7.2.1 Results and Discussion

A MLV suspension of 28.5 mol % cholesterol in chain perdeuterated DPPC-d_{62} was studied with deuterium NMR at ambient and elevated pressure, as well as at a fixed temperature as the pressure was varied. At ambient pressure, experiments were carried out between 50°C and 0°C as the temperature was decremented in 3°C steps with equilibration of approximately 20 to 30 minutes prior to collection of each free induction decay. Spectra consist of superimposed Pake powder doublets which gradually broaden as the temperature is decreased to approximately 20°C. At lower temperatures, the DPPC-d_{62} lineshape loses its axially symmetric features in a continuous way. This is in accord with a previous observation of a very broad feature in the thermograms of 30 mol % cholesterol in DPPC [178]. At 0°C the individual doublets are indistinguishable and the spectrum becomes more and more similar to a pure lipid gel spectrum with a vestige of an axially symmetric shape. The first spectral moments (Figure 7.10, empty circles) are much higher in this case than the corresponding values in the liquid crystalline phase of pure DPPC (solid circles) at the same temperature, yet they remain lower than M_1 in the DPPC $P_{\beta'}$ phase. This behaviour is consistent with earlier measurements [162, 166, 167, 170, 172, 174, 175].

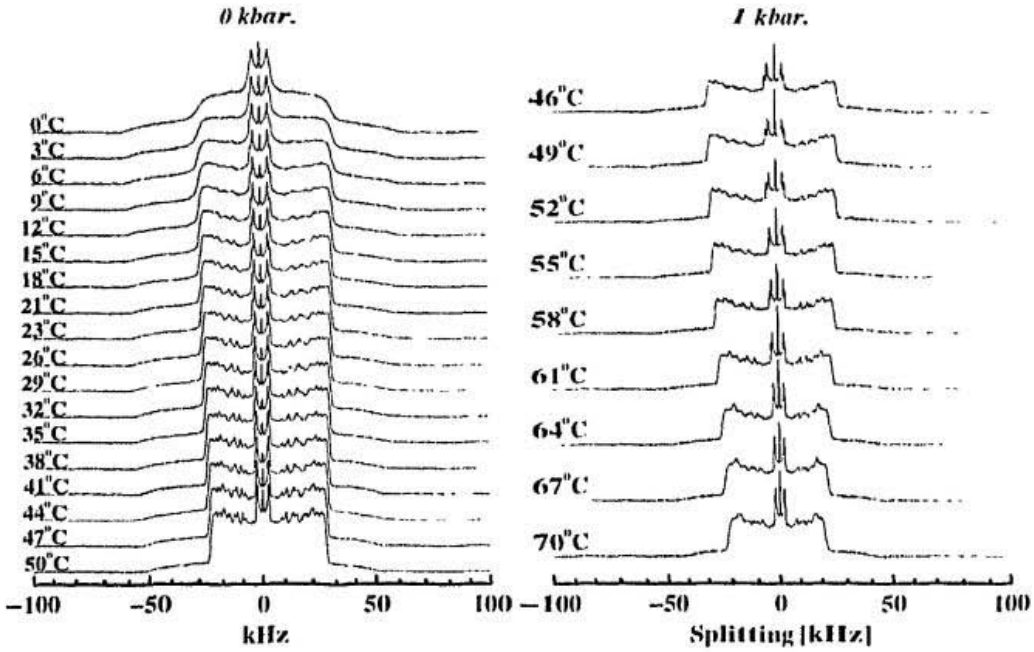

Figure 7.9: Representative deuterium NMR spectra of 28.5 mol % cholesterol in DPPC-d_{62} at ambient pressure (left) and 1 kbar (right).

Hydrostatic pressure of 1 kbar was applied to the DPPC-d_{62}/cholesterol suspension and spectra were collected as the temperature was lowered in steps of 3°C from 70°C to 46°C. Higher M_1 values and broader spectra suggest that pressure has an ordering effect on the phosphatidylcholine chains (Figure 7.10). Spectra of DPPC d_{62} with 28.5 mol% cholesterol are shown in Figure 7.9 for ambient pressure and 1 kbar. Near the pure lipid transitions, corresponding to each pressure, there are no qualitative differences between the effect of temperature on the spectra at 1 kbar and at ambient pressure.

Figure 7.11 shows the spectra of the DPPC/cholesterol mixture as the system was cooled from 78°C to 42°C at 2.1 kbar. The bilayer at this pressure is in the liquid ordered phase down to almost 65°C. Between 63°C and 45°C the DPPC/cholesterol

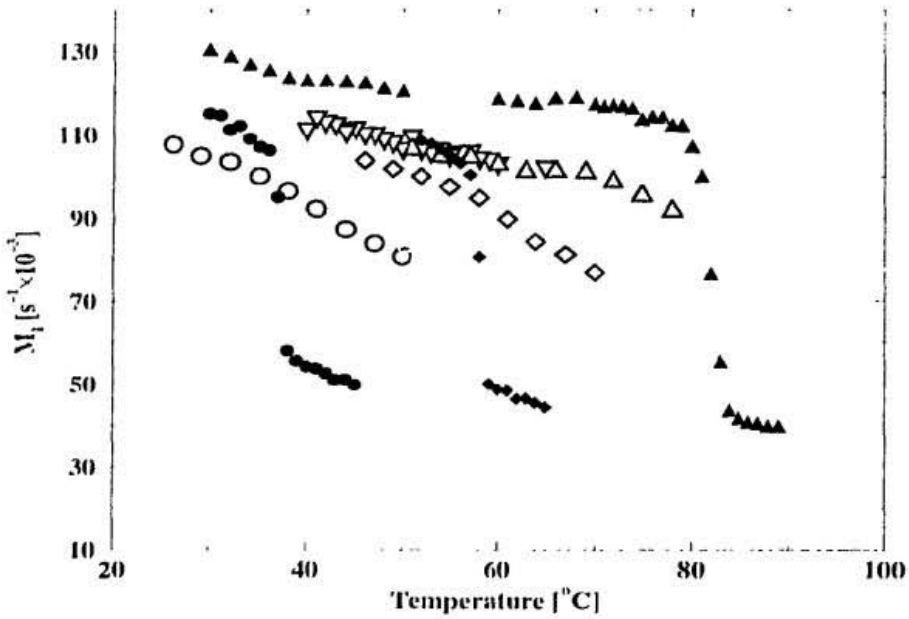

Figure 7.10: First spectral moments for pure DPPC-d_{62} (solid symbols) and 28.5 mol % cholesterol in DPPC-d_{62} (open symbols) at ambient pressure (circles), 1 kbar (diamonds) and 2.2 kbar (triangles) (2.1 kbar for the mixture).

system undergoes a continuous phase change to a gel phase. The spectra in this gel phase (Figure 7.11) closely resemble the lineshapes observed in the $P_{\beta'}$ phase of the pure lipid bilayer (Figure 7.1(a)). At ambient pressure the border between the liquid ordered phase and the gel-l_o two phase region of the PC/cholesterol phase diagram [175] is almost vertical and falls between 20 and 25 mol % cholesterol in the bilayer. At a cholesterol concentration of 28.5 mol % therefore, the gel phase could be observed only at very low temperature. This is largely the case with the present ambient pressure experiment: cooling down to 0°C preserves the axial symmetry of the molecular motions with only a hint of a gel subphase at 0°C (Figure 7.9). At 2.1 kbar the sample is in a l_o phase above 70°C. As the temperature is lowered to

42°C it undergoes a continuous phase change to a gel phase (Figure 7.11). Thus elevated pressure appears to favour somewhat the formation of gel phase over the l_o phase.

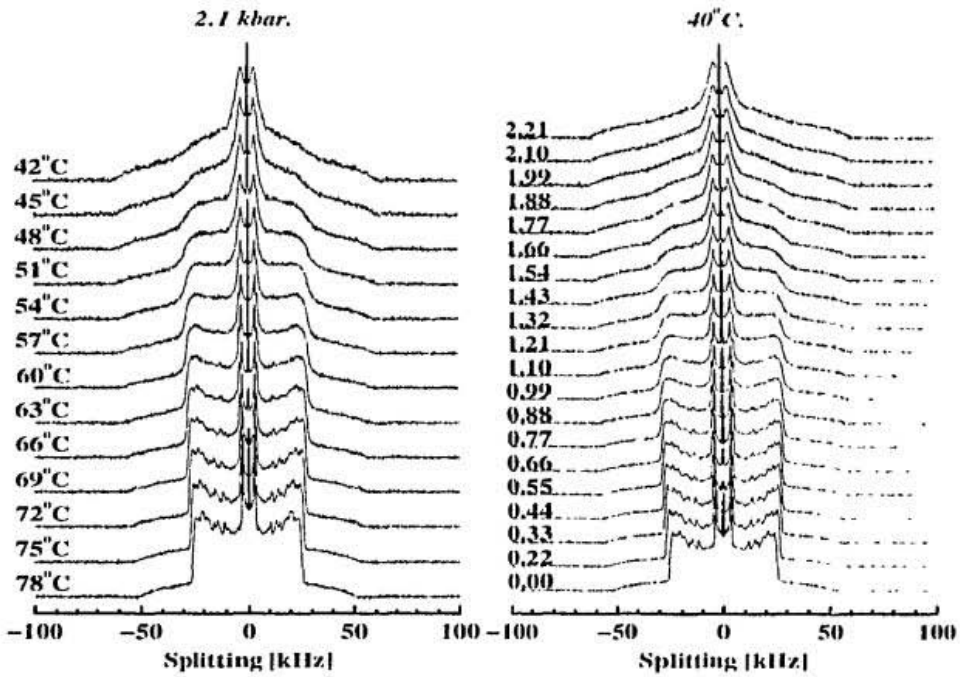

Figure 7.11: Representative deuterium NMR spectra of 28.5 mol% cholesterol in DPPC-d_{62} at 2.1 kbar as the temperature was varied (a) and at 40°C as the pressure was varied (b). Pressure is shown in kbar next to each spectrum.

Probably the most striking result from the isobaric experiment at 2.1 kbar is the suppression of the bilayer interdigitation, observed under like conditions in the pure lipid system (Figure 7.3). A concentration of 30 mol % cholesterol has been observed to inhibit pressure-induced interdigitation in DMPC [72] and alcohol-induced interdigitation in DPPC [98]. Figure 7.11(a) shows axially symmetric spectra with width increasing as the temperature is decreased at 2.1 kbar. The spectral lineshape gradually changes to one characteristic of a gel phase. The behaviour of the first spectral

moments with temperature (Figure 7.10, empty triangles) is continuous, with only a slight change in the slope of M_1 versus temperature indicating the occurrence of the gel phase. First moments for pure DPPC-d_{62} at 2.2 kbar are shown throughout the L_α, L_i and $GIII$ phases (Figure 7.10, solid triangles) as a reference.

The above observations on the phase behaviour of the PC/cholesterol system lead to the very important conclusion that cholesterol remains in the membrane even at 2.1 kbar.

A heating experiment was carried out at 2.1 kbar between 46°C and 65°C in 5°C intervals. The temperature behaviour of the system over this interval was found to be completely reversible.

A decompression experiment was performed at 40°C between 2.21 kbar and ambient pressure. As the pressure was lowered in steps of 0.11 kbar, the samples were allowed to reach equilibrium for 20 to 30 minutes per point prior to spectral acquisition. The corresponding spectra are shown in Figure 7.11(b). The spectrum at 2.21 kbar at 40°C again closely resembles the spectra of the $P_{\beta'}$ phase in pure DPPC. The spectra below 1 kbar can be considered as characteristic of the fluid phase and the spectra above 2 kbar are typical of the gel phase. The DPPC/cholesterol system undergoes a continuous phase change between these two pressures.

The first spectral moments for the pressure experiment are shown in Figure 7.12 as a function of pressure together with the corresponding transverse relaxation times. As the pressure is lowered, M_1 decreases in a continuous fashion, displaying a region of almost constant values between 0.75 kbar and 1.25 kbar. A concomitant increase in T_{2e} is observed, although this increase is slightly shifted towards lower pressures. In the gel phase T_{2e} is essentially constant and M_1 decreases monotonically with decreasing pressure.

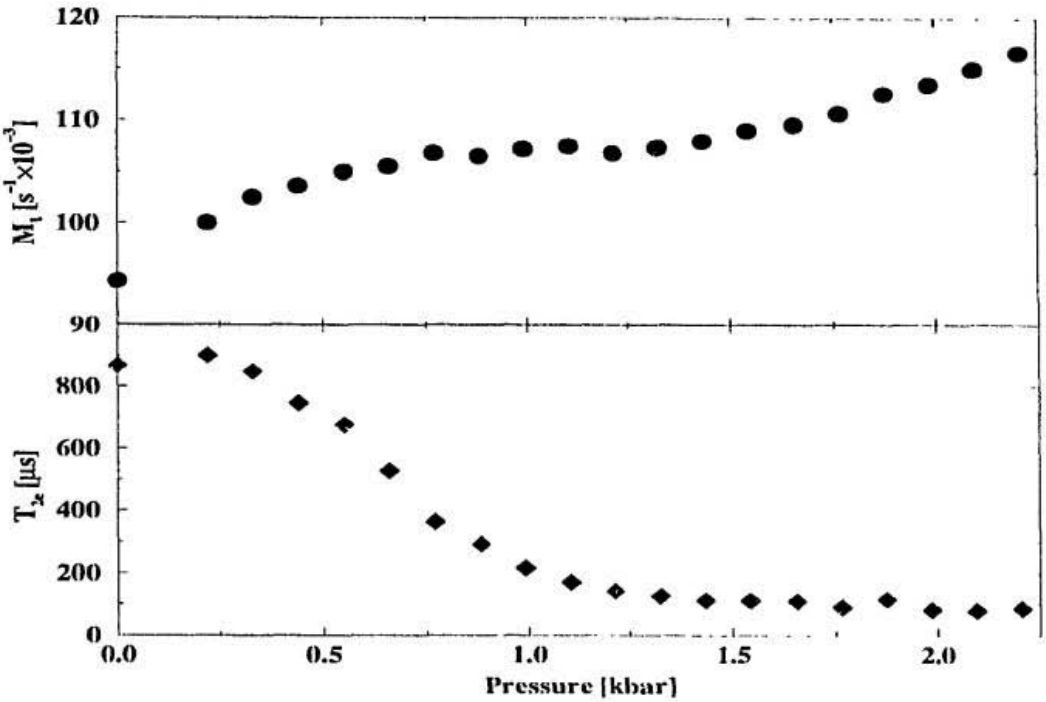

Figure 7.12: First spectral moments and transverse relaxation times, T_{2c}, of 28.5 mol % cholesterol in DPPC-d_{62} as a function of pressure at 40°C.

7.2.2 Summary

Cholesterol orders the DPPC fluid phase and disorders its gel phase both at low and elevated pressure. Addition of 28.5 mol % cholesterol to a DPPC-d_{62} membrane removes the sharp transition observed in pure phosphatidylcholine at ambient pressure. A pure gel phase is formed below 45°C when the PC/cholesterol system is cooled at 2.1 kbar. When compressed to 2.21 kbar at 40°C the resulting state of the lipid mixture is again a pure gel. Upon isothermal decompression this gel phase is converted into a fluid ordered phase in a continuous fashion. It can be concluded, therefore, that hydrostatic pressure affects very little the continuous character of the DPPC/cholesterol mixture at the above concentration. Measurements of the transverse relaxation rates indicate a continuous change in the molecular dynamics

throughout this region from higher relaxation rates, which are typical of the high pressure gel phase, to lower rates, which are observed in the low pressure fluid phase. Within the high pressure phase the transverse relaxation rate is essentially constant over the observed pressure interval. Cholesterol at a concentration of 28.5 mol % prevents the formation of a high pressure interdigitated gel, which is the stable phase of DPPC at 2.2 kbar. It is concluded that, even at pressures as high as 2.2 kbar, cholesterol is not excluded from the phospholipid bilayer.

Chapter 8

Concluding Remarks

The properties of an important class of biomolecules, the phospholipids, were studied under hydrostatic pressure. Various aspects of the molecular behaviour of three diacylphosphatidylcholines with 12, 14 and 16 carbons in their chains were investigated at pressures between ambient and 2.7 kbar and temperatures between −20 and 80°C. A special beryllium copper probe was designed and built, allowing for deuterium NMR measurements to be carried out under such a wide range of experimental conditions. In addition to its ability to operate at constant temperature, the new probe is equipped with a pressure stabilizer, allowing for experimentation under isobaric conditions. Simple design and operation, low cost, modular coil design and plastic-encapsulated lipid samples are some of the main features of the device. The probe was used in a 3.5 T wide-bore superconducting magnet with a locally constructed solid state spectrometer [128].

The chain region of all three phospholipids was studied under a variety of pressure and temperature conditions. Pressure was found to have an ordering effect on the acyl chains at constant temperature. As a result of this, the thickness of the hydrocarbon region was found to increase with pressure. This corresponds to a decrease in the bilayer area per molecule.

Headgroups were found to respond to a decrease in molecular area by tipping of the whole choline moiety away from the bilayer surface. Conformational changes in response to increasing or decreasing molecular area were observed as a result of variation of both temperature and pressure. The headgroup tilt produced by lateral

compression was found to be very similar to the conformational changes resulting from the presence of a bilayer surface charge. The response of the headgroups to changes in molecular area can thus be used as a molecular probe, or indicator for following such changes. The pressure-induced headgroup tilt towards the bilayer normal, together with the increase in the hydrophobic region thickness, suggest an overall increase in the membrane thickness.

Elevated pressure was found to increase the discontinuity across the main transition of some bilayer properties, such as orientational order, bilayer thickness and area per lipid molecule, enhancing in this way the first order character of the transition. When pressure was increased at constant temperature, the main transition was observed to display stronger first order characteristics at the higher transition temperatures. These were taken as an indication that high pressure suppresses the role of thermodynamic fluctuations and drives the main transition away from a critical point. An interesting consequence of this is the faster change in bilayer area per molecule in the vicinity of the transition for DPPC than for DMPC at the same temperature. As a result, the headgroup conformational changes in DPPC headgroups are more pronounced than in DMPC.

A simple phenomenological model [22], based on a Landau expansion of the free energy, was used for comparison between the elevated and the ambient pressure properties of the bilayer. Analysis based on this model provided additional support to the suggestion that the bilayer moves away from a critical point with increasing pressure.

Hydrostatic pressure was observed to affect the temperature of the various lipid phase transitions in different ways. The main transition in DMPC was found to be more sensitive to pressure than the subtransition. In DLPC, high pressure was also found to decouple the two transitions between the liquid crystalline, the gel and

the crystalline phases, which overlap at ambient pressure, thereby allowing a gel phase to be observed over a finite temperature interval. A region of slow molecular dynamics was observed at the lower temperature end of the liquid crystalline phase. This region was identified as the L_x phase, recently observed by Hatta and coworkers [36] at ambient pressure. Both the gel and the L_x phase were found to be metastable with respect to the crystalline phase.

In DPPC the difference in sensitivity to pressure of the various phase transitions leads to the observation of a number of new phases at elevated pressure. The crystalline (L_c) phase was shown to be characterized by very slow molecular dynamics and all motions in the X phase were practically frozen. Metastability of the phases adjacent to the boundaries of the (L_c) and the X phases was suggested. When cooled at 2.2 kbar, DPPC was found to enter an interdigitated gel (L_i) directly from the liquid crystalline (L_α) phase. A new faster method for obtaining a crystalline (L_c) phase by isothermal decompression was proposed.

Addition of cholesterol to the DPPC membrane was shown to fluidize the bilayer even at pressures as high as 2.2 kbar. The high pressure phase behaviour of 28.5 mol % cholesterol/DPPC mixture was described as a continuous change from a liquid ordered to a gel phase. No indication of phase separation or domain formation was found. Cholesterol was found to remain in the bilayer even at 2.2 kbar. Cholesterol was also found to completely prevent the formation of a high pressure interdigitated gel (L_i).

This work provides valuable information on the pressure behaviour of phospholipids, as well as new insights into a number of their ambient pressure properties from the perspective of another thermodynamic dimension. It lays the foundation for future studies of various types of soft materials and in particular membrane lipids, their diffusion properties and lipid-lipid and lipid-protein interactions.

Bibliography

[1] Ceve G. and Marsh D. Phospholipid Bilayers. John Wiley & Sons, Inc., New York, 1987.

[2] Bloom M., Evans E., and Mouritsen O.G. Q. Rev. Biophys., **24**:293-397, 1991.

[3] Yeagle P.L. The Membranes of Cells. Academic Press, Inc., San Diego, 1993.

[4] Lehninger A.L., Nelson D.L., and Cox M.M. Principles of Biochemistry. Worth Publishers, Inc., New York, 1993.

[5] Marsh D. Handbook of Lipid Bilayers. CRC Press, Inc., Boca Raton, 1990.

[6] Yeagle P. The Structure of Biological Membranes. CRC Press, Inc., Boca Raton, 1992.

[7] Seddon J.M. and Ceve G. Phospholipids Handbook, page 403. Marcel Dekker, Inc., New York, 1993.

[8] Luzzati V. Biological Membranes, volume 2, pages 71-123. Academic Press, London, 1968.

[9] Chapman D., Williams R.M., and Ladbrooke B.D. Chem. Phys. Lipids, **1**:445, 1967.

[10] Powers L. and Pershan P.S. Biophys. J., **20**:137, 1977.

[11] Janiak M.J., Small D.M., and Shipley G.G. J. Biol. Chem., **254**:6068-6078, 1979.

[12] Seddon J.M., Cevc G., Kaye R.D., and Marsh D. Biochemistry, **23**:2634, 1984.

[13] Hauser H., Pascher I., Pearson H., and Sundell S. Biochim. Biophys. Acta, **650**:21–51, 1981.

[14] Flory P.J. Statistical Mechanics of Chain Molecules. John Wiley & Sons, Inc., New York, 1969.

[15] Seelig A. and Seelig J. Biochemistry, **13**:4839–4845, 1974.

[16] deGennes P.G. and Prost J. The Physics of Liquid Crystals. Oxford University Press, New York, 1993.

[17] Petrov A.G., Todorov A.T., Bonev B.B., Blinov L.M., Jablonski S., Fubaheyus D.B., and Tsvetkova N. Proc. IInd Intl. Conf. Ferroelectrics, Goetheborg, Sweden, , 1990.

[18] Cevc G. and Seddon J.M. Phospholipids Handbook, page 351. Marcel Dekker, Inc., New York, 1993.

[19] Braganza L.F. and Worcester D.L. Biochemistry, **25**:2591–2596, 1986.

[20] Davis J.H. Biophys. J., **27**:339–358, 1979.

[21] MacKay A.L. Biophys. J., **35**:301–313, 1981.

[22] Morrow M.R., Whitehead J.P., and Lu D. Biophys. J., **63**:18–27, 1992.

[23] Madelmont C. and Perron R. J. Colloid Interface Sci., **95**:471–472, 1983.

[24] Doniach S. J. Chem. Phys., **68**:4912–4916, 1978.

[25] Pink D., Georgallas A., and Zuckermann M.J. Z. Physik B Condensed Matter. **40**:103 110, 1980.

[26] Jähnig F. Biophys. J., **36**:329 345, 1981.

[27] Hatta I., Suzuki K., and Imaizumi S. J. Phys. Soc. Japan. **50**:2790 2797. 1983.

[28] Hatta I., Suzuki K., and Akutsu Y. J. Phys. Soc. Japan. **53**:882 888, 1984.

[29] Lemmich J., Mortensen K., Ipsen J.H., Honger T., Bauer R., and Mouritsen O. Phys. Rev. Let., **75**:3958 3961, 1995.

[30] Nagano H., Nakanishi T., Yao H., and Ema K. Phys. Rev. E, **52**:4244 4250, 1995.

[31] Finegold L. and Singer M.A. Biochim. Biophys. Acta, **855**:417–420. 1986.

[32] Morrow M.R. and Davis J.H. Biochim. Biophys. Acta, **904**:61–70, 1987.

[33] Lewis R.N.A.H., Mak N., and McElhaney R.N. Biochemistry, **26**:6118 6126. 1987.

[34] Lewis R.N.A.H and McElhaney R.N. Biochemistry, **29**:7946 7953. 1990.

[35] Finegold L., Shaw W.A., and Singer M.A. Chem. Phys. Lipids, **53**:177 184. 1990.

[36] Hatta I., Matuoka S., Singer M.A., and Finegold L. Chem. Phys. Lipids, **69**:129 136, 1994.

[37] Ruocco M.J. and Shipley G.G. Biochim. Biophys. Acta, **961**:309 320. 1982.

[38] Büldt G., Gally H.U., Seelig J., and Zaccai G. J. Mol. Biol., **134**:673 691, 1979.

[39] Seelig J., Macdonald P.M., and Scherer P.G. Biochemistry, **26**:7535 7541, 1987.

[40] Gally H.-U., Niederberger W., and Seelig J. Biochemistry, **14**:3674 3652, 1975.

[41] Akutsu H. and Seelig J. Biochemistry, **20**:7366 7373, 1981.

[42] Macdonald P.M. and Seelig J. Biochemistry, **27**:6769 6775, 1988.

[43] Dempsey C., Bitbol M., and Watts A. Biochemistry, **28**:6590 6596, 1989.

[44] Kuchinka E. and Seelig J. Biochemistry, **28**:4216 4221, 1989.

[45] Scherer P.G. and Seelig J. Biochemistry, **28**:7720 7728, 1989.

[46] Roux M., Neumann J.-M., Hodges R.S., Devaux P.F., and Bloom M. Biochemistry, **28**:40, 1989.

[47] Roux M. and Bloom M. Biochemistry, **29**:7077 7089, 1990.

[48] Macdonald P.M., Leisen J., and Marassi F. Biochemistry, **30**:3558 3566, 1991.

[49] Marassi F.M. and Macdonald P.M. Biochemistry, **31**:10031 10036, 1992.

[50] Bechinger B. and Seelig J. Chem. Phys. Lipids, **58**:1 5, 1991.

[51] Ulrich A. and Watts A. Biophys. J., **66**:1441 1449, 1994.

[52] Trudell J.R., Payan D.G., Chin J.H., and Cohen E.N. Biochim. Biophys. Acta, **373**:436 443, 1974.

[53] Trudell J.R., Payan D.G., Chin J.H., and Cohen E.N. Proc. Natl. Acad. Sci. USA, **72**:210 213, 1975.

[54] Liu N.-L and Kay R.L. Biochemistry, **16**:3484–3486, 1977.

[55] Macdonald P.M. Biochim. Biophys. Acta, **507**:26–37, 1978.

[56] Utoh S. and Takemura T. Jap. J. Appl. Physics, **24**:356–360, 1985.

[57] Tosh R.E. and Collings P.J. Biochim. Biophys. Acta, **859**:10 14, 1986.

[58] Mason J.T. and O'Leary T.J. Biophys. J., **58**:277 281, 1990.

[59] Mountcastle D.B., Biltonen R.L., and Halsey M.J. Proc. Natl. Acad. Sci. USA, **75**:4906 4910, 1978.

[60] Wu W.-G., Chong P.L.-G., an ' Huang C.-H. Biophys. J., **47**:237–242, 1985.

[61] Wong P.T.T. and Mantsch H.H. Biochemistry, **24**:4091 4096, 1985.

[62] Wong P.T.T. and Mantsch H.H. J. Chem. Phys., **83**:3268–3274, 1985.

[63] Wong P.T.T. and Mantsch H.H. J. Raman Spectrosc., **17**:335–340, 1986.

[64] Wong P.T.T., Weng S.F., and Mantsch H.H. J. Chem. Phys., **85**:2315–2319, 1986.

[65] Wong P.T.T. Current Perspectives in High Pressure Biology, pages 287 314. Academic Press Inc., London, Ltd., 1987.

[66] Wong P.T.T. and Mantsch H.H. Biophys. J., **54**:781–790, 1988.

[67] Wong P.T.T. and Mantsch H.H. Chem. Phys. Lipids, **46**:213–224, 1988.

[68] Wong P.T.T. and Huang C.-H. Biochemistry, **28**:1259–1263, 1989.

[69] Wong P.T.T., Chagwedera T.E., and Mantsch H.H. Biophys. J., **56**:845 850, 1989.

[70] Siminovitch D.J., Wong P.T.T., and Mantsch H.H. Biochim. Biophys. Acta, **900**:163 167, 1987.

[71] Siminovitch D.J., Wong P.T.T., Berchtold R., and Mantsch H.H. Chem. Phys. Lipids, **46**:79 87, 1988.

[72] Auger M., Jarrell H.C., Smith. I.C.P., Siminovitch, D.J. Mantsch H.H., and Wong P.T.T. Biochemistry, **27**:6086 6093, 1988.

[73] Hübner W., Wong P.T.T., and Mantsch H.H. Biochim. Biophys. Acta, **1027**:229 237, 1990.

[74] Auger M., Smith. I.C.P., Mantsch H.H., and Wong P.T.T. Biochemistry, **29**:2008 2015, 1990.

[75] Bucket R., Carrier D., Wong P.T.T., Jona I., and Martonosi A. Biochim. Biophys. Acta, **1023**:107 118, 1990.

[76] Zakim D. and Wong P.T.T. Biochemistry, **29**:2003 2007, 1990.

[77] Carrier D., Mantsch H.H., and Wong P.T.T. Biochemistry, **29**:251 258, 1990.

[78] Philip R.B., McIver D.J.L., and Wong P.T.T. Biochim. Biophys. Acta, **1021**:91 95, 1990.

[79] Tamura K., Kaminoh Y., and Ueda I. Biochim. Biophys. Acta, **1066**:219 224, 1991.

[80] Jonas J., Xie C.-L., Grandinetti P.J., Campbell D.M., and Driscoll D. Proc. Natl. Acad. Sci. USA, **85**:4115 4117, 1988.

[81] Jonas J., Grandinetti P.J., and Driscoll D. J. Mag. Res., **87**:536–547, 1990.

[82] Jonas J., Koziol P., Peng X., Reiner C., and Campbell D.M. J. Mag. Res., Ser. B, **102**:299–309, 1986.

[83] Driscol D.A., Jonas J., and Jonas A. Chem. Phys. Lipids, **58**:97–104, 1991.

[84] Driscol D.A., Samarasinghe S., Adamy S., Jonas J., and Jonas A. Biochemistry, **30**:3322–3327, 1991.

[85] Peng X. and Jonas J. Biochemistry, **31**:6383–6390, 1992.

[86] Peng X. and Jonas J. Biophys. J., **68**:1137–1144, 1995.

[87] Bonev B.B. and Morrow M.R. Biophys. J., **69**:518–523, 1995.

[88] Bonev B.B. and Morrow M.R. Biophys. J., **70**:2727–2735, 1996.

[89] Braganza L.F. and Worcester D.L. Biochemistry, **25**:7484–7488, 1986.

[90] Winter R. and Pilgrim W.-C. Ber. Bunsenges. Phys. Chem., **93**:708–717, 1989.

[91] Winter R., Xie C.-L., Jonas J., Thyiagarajan P., and Wong, P.T.T. Biochim. Biophys. Acta., **982**:85–88, 1989.

[92] Shyamsunder E., Botos P., and Gruner S.M. J. Chem. Phys., **90**:1293–1295, 1989.

[93] McIntosh T.J., Magid A.D., and Simon S.A. Biophys. J., **55**:897–904, 1989.

[94] Caffrey M., Hogan J., and Mencke A. Biophys. J., **60**:456–466, 1991.

[95] Mencke A.P. and Caffrey M. Biochemistry, **30**:2453–2463, 1991.

[96] Kamaya H., Ueda I., Moore P.S., and Eyring H. Biochim. Biophys. Acta, **550**:131–137, 1979.

[97] Prasad S.K., Shashidhas R., Gaber B.P., and Chandrasekhar S.C. Chem. Phys. Lipids, **143**:227–235, 1987.

[98] Komatsu H. and Rowe E.S. Biochemistry, **30**:2163–2170, 1991.

[99] Sassaroli M., Vauhkonen M., Somerharju P., and Scarlata S. Biophys. J., **64**:137–149, 1993.

[100] Suezaki Y., Kamaya H., and Ueda I. Biochim. Biophys. Acta, **818**:31–37, 1985.

[101] Suezaki Y., Tamura K., Takasaki M., Kamaya H., and Ueda I. Biochim. Biophys. Acta, **1066**:225–228, 1991.

[102] Wong P.T.T. Ann. Rev. Biophys. Bioeng., **13**:1–24, 1984.

[103] Wong P.T.T., Siminovitch D.J., and Mantsch H.H. Biochim. Biophys. Acta, **947**:139–171, 1988.

[104] Kaneshina S., Kamaya H., and Ueda I. Biochim. Biophys. Acta, **777**:75–83, 1984.

[105] Macdonald P.M. Biochim. Biophys. Acta, **775**:141–149, 1984.

[106] Macdonald P.M. Phil. Trans. R. Soc. London, **304**:141–149, 1984.

[107] Jannasch H.W. Current Perspectives in High Pressure Biology, pages 1–16. Academic Press Inc., London, Ltd., 1987.

[108] Yayanos A.A. and Delong E.F. Current Perspectives in High Pressure Biology, pages 17–32. Academic Press Inc., London, Ltd., 1987.

[109] Marquis R.E. and Bender G.R. Current Perspectives in High Pressure Biology, pages 65–74. Academic Press Inc., London, Ltd., 1987.

[110] Otter, T., Bourns B., Franklin S., Reider C., and Salmon E.D. Current Perspectives in High Pressure Biology, pages 75–94. Academic Press Inc., London, Ltd., 1987.

[111] Brauer R.W. Current Perspectives in High Pressure Biology, pages 129–136. Academic Press Inc., London, Ltd., 1987.

[112] Heremans K. Ann. Rev. Biophys. Bioeng., **11**:1–21, 1982.

[113] Cevc G. Phospholipids Handbook, page 957. Marcel Dekker, Inc., New York, 1993.

[114] Abragam A. The Principles of Nuclear Magnetism. Oxford University Press, London, 1961.

[115] Ernst R., Bodenhausen G., and Wokaun A. Principles of NMR in One and Two Dimensions. Oxford University Press, London, 1986.

[116] Slichter C.P. Principles of Magnetic Resonance. Springer-Verlag, Berlin, 1990.

[117] Davis J.H. Isotopes in Physical and Biomedical Science, volume 2. Elsevier Science Publishers, Amsterdam, 1991.

[118] Seelig J. Q. Rev. Biophys., **10**:353–418, 1977.

[119] Davis J.H. Biochim. Biophys. Acta, **737**:117–171, 1983.

[120] Bloom M. Proceedings of Enrico Fermi International School on the Physics of Magnetic Resonance in Biology and Medicine. Soc. Italiana di Fizica, Bologna, 1990.

[121] Davis J.H. Advances in Magnetic Resonance, volume 13, pages 195 223. Academic Press, New York, 1965-1990.

[122] Davis J.H., Jeffrey K.R., Bloom M., and Valic M.I. Chem. Phys. Let., **42**:390 394, 1976.

[123] Vega S. and Pines A. J. Phys. Chem., **66**:5624 5644, 1977.

[124] Bloom M., Davis J.H., and Valic M. Can. J. Phys., **58**:1510 1517.

[125] Jeffrey K.R. Bull. Mag. Res., **3**:69 82, 1981.

[126] Sternin E., *Ph.D. Thesis*, University of British Columbia, Vancouver, 1988.

[127] Pauls K.P., MacKay A. L., Söderman O., Bloom M., Tanjea A.K., and Hodges R.S. Eur. Biophys. J., **12**:1 11, 1985.

[128] Morrow M.R. Biochim. Biophys. Acta, **1023**:197 205, 1990.

[129] Prosser R.S., Davis J.H., Dahlquist F.W., and Lindorfer M.A. Biochemistry, **30**:4687–4696, 1991.

[130] Gupta C.M., Radhakrishnan R., and Khorana H.G. Proc. Natl. Acad. Sci. USA, **74**:4315–4319, 1977.

[131] Hsiao C.Y.Y., Ottaway C.A., and Wetlaufer D.B. Lipids, **9**:913 915, 1974.

[132] Small D.M. Handbook of Lipid Research, Vol. 4: The Physical Chemistry of Membranes, volume 4. Plenum Press, New York, 1985.

[133] Ruggiero A. and Hudson B. Biophys. J., **55**:1111 1124, 1989.

[134] Mitaku S., Jippo T., and Kataoka R. Biophys. J., **42**:137 144, 1983.

[135] Owicki J.C., Springgate M.W., and McConnell H.M. Proc. Natl. Acad. Sci. USA, **75**:1616–1619, 1978.

[136] Ikeda H. Prog. Theor. Physics. **61**:1023–1033, 1979.

[137] Morrow M.R. and Whitehead J. Biochim. Biophys. Acta. **941**:271–277, 1988.

[138] Zhang Z., Sperotto M.M., Zuckermann M.J., and Mouritsen O.G. Biochim. Biophys. Acta, **1147**:154–160, 1993.

[139] Goodstein D.L. States of Matter. Prentice-Hall, Engewood Cliffs, 1975.

[140] Lifshitz E.M. and Pitaevskii L.P. Statistical Physics. Pergamon Press Ltd., Oxford, 1980.

[141] Huang K. Statistical Mechanics. John Wiley & Sons Inc., New York, 1987.

[142] Goldenfeld N. Phase Transitions and Renormalisation Group. Addison-Wessley, Reading, 1992.

[143] Schindler H. and Seelig J. Biochemistry. **14**:2238–2287, 1975.

[144] Lis L.J., McAlister M., Fuller N., Rant R.P., and Parsegian V.A. Biophys. J., **37**:657–666, 1982.

[145] Böttner M., Ceh D., Jacobs U., and Winter R. Zeitschr. Phys. Chem., **184**:205–218, 1994.

[146] Nagle J.F. J. Chem. Phys., **58**:252–264, 1973.

[147] Marčelja S. Biochim. Biophys. Acta, **367**:165–176, 1974.

[148] Owicki J.C. and McConnell H.M. Proc. Natl. Acad. Sci. USA, **76**:4750–4754, 1979.

[149] Mabrey S. and Sturtevant J.M. Proc. Natl. Acad. Sci. USA, **73**:3862 3866, 1976.

[150] Pàli T., Bartucci R., Horváth L., and Marsh D. Biophys. J., **64**:1781 1788, 1993.

[151] Marassi F.M. and Macdonald P.M. Biochemistry, **30**:10558 10566, 1991.

[152] Morrow M.R., Taneva S., Simatos G., Alwood L.A., and Keough K.M.W. Biochemistry, **32**:11338 11344, 1993.

[153] Li W., *M.Sc. Thesis*, Memorial University of Newfoundland, St. John's, 1995.

[154] Rydall J.R. and Macdonald P. Biochim. Biophys. Acta, **1111**:211 220, 1992.

[155] Pinherto T.J.T., Duralski A.A., and Watts A. Biochemistry, **33**:4896 4902, 1994.

[156] Cevc G. Phospholipids Handbook, page 939. Marcel Dekker, Inc., New York, 1993.

[157] Seddon J.M., Harlos K., and Marsh D. J. Biol. Chem., **24**:4844 4851, 1983.

[158] Finegold L. and Singer M.A. Chem. Phys. Lipids, **35**:291 297, 1984.

[159] Ruocco M.J., Siminovich D.J., and Griffin R.G. Biochemistry, **24**:2406 2411, 1985.

[160] Trahms L., Klabe W.D., and Boroske E. Biophys. J., **42**:285 293, 1985.

[161] Ruocco M.J., Makriyannis A., Siminovich D.J., and Griffin R.G. Biochemistry, **24**:4844 4851, 1985.

[162] Yeagle P.L. Biochim. Biophys. Acta, **815**:33 36, 1985.

[163] Yeagle P.L. Biochim. Biophys. Acta, **822**:267–287, 1985.

[164] Yeagle P.L., Albert A.D., Boesze-Battaglia K., Young J., and Frye J. Biophys. J., **57**:413–424, 1990.

[165] Weisz K., Gröbner G., Mayer C., Stohrer J., and Kothe G. Biochemistry, **31**:1100 1112, 1992.

[166] Reinl H., Brumm T., and Bayerl T. Biophys. J., **61**:1025–1035, 1992.

[167] Thewalt J.L. and Bloom M. Biophys. J., **63**:1176–1181, 1992.

[168] Nezil F.A. and Bloom M. Biophys. J., **63**:1176–1183, 1992.

[169] Bayerl T. and Sackman E. Cholesterol in Model Membranes. pages 13–44. CRC Press, Inc., Boca Raton, 1993.

[170] Davis J.H. Cholesterol in Model Membranes, pages 67–136. CRC Press, Inc., Boca Raton, 1993.

[171] Finegold L. and Singer M. Cholesterol in Model Membranes, pages 137–158. CRC Press, Inc., Boca Raton, 1993.

[172] Sankaram M.B. and Thompson T.E. Biochemistry, **29**:10676–10684, 1990.

[173] Sankaram M.B. and Thompson T.E. Proc. Natl. Acad. Sci. USA, **88**:8686–8690, 1991.

[174] Keough K.M.W., Morrow M.R., and Bittman R. Encyclopodia of NMR, pages 3601 6307. John Wiley & Sons, New York, 1996.

[175] Vist M.R. and Davis J.H. Biochemistry, **29**:451–464, 1990.

[176] Pink D.A. and Carrol C.E. Phys. Lett., **66A**:157–160, 1978.

[177] Ipsen J.H., Karlström G., Mouritsen O.G., and Wennerström O.G. Biochim. Biophys. Acta, **905**:162-72, 1987.

[178] Ipsen J.H., Mouritsen O.G., and Zuckermann M.J. Biophys. J., **56**:661 667, 1989.

[179] Ipsen J.H., Mouritsen O.G., and Bloom M. Biophys. J., **57**:405 412, 1990.

[180] Scott H.L. Biophys. J., **59**:445 455, 1991.